ISSN: 2153-1196 Volume 12, Number 10, August 2021

Scientific Research Publishing

Journal of Modern Physics

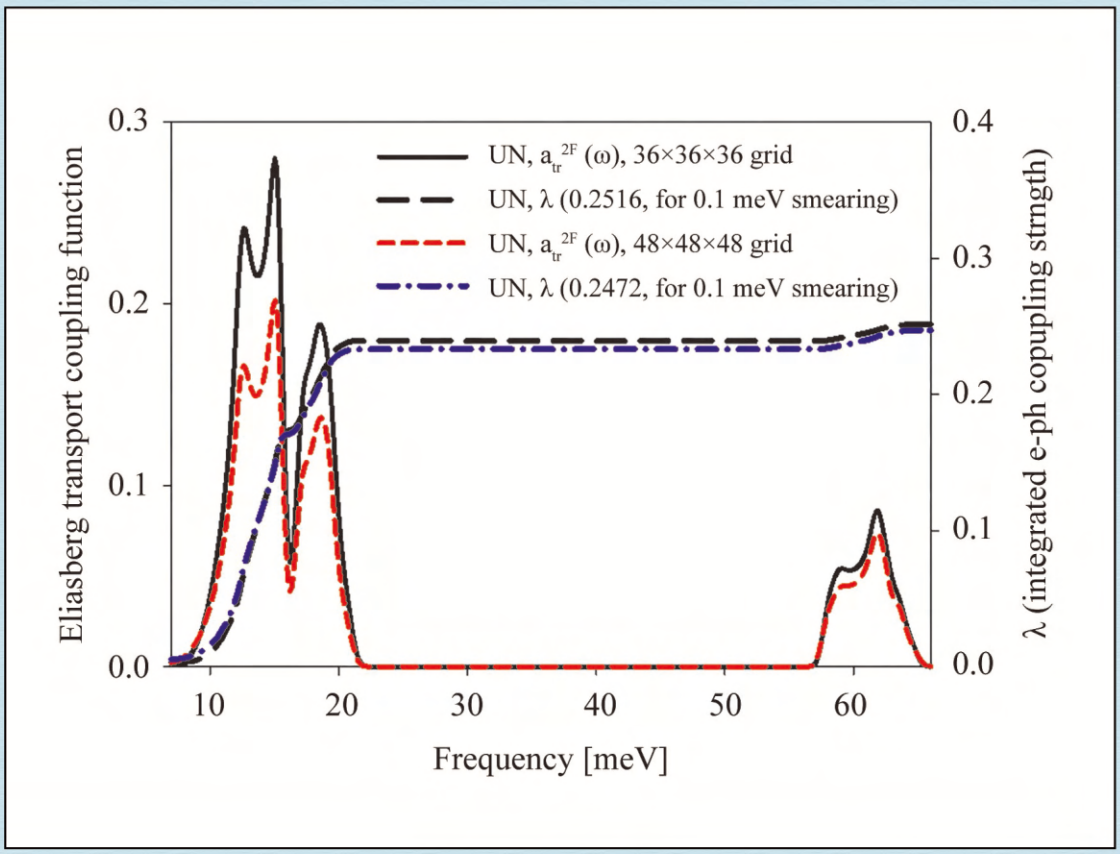

ISSN: 2153-1196

https://www.scirp.org/journal/jmp

Journal Editorial Board

ISSN: 2153-1196 (Print) ISSN: 2153-120X (Online)
https://www.scirp.org/journal/jmp

Editor-in-Chief

Editorial Board

Journal of Modern Physics, 2021, 12, 1401-1474
https://www.scirp.org/journal/jmp
ISSN Online: 2153-120X
ISSN Print: 2153-1196

Table of Contents

Volume 12 Number 10 August 2021

The figure on the front cover is from the article published in Journal of Modern Physics, 2021, Vol. 12, No. 10, pp. 1409-1417 by Barbara Szpunar, Jayangani I. Ranasinghe and Jerzy A. Szpunar.

Journal of Modern Physics (JMP)
Journal Information

SUBSCRIPTIONS

The *Journal of Modern Physics* (Online at Scientific Research Publishing, https://www.scirp.org/) is published monthly by Scientific Research Publishing, Inc., USA.

Subscription rates:
Print: $89 per issue.
To subscribe, please contact Journals Subscriptions Department, E-mail: sub@scirp.org

SERVICES

Advertisements
Advertisement Sales Department, E-mail: service@scirp.org

Reprints (minimum quantity 100 copies)
Reprints Co-ordinator, Scientific Research Publishing, Inc., USA.
E-mail: sub@scirp.org

COPYRIGHT

PRODUCTION INFORMATION

For manuscripts that have been accepted for publication, please contact:
E-mail: jmp@scirp.org

Journal of Modern Physics, 2021, 12, 1401-1408
https://www.scirp.org/journal/jmp
ISSN Online: 2153-120X
ISSN Print: 2153-1196

Persistence Exponent for the Simple Diffusion Equation: The Exact Solution for Any Integer Dimension

Devashish Sanyal

Department of Theoretical Physics, Institute of Physics, Bhubaneswar, India
Email: deva_sans@yahoo.co.in

How to cite this paper: Sanyal, D. (2021) Persistence Exponent for the Simple Diffusion Equation: The Exact Solution for Any Integer Dimension. *Journal of Modern Physics*, **12**, 1401-1408.
https://doi.org/10.4236/jmp.2021.1210083

Received: June 28, 2021
Accepted: August 1, 2021
Published: August 4, 2021

Abstract

The persistence exponent θ_o for the simple diffusion equation $\phi_t(x,t)=\Delta\phi(x,t)$, with random Gaussian initial condition, has been calculated exactly using a method known as selective averaging. The probability that the value of the field ϕ at a specified spatial coordinate remains positive throughout for a certain time t behaves as $t^{-\theta_o}$ for asymptotically large time t. The value of θ_o, calculated here for any integer dimension d, is $\theta_o=\frac{d}{4}$ for $d\le 4$ and 1 otherwise. This exact theoretical result is being reported possibly for the first time and is not in agreement with the accepted values $\theta_o=0.12,0.18,0.23$ for $d=1,2,3$ respectively.

Keywords

Non-Equilibrium Statistical Mechanics, Diffusion Equation, Persistence Exponent, Probability Theory

1. Introduction

The problem in the present paper is to find the persistence exponent for the simple diffusion equation $\phi_t(x,t)=\Delta\phi(x,t)$. The diffusion equation is an equation that has no stochasticity. In the present problem, the stochasticity is introduced through the random initial conditions. The problem is about evaluating the probability of a certain event. The event is that ϕ at a specified location remains positive throughout the time evolution till a certain time t *i.e.* the ϕ at the location does not change sign even once. This probability for asymptotically large time is characterised by an exponent θ_o called the persistence exponent.

Persistence exponent for the diffusion equation has been a subject of interest to physicists [1]-[7] etc., researchers in mathematics and statistics [8] [9] etc. as well as experimentalists [10]. The interest in the persistence exponent is just not confined to the diffusion equation but to other areas of non-equilibrium physics. Among them random walk [11], walk in a random environment with or without bias [12], surface growth [13], diffusing particle in a random potential with a small concentration of absorbers [14], behaviour of financial markets [15] etc. are worth mentioning. There are few exact calculations for the persistence exponent in the literature. The case of a simple random walk in one dimension gives the exponent $\theta_o = \frac{1}{2}$. Even the calculation of persistence exponents for Gaussian processes may not be straight forward.

We revisit the problem of simple diffusion. It is strongly non-Markovian in nature. The problem involves the partial differential equation $\phi_t = \Delta\phi$ with random Gaussian initial conditions. It appears to remain an unsolved problem even though results [1] [2] and several others have been reported. The problem of diffusion may require a better understanding in the context of persistence. The article tries to find an exact solution to the problem.

2. Simple Diffusion Equation, Random Initial Conditions and Persistence Exponent

The diffusion equation $\phi_t = \Delta\phi$ is a coarse grained differential equation whose solution is uniquely determined by the initial condition. In the present problem, the initial condition is not fixed but is chosen from a distribution. The initial value of ϕ at every coordinate is chosen from a Gaussian distribution with mean 0, variance k and the initial values of ϕ at any two coordinates are statistically independent.

In order to calculate persistence exponent θ_o we have to calculate the probability that the field ϕ at a specified coordinate does not flip sign even once throughout a time t. This probability $\mathcal{P}^+(t)$ of ϕ always remaining +ve behaves in the limit of asymptotically large time as $\mathcal{P}^+(t) \sim t^{-\theta_o}$. This is true for a non-stationary process like in the present case. In this article any position x coordinate is a vector quantity in a d dimensional space. The moments of the initial condition distribution described above are given by

$$\langle \phi(x,0) \rangle = 0 \tag{1-a}$$

$$\langle \phi(x_1,0)\phi(x_2,0) \rangle = k\delta^{(d)}(x_1 - x_2) \tag{1-b}$$

where k is the variance of the distribution. The solution for the diffusion equation may be written in terms of the initial condition as

$$\phi(x,t) = \int \mathrm{d}^d x' G(x - x', t)\phi(x',0) \tag{2}$$

where $G(x,t) = (4\pi t)^{-d/2} \exp(-x^2/4t)$. The plan for the evaluation of the exponent is as follows. First, we have to calculate the probability of ϕ attaining a

specific final value β at a certain $x = x_o$ starting from a definite initial value α of ϕ at $x = x_o$. In order to evaluate it we use the method of selective averaging. The paths that take the initial α to the final value β also comprise those where $\phi(x_o)$ flips sign at least once during time evolution. The probability of such paths is to be subtracted out. Finally, there has to be an integration over the final β from 0 to ∞, followed by an integration over α from 0 to ∞.

Selective averaging means averaging over the initial field $\phi(x,0)$, except when $x = x_o$. In other words, the averaging is done over all the initial configurations such that ϕ at $x = x_o$ is kept fixed at α (say) *i.e.* $\phi(x_o,0) = \alpha$ while for $x \neq x_o$ ϕ varies according to Gaussian distribution. In this paper the selective distribution, denoted by subscript *s*, is characterized by the moments,

$$\langle \phi(x,0) \rangle_s = \alpha \delta^{(d)}(x - x_o) \tag{3-a}$$

$$\langle \phi(x_1,0)\phi(x_2,0) \rangle_s = \left\{ k + \left[\alpha^2 - k \right] \delta^{(d)}(x_1 - x_o) \right\} \delta^{(d)}(x_1 - x_2) \tag{3-b}$$

It may be verified from (3-a), (3-b) that if $x \neq x_o$, $x_1 \neq x_o$, $x_2 \neq x_o$, we get (1-a), (1-b) and for $x = x_1 = x_2 = x_o$, (3-a), (3-b) give α, α^2 as expected. Using (3-a), (3-b), we can calculate the moments of the random variable $\phi(x_o,t)$,

$$\langle \phi(x_o,t) \rangle_s = (4\pi t)^{-d/2} \alpha \tag{4}$$

$$\begin{aligned} \langle \phi^2(x_o,t) \rangle_s &= \int \mathrm{d}^d x_1' \mathrm{d}^d x_2' (4\pi t)^{-d} \exp\left[-\frac{(x_o - x_1')^2}{4t} \right] \\ &\quad \times \exp\left[-\frac{(x_o - x_2')^2}{4t} \right] \langle \phi(x_1',0)\phi(x_2',0) \rangle_s \\ &= k \int \mathrm{d}^d x_1' (4\pi t)^{-d} \exp\left[-\frac{(x_o - x_1')^2}{2t} \right] - \frac{k}{(4\pi t)^d} + \frac{\alpha^2}{(4\pi t)^d} \end{aligned} \tag{5}$$

While evaluating the second order moment, we have used the relation in (3-b). Hence the mean and the variance of the distribution for $\phi(x_o,t)$, represented by μ and σ^2 respectively, are

$$\mu = \langle \phi(x_o,t) \rangle_s = (4\pi t)^{-d/2} \alpha \tag{6-a}$$

$$\begin{aligned} \sigma^2 &= \langle \phi^2(x_o,t) \rangle_s - \langle \phi(x_o,t) \rangle_s^2 \\ &= k(4\pi)^{-d} 2^{(d/2-1)} k_d \Gamma(d/2) t^{-d/2} - k(4\pi t)^{-d} \end{aligned} \tag{6-b}$$

In the above equation k_d denotes the angular integration in d dimensional space while Γ represents the usual Gamma function. It may be mentioned that $\phi(x,t)$ in (2) is Gaussian irrespective of whether $\phi(x',0)$, the initial Gaussian field, is correlated or not. In the present case, though, the initial field is uncorrelated and $\phi(x,t)$ can be proved to be Gaussian using characteristic functions in probability theory [16]. It may be noted that the δ function distribution is the limiting case of a Gaussian distribution. The expression for the conditional

probability for starting at α and being between β and $\beta+\mathrm{d}\beta$ at time t_1 is

$$P(\beta|\alpha)\mathrm{d}\beta=\frac{1}{\sqrt{2\pi}\sigma}\exp\left[\frac{-(\beta-\mu)^2}{2\sigma^2}\right]\mathrm{d}\beta \tag{7}$$

where $\mu=\mu(\alpha,t_1)$ and $\sigma=\sigma(t_1)$. This probability considers all the paths that start from α to be between β and $\beta+\mathrm{d}\beta$ at time t_1 including ones that flip en route β as depicted in **Figure 1**. **Figure 1** is the projection of the trajectory of the system in the infinite dimensional $\Phi-t$ space on to the $\phi(x_o)-t$ plane.

$A(0,\alpha)$ represents the starting point and $B(t_1,\beta)$, the destination. AB represents a path along which $\phi(x_o)$ does not flip and ADB (blue curve) is a typical path along which $\phi(x_o)$ flips. Such paths have to be excluded. The probability of reaching from A to the neighborhood B at asymptotically large time t_1 without flipping is given by,

$$P^{+}(\beta|\alpha)\mathrm{d}\beta=P(\beta|\alpha)\mathrm{d}\beta-P(\beta|-\alpha)\left(1+O\left(t^{-1}\right)\right)\mathrm{d}\beta \tag{8}$$

The second term represents the probability of paths such as $\bar{A}DB$ originating from $\bar{A}(0,-\alpha)$ and terminating in the neighborhood of B at t_1. (8) is not be confused with the method of images in [17]. (8) follows a very different logic in the present case and holds good asymptotically. To prove (8) we will show that there is a one to one mapping from a path $A\to B$ to a path $\bar{A}\to B$ and that the probability of two such paths converges asymptotically. This part is explained in 1) in what follows. Further, to justify (8) we have to show that the "number" of paths $A\to B$ that flip and the "number" of paths $\bar{A}\to B$ converge asymptomatically. This is done in 2). In the subsequent analysis we will consider a d dimensional lattice—lattice spacing being infinitesimally small—instead of continuum for the sake of notational convenience only. The reason for (8) follows.

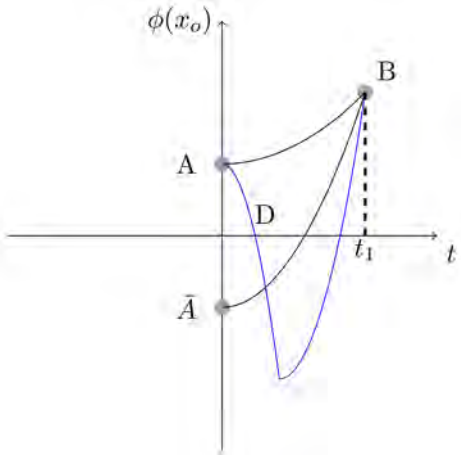

Figure 1. Projection of $\Phi-t$ trajectory onto the $\phi(x_o)-t$ plane.

1) An initial configuration at A of Figure 1 given by $X_{AB}=\{\cdots,\alpha_1,\alpha,\alpha_2,\cdots\}$, is considered, where $\alpha_1,\alpha_2,\cdots$ are the initial values of ϕ at coordinates $x\neq x_o$. The corresponding path takes initial $\phi(x_o)=\alpha$ to B, then it may be concluded from (2) that $X_{\bar{A}B}=\{\cdots,f\alpha_1,-\alpha,f\alpha_2,\cdots\}$ ($f=\dfrac{\beta+(4\pi t)^{-d/2}\alpha}{\beta-(4\pi t)^{-d/2}\alpha}$) is a configuration at $\bar{A}$ which takes initial $\phi(x_o)=-\alpha$ to B. Hence there is a one to one mapping of paths from $A\to B$ to those from $\bar{A}\to B$. It may be underlined here that $f\to 1$ as $t\to\infty$. This implies that the probability of the two paths approach each other asymptotically.

2) In this part we will address the fact that in the asymptotically large time limit it is a very good approximation to say that there is a one to one correspondence between the paths from A that flip to those from $\bar{A}\to B$. This may be used as it is a controlled approximation for it improves with increasing t. In order to see this point let us consider a point $C(t_2,\beta)$ (not shown in the Figure 1) where $t_2>t_1$. Let $Y_{AB}=\{\cdots,\gamma_1,\alpha,\gamma_2,\cdots\}$ be the initial configuration corresponding to path ADB (the path in blue in Figure 1) where $\gamma_1,\gamma_2,\cdots$ are the initial values of ϕ at coordinates $x\neq x_o$. This path crosses zero while reaching B. It can be shown that $Y_{AC}=\{\cdots,f_1\gamma_1,\alpha,f_1\gamma_2,\cdots\}$ ($f_1=\left(\dfrac{t_2}{t_1}\right)^{d/2}\dfrac{\beta-(4\pi t_2)^{-d/2}\alpha}{\beta-(4\pi t_1)^{-d/2}\alpha}$) is the corresponding initial configuration for a path $A\to C$. The exact expression for f_1 contains a coordinate dependent term whose leading order behavior for large t is 1. Since $t_2>t_1$, we have $f_1>1$ for sufficiently large t_1. Let the time coordinate at D be t_D, then $\phi(x_o,t_D)=0$ for the path ADB. Then one may arrive from (2) that $\phi(x_o,t_D)<0$ for the initial configuration Y_{AC}. Hence, one can conclude that the path corresponding to Y_{AC} must have flipped at an earlier time than t_D. Therefore, if a path from $A\to B$ flips, the corresponding path from $A\to C$ flips at an earlier time. Since $t_2>t_1$, the "number" of paths flipping while going from $A\to C$ is more than those from $A\to B$. Thus the "number" of paths from $A\to B$ that flip is a fraction f_2 of those from $\bar{A}\to B$ where $f_2=1-O\left(t_1^{-a}\right)$ for large t_1, a being some positive number.

On account of 1), 2) we say that the probability of the paths (like ADB in Figure 1) that flip while reaching B in the large time limit is given by $P(\beta|-\alpha)h_{\text{correction}}$, where $h_{\text{correction}}=1+O\left(t^{-b}\right)$, $b=1$, being Taylor expansion in t^{-1}. In principle, the coefficient of t^{-b} may be a function of β. When integrating over β —as will be done later—the contribution to the integral comes from the vicinity of $\beta=-\mu\sim t^{-d/2}$ which is vanishingly small in the asymptotic limit. Also, $\mathrm{d}\beta\sim\sigma\sim t^{-d/4}$. The coefficient is Taylor expanded about $\beta=0$ and only the zeroth order term or the term independent of β is retained. So the probability of $\phi(x_o)$ not changing sign when reaching the neighborhood ($\mathrm{d}\beta$) of B is, for asymtotically large time,

$$\begin{aligned}&\lim_{t\to\infty}\left[P(\beta|\alpha)\mathrm{d}\beta-P(\beta|-\alpha)h_{\text{correction}}\mathrm{d}\beta\right]\\&=P(\beta|\alpha)\mathrm{d}\beta-P(\beta|-\alpha)\left(1+O\left(t^{-1}\right)\right)\mathrm{d}\beta\end{aligned}\tag{9}$$

This leads us to (8). The final β may have any value as long as it remains positive. The probability of $\phi(x_o)$ starting from α and reaching a final positive value without ever changing sign is

$$\mathbb{P}^+(\alpha) = \int_0^\infty d\beta P^+(\beta \mid \alpha) \tag{10}$$

We would now calculate (10) for asymptotically large value of *t*. Under the circumstances the second term on the R.H.S of (6-b) can be neglected. Further $\frac{\mu^2}{\sigma^2} \sim \alpha t^{-d/2}$. Hence for $\alpha \ll t^{d/2}$, $\mu^2/\sigma^2 \ll 1$. The expression (10) is evaluated using the identity [18]

$$\boxed{\int_0^\infty dx \exp\left(\frac{-x^2}{4\beta} - \gamma x\right) = \sqrt{\pi\beta}\exp\left(\beta\gamma^2\right)\left[1 - erf\left(\gamma\sqrt{\beta}\right)\right]} \tag{11}$$

Evaluation leads to a sum of two terms—one is proportional to $t^{-d/4}$ and the other is proportional to t^{-1}. Hence we obtain

$$\mathbb{P}^+(\alpha) \sim \alpha t^{-d/4} \tag{12}$$

for $d \le 4$. In arriving at the above result the asymptotic expansion of "error function" *erf* has been used for small argument. Finally, the expression for $\mathcal{P}^+(t)$ is obtained by integrating α over a Gaussian distribution.

$$\mathcal{P}^+(t) = \int_0^\infty d\alpha \mathbb{P}^+(\alpha) Q(\alpha) \tag{13}$$

where $Q(\alpha)$ is the Gaussian distribution for initial $\phi(x_o, o) = \alpha$ with variance *k* as mentioned at the beginning. If $k \ll t^{d/2}$, it may be concluded from (12) and (13) that $\mathcal{P}^+(t) \sim t^{-d/4}$ or t^{-1} depending on whether $d \le 4$ or not. This gives $\theta_o = d/4$ or 1.

3. Result and Conclusion

In the previous section, exact calculation has been carried out to determine the probability $\mathcal{P}^+(t)$ of the sign of the field ϕ remaining positive throughout an asymtotically large time *t*. The probability is $\mathcal{P}^+(t) \sim t^{-d/4}$. Hence, the persistence exponent is $\theta_o = d/4$ valid for any arbitrary integer dimension $d \le 4$. The exponents for $d = 1, 2, 3$ are 0.25, 0.50, 0.75 respectively.

The result may be experimentally verified for a system initially at thermal equilibrium defined by a temperature T. The equilibrium is then disturbed in a suitable manner. The time evolution of the coarse grained temperature at any point satisfies the simple diffusion equation; hence, this time evolution can be studied to find the persistence exponent.

The answer for the exponent θ_o obtained in this paper is in disagreement with all the papers cited in the beginning. The first results for the persistence exponent in the case of the diffusion problem were published in [1] [2] back to back. The papers used a two time correlation function and explicitly applied the approximation (IIA), Independent Interval Approximation, to get to the answer. Application of the two time correlation function is not suitable here and so is

IIA which is a Markovian approximation. Further, the papers use Monte Carlo simulation to confirm the result. Monte Carlo method appears to be unsuitable for this problem. Hence all the papers that reproduce the results of [1] [2] are not expected to give the correct answer. In [3], the authors have defined a correlation function $C(T)$, just like [1] [2], to carry the calculation forward. Let us also consider [6] where the authors have used Kac Polynomials [19] to obtain the "exact exponent" in 2d. The answer obtained agrees perfectly with [1] [2]. In the course of the calculation, they have used that the zero crossing property is governed by the covariance $c(T)=\operatorname{sech}\left(\frac{T}{2}\right)$ [6] of the stationary Gaussian process *i.e.* the diffusion equation with time redefined. Similarly in [4], correlator in time $F_{\varepsilon}(\tau-\tau')$ has been used in the calculation. The point is that the covariance/correlator/correlation function is a misleading quantity for the problem for reasons mentioned below. The model presented in the paper has randomness only in the initial condition. Once the system starts evolving, there is no further randomness. It evolves in accordance with the kernel in (2). It is encoded in the initial condition when and where the ϕ will flip. The probability of each path is uniquely determined by the probability of initial condition, hence the problem with covariance/correlator. The covariance function imposes stochasticity on the present problem throughout the entire time evolution. We now have a different model with the same correlation function but no unique dependence of the probability of the path on initial condition. It also makes the problem Markovian. Hence, all the previous results are in perfect agreement though the calculated exponent will be different from the actual value. The value of the exponent does not depend on only correlation function, but it depends on other details of the model too. Further, there even appears to be experimental proof [10] for the results of [1] [2]. The experimental setup of [10] does not represent the diffusion model described in this paper. The setup satisfies the approximations of the previous papers and hence the agreement with their result.

Acknowledgements

The author would like to thank CSIR, India for Fellowship during the course of the work (2004) at IACS, India.

Conflicts of Interest

The author declares no conflicts of interest regarding the publication of this paper.

References

[1] Majumdar, S.N., Sire, C., Bray, A.J. and Cornell, S.J. (1996) *Physical Review Letters*, **77**, 2867-2870. https://doi.org/10.1103/PhysRevLett.77.2867

[2] Derrida, B., Hakim, V. and Zeitak, R. (1996) *Physical Review Letters*, **77**, 2871-2874. https://doi.org/10.1103/PhysRevLett.77.2871

[3] Ehrhardt, G.C.M.A. and Bray, A.J. (2002) *Physical Review Letters*, **88**, Article ID: 070601. https://doi.org/10.1103/PhysRevLett.88.070601

[4] Hilhorst, H.J. (2000) *Physica A*: *Statistical Mechanics and Its Applications*, **277**, 124-126. https://doi.org/10.1016/S0378-4371(99)00509-9

[5] Schehr, G. and Majumdar, S.N. (2008) *Journal of Statistical Physics*, **132**, 235-273. https://doi.org/10.1007/s10955-008-9574-3

[6] Poplavskyi, M. and Schehr, G. (2018) *Physical Review Letters*, **121**, Article ID: 150601. https://doi.org/10.1103/PhysRevLett.121.150601

[7] Barbier-Chebbah, A., Benichou, O. and Voituriez, R. (2020) *Physical Review E*, **102**, Article ID: 062115. https://doi.org/10.1103/PhysRevE.102.062115

[8] Aurzada, F. and Simon, T. (2015) Persistence Probabilities and Exponents. In: *Lévy Matters V*, Springer, Berlin, 183-224. https://doi.org/10.1007/978-3-319-23138-9_3

[9] Dembo, A. and Mukherjee, S. (2015) *The Annals of Probability*, **43**, 85-118. https://doi.org/10.1214/13-AOP852

[10] Wong, G.P., Mair, R.W., Walsworth, R.L. and Cory, D.G. (2001) *Physical Review Letters*, **86**, 4156-4159. https://doi.org/10.1103/PhysRevLett.86.4156

[11] Schwarz, J.M. and Maimon, R. (2001) *Physical Review E*, **64**, Article ID: 016120. https://doi.org/10.1103/PhysRevE.64.016120

[12] Le Doussal, P., Monthus, C. and Fisher, D.S. (1999) *Physical Review E*, **59**, 4795-4840. https://doi.org/10.1103/PhysRevE.59.4795

[13] Krug, J., Kallabis, H., Majumdar, S.N., Cornell, S.J., Bray, A.J. and Sire, C. (1997) *Physical Review E*, **56**, 2702-2712. https://doi.org/10.1103/PhysRevE.56.2702

[14] Le Doussal, P. (2009) *Journal of Statistical Mechanics*: *Theory and Experiment*, No. 7, P07032. https://doi.org/10.1088/1742-5468/2009/07/P07032

[15] Constantin, M. and Das Sarma, S. (2005) *Physical Review E*, **72**, Article ID: 051106. https://doi.org/10.1103/PhysRevE.72.051106

[16] Mathews, J. and Walker, R.L. (1970) Mathematical Methods of Physics. Volume 501, WA Benjamin, New York.

[17] Chadrasekhar, S. (1989) Stochastic, Statistical and Hydromagnetic Problems in Physics and Astronomy. Selected Papers Vol. 3.

[18] Gradshteyn, I.S. and Ryzhik, I.M. (2014) Table of Integrals, Series, and Products. Academic Press, Cambridge.

[19] Kac, M. (1943) *Bulletin of the American Mathematical Society*, **49**, 314-320. https://doi.org/10.1090/S0002-9904-1943-07912-8

Journal of Modern Physics, 2021, 12, 1409-1417
https://www.scirp.org/journal/jmp
ISSN Online: 2153-120X
ISSN Print: 2153-1196

Electronic Transport of Uranium Mononitride

Barbara Szpunar[1*], Jayangani I. Ranasinghe[1], Jerzy A. Szpunar[2]

[1]Department of Physics and Engineering Physics, University of Saskatchewan, Saskatoon, Canada
[2]Department of Mechanical Engineering, University of Saskatchewan, Saskatoon, Canada
Email: *B.Szpunar@usask.ca

How to cite this paper: Szpunar, B., Ranasinghe, J.I. and Szpunar, J.A. (2021) Electronic Transport of Uranium Mononitride. *Journal of Modern Physics*, **12**, 1409-1417.
https://doi.org/10.4236/jmp.2021.1210084

Received: April 14, 2021
Accepted: August 1, 2021
Published: August 4, 2021

Abstract

We investigated the electronic heat capacity, thermal conductivity, and resistivity of UN using Quantum Espresso and EPW code. GGA, PBEsol functional was used. The calculated electronic heat coefficient was found to be significantly reduced (0.0176 $J \cdot mol^{-1} \cdot K^{-2}$ versus 0.0006 $J \cdot mol^{-1} \cdot K^{-2}$) when the non-local hybrid functional (B3LYP) was used. Furthermore, we calculated electrical resistivity using a very transparent Ziman's formula for metals with the Eliashberg transport coupling function as implemented in EPW code for non-spin-polarized calculations. The number of mobile electrons in UN, as a function of temperature, was derived from the ratio of the calculated resistivity and available experimental data. The electronic thermal conductivity was evaluated from the calculated electronic resistivity via Wiedemann-Franz law with the number of mobility electrons (n_{av}) incorporated (averaged over the temperature range 300 K - 1000 K). Both the electronic thermal conductivity and resistivity, as calculated using newly evaluated n_{av}, compare well with experimental data at ~700 K, but to reproduce the observed trend as a function of temperature, the number of mobile electrons must decrease with the temperature as evaluated.

Keywords

UN, Electronic Thermal Conductivity, Electronic Structure, Number of Mobility Electrons, Quantum ESPRESSO, EPW Codes

1. Introduction

Urania fuel, which is used in conventional nuclear reactors, is not suitable for some designs of new generation reactors (e.g., SuperCritical Water Reactor) due to its low thermal conductivity [1]. In the context of finding a sustainable development solution to the use of non-renewable energy sources, innovative research towards enhanced accident-tolerant nuclear fuel (EATF) that can with-

stand the loss of coolant for a long time is gaining momentum. EATF materials must have higher thermal conductivities to prevent meltdown [2]. High-density metallic compounds, uranium silicide (U_3Si_2) and uranium and thorium nitrides (UN, ThN) [3], have been proposed as alternative EATFs [2] for implementation as lower enrichment fuel.

In our previous papers [4] [5], we have investigated UN, which has the same cubic structure ($Fm\bar{3}m$ symmetry) as ThN, and may be used in combination to enhance thermal conductivity as both are metals. In these metallic fuels, thermal conductivity does not deteriorate with increasing temperature like the lattice-governed thermal conductivity in insulators (e.g. urania [6]). This is due to the increasing presence of electronic carriers with mobility as temperature rises. Since both electronic conductivity and electronic contribution to thermal conductivity are related to electron mobility, they can be derived from each other via the Wiedemann-Franz proportionality law (WFL), which is very useful in determining the contribution from electrons to the measured total thermal conductivity.

Enhanced computational capabilities have led to significant developments in extending the potentialities of based on density functional theory (DFT) codes. *Ab initio* calculations based on DFT have become an essential theoretical tool in investigating novel nuclear materials. In this study, we used first-principles, predictive calculations based on DFT, where ground state energy is calculated using functionals dependent on the electronic density only. Unlike urania, fewer such studies have been done on these alternative fuels. In particular number of mobility, electrons need to be investigated, since they are crucial in enhancing the thermal conductivity of metals at high temperatures. High thermal conductivity in metallic fuels allows for fast heat dissipation and makes reactors safer and more economical.

In an evaluation of the electronic heat capacity, very accurate calculations of electrondensities of states are required. In our previous work on thoria [7], we found that the non-local hybrid functional (B3LYP) [8] modified the electronic structure significantly and led to a larger bandgap. It was therefore of interest to examine the electronic structure of UN using B3LYP to find how it might affect the value of the electronic heat capacity coefficient of UN, as evaluated here.

2. Calculation Methodology

To evaluate the geometrical and electronic structures of UN we used Quantum ESPRESSO (QE) code [9], since there is already an interface provided between QE and EPW (Electron-Phonon coupling using Wannier functions) code [10], which we used to evaluate electronic transport.

We calculated the electronic heat capacity coefficient (γ), which is proportional to the electron density of states at Fermi energy at the equilibrium lattice constants using the density of states of electrons per eV at the Fermi energy ($\rho(\varepsilon_F)$) for UN from:

$$C_e(T) = \pi/3 \times 6.242 \times 10^{18} \rho(\varepsilon_F) N_A k_B^2 T \equiv \gamma T \quad (1)$$

The respective electronic heat capacity is proportional to γ and increases linearly with temperature and can be evaluated using Equation (1). A very accurate evaluation of the electronic structure was required; therefore, in addition to generalized gradient approximation (GGA) of the Perdew, Burke, and Ernzerhof functional developed for solids (PBEsol) [11] DFT, we used non-local Becke three-parameter hybrid exchange (B3)+LYP functional (B3LYP) [8] to modify the electronic structure around Fermi energy, and the respective electronic heat coefficients were compared. We used the same norm-conserved pseudopotentials and setup for the electronic structure calculations as detailed in our previous work on UN [5].

Using the density functional perturbation theory (DFPT) method as implemented in QE code [12], we evaluated previously [5] the phonons' dispersion relation and the densities of states of UN.

We computed the electrical resistivity calculation ($\rho_{calc}(T)$) using a very transparent Ziman's formula for metals (Equation 54 in Ref. [10]) with the Eliashberg transport coupling function: $\alpha_{tr}^2 F(\omega)$ (Equation 55 in Ref. [10]) and a hard-coded number of mobility electrons (nc) per cell equal to 8 (assumed for lead as an example) as implemented in EPW code [10]:

$$\rho_{calc}(T) = \frac{4\pi m_e}{ne^2 k_B T} \times \int_0^\infty \mathrm{d}\omega \hbar \alpha_{tr}^2 F(\omega) n(\omega, T)\left[1 + n(\omega, T)\right] \quad (2)$$

where n = nc/omega and omega is the calculated in the code volume of the primitive cell in a.u.. Note that in the new version (QE 6.7) nc is a parameter with the default value equal to (4).

We also calculated integrated electron-phonon strength (λ) as a function of frequency (ω) [10]:

$$\lambda = \int_0^\omega \frac{\alpha_{tr}^2 F(\omega)}{\omega} \mathrm{d}\omega \quad (3)$$

The cumulative electron-phonon strength and Eliashberg transport coupling function could be used in future comparisons with other metallic fuels. Additionally, since the experimental resistivity is known for UN, we evaluated the effective number of electron carriers in electronic transport ($n_{eff}(T)$):

$$n_{eff}(T) = \frac{8\rho(T)_{calc}}{\rho(T)_{exp}} \quad (4)$$

When replacing n, the number of mobility electrons in Equation (2) with $n_{eff}(T)$, the calculated resistivity would become equal to the experimental. We also calculated averages of an effective number of electron carriers in the 300 K - 1000 K temperature range (n_{av}) and calculated resistivity by replacing n with n_{av}.

The electronic contribution to the thermal conductivity (κ_e) can be calculated via Wiedemann-Franz law [13] from the electrical conductivity (σ) or resistivity ($\rho(T) = \sigma(T)^{-1}$):

$$\kappa_e = \frac{\pi}{3}\left(\frac{k_B}{e}\right)^2 \sigma T \tag{5}$$

where k_B is the Boltzmann constant, e is the electron charge, and T is the temperature in K. We calculated electronic thermal conductivity using the n_{av} number of mobility electrons of Un and compared results with the experiment.

3. Results and Discussion

Here we adopted for UN the same parameters and norm-conserving pseudopotentials: U.pbesol-n-nc.UPF and N.pbesol-nc.UPF from QE code as in our previous studies [5]. We assumed $5f^3$, $6d^1$, $7s^2$ for U and $2s^2$, $2p^3$ for N as the electronic configurations. The evaluated lattice constants for non-magnetic UN (0.489 nm) and using this setup [5] agreed very well with the experimental value of 0.489 [14].

3.1. Electrons' Density of States and Electronic Heat Capacity

Using QE code, we previously performed [5] non-spin-polarized calculations to evaluate the electronic structure of UN at the equilibrium lattice constants. In addition, we used here the non-local hybrid exchange functional (B3LYP) [8] to try to modify its electronic structure around Fermi energy as demonstrated before during an evaluation of the bandgap of ThO_2 [7]. However, there are no pseudopotentials developed for B3LYP either for N or U atoms and the calculations are very computationally demanding. Therefore, we reduced the kinetic energy cutoff for wave functions to 200 Ry (2721 eV) and used existing pseudopotentials for other functionals: N.blyp-hgh.UPF and the used above U.pbesol-n-nc.UPF. Otherwise, we used a similar setup and the same lattice constants as previously determined for PBEsol calculations [5].

In **Figure 1(a)** and **Figure 1(b)**, we compare the electronic structure of UN evaluated using a) PBEsol and b) B3LYP functionals. We present the evaluated per formula unit (f.u.,: UN) total electronic density of states of UN (solid black line) together with the projected partial electron densities of states (plotted with 0.1 eV energy step) of nitrogen: 2p (dashed-dot-dot blue line), and 2s (dashed-long pink line) and for uranium: 6d (dark red dotted line) and 5f (dashed medium green line) electron densities of states. The Fermi energy is indicated by the grey dashed line. The integrated (with 0.01 eV energy step) total number of electrons as a function of energy is indicated as dashed-dot red lines, with the total number of electrons at Fermi energy: 11e. In both calculations (**Figure 1(a)** and **Figure 1(b)**) 2p electrons of the N atom are located below 10 eV while 2s electrons are located below 0 eV energy.

Similar to our previous results for thoria [7], we found that the non-local hybrid functional B3LYP pushed 5f electrons of U up and away from Fermi energy (**Figure 1(b)**) when compared with our calculations using PBEsol in **Figure 1(a)**. This resulted in a lower density of states at Fermi energy ($\rho(\varepsilon_F)$) as the hybridized states of 6d and 5f U electrons also moved up just above it, as shown in **Ta-**

ble 1, second row.

Our calculations predict a significant reduction of the electronic heat coefficient (γ) for UN (B3LYP result), as shown in Table 1. It would be interesting to examine an experimental evaluation although recently Parker *et al.*, using the experimental fit [15] for ThN, also found γ to be very small (0.001 J·mol^{-1}·K^{-2}).

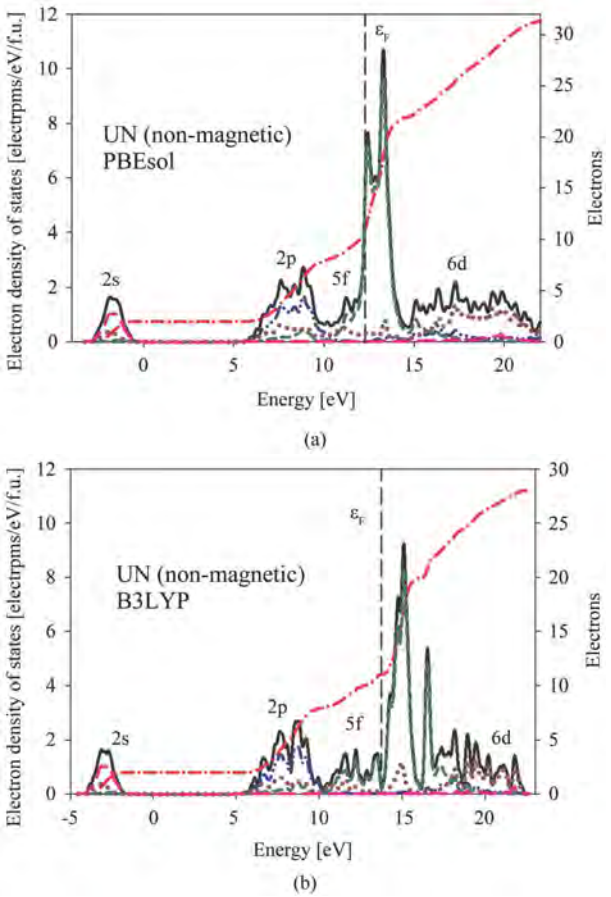

Figure 1. The calculated total (black solid line) electron densities of states of UN using (a) PBEsol functional and (b) non-local hybrid functional (B3LYP) are presented. The projected partial electron densities of states of nitrogen 2p (dashed-dot-dot blue line), and 2s (dashed-long, pink line) and for uranium: 6d (dark red dotted line) and 5f (dashed medium green line) electron densities of states are shown as indicated. The dashed grey lines indicate the Fermi energy. The integrated total number of electrons (left y axis) as a function of energy is indicated as dashed-dot red lines.

Table 1. The comparison of the calculated electron density of states at Fermi energy, the electronic heat capacity coefficient, and Fermi Energy of UN using PBEsol and B3LYP functionals.

Calc. QE This work	UN (PBEsol)	UN (B3LYP)
$\rho(\varepsilon_F)$ [electr./eV/FU]	7.472	0.253
γ [J·mol^{-1}·K^{-2}]	0.0176	0.0006
E_F [eV]	12.31	13.72

3.2. Electronic Resistivity

We calculated phonons' dispersion and the density of states as before [5] but used a finer grid: 6 × 6 × 6. Next, using EPW code, we calculated the Eliashberg transport coupling function: $\alpha_{tr}^2 F(\omega)$ (Equation 55 in Ref. [10]) together with the integrated electron-phonon strength (λ) as a function of frequency (ω) using Equation (3). In **Figure 2**, we present the results by a dashed red line and dashed-dot blue line, respectively. The integration was done on a 48 × 48 × 48 homogeneous k-point mesh and a 48 × 48 × 48 homogeneous q-point mesh with Gaussian smearing of 100 meV for the electrons, and 0.1 meV for the phonons. The total integrated electron-phonon strength of 0.2472 only slightly increases (0.2516) when 36 × 36 × 36 grids are used while the Eliashberg transport coupling function (indicated by a solid black line), which is presented here using 0.5 meV smearing, shows a more visible effect of grid change (**Figure 2**).

Next, we calculated the electrical resistivity of UN and the number of mobility electrons using Equations (2) and (4), and the results are presented in **Figure 3** and **Figure 4**. We used porosity-free experimental resistivity for UN by Hayes *et al.* [16]. We note that both the resistivity and the evaluated number of mobility electrons are not much affected by a change in the grid. The averages over a number of mobility electrons in the temperature range 300 K - 1000 K are slightly higher for the finer grid (n_{av}: 0.343 e versus 0.337 e). We found that Ziman's formula (Equation (2)) predicts a stronger decrease of resistivity for decreasing temperatures than experiment when assuming that the number of mobility electrons is constant and equal to n_{av}, as indicated in **Figure 3**. To reproduce the experimentally observed temperature dependence of the resistivity of UN as presented in **Figure 3** (black solid line), a variable with a temperature-dependent number of electrons was needed, as evaluated in **Figure 4**.

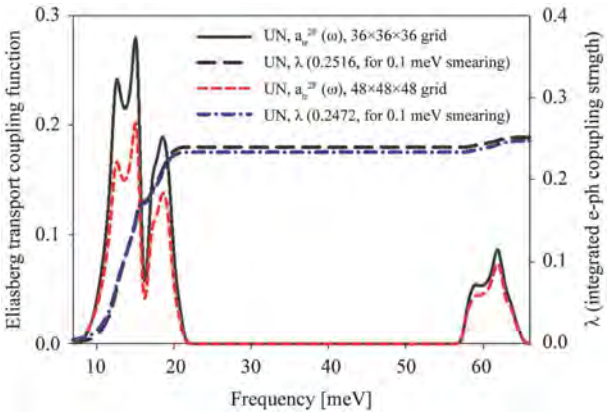

Figure 2. The calculated Eliashberg transport coupling function for UN: $\alpha_{tr}^2 F(\omega)$ together with the integrated electron-phonon strength (λ) as a function of frequency (ω) using the same homogeneous grid for k-point and q-point meshes: 48 × 48 × 48 is shown by dashed red line while for the 36 × 36 × 36 grid a solid black line is used. The respective integrated electron-phonon strengths (right y axis) are indicated by the dashed-dot blue line and dashed long black line, respectively.

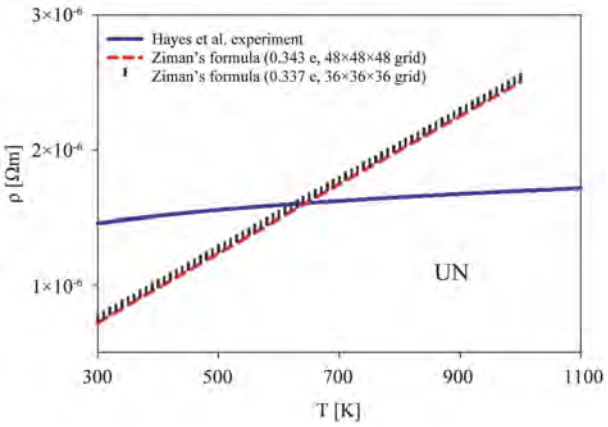

Figure 3. The calculated electrical resistivity of UN using Equation (2) for two grids as indicated and a constant number of mobility electrons (n_{av}): 0.343 e and 0.337, respectively, versus experimental correlations [16] are shown, as indicated.

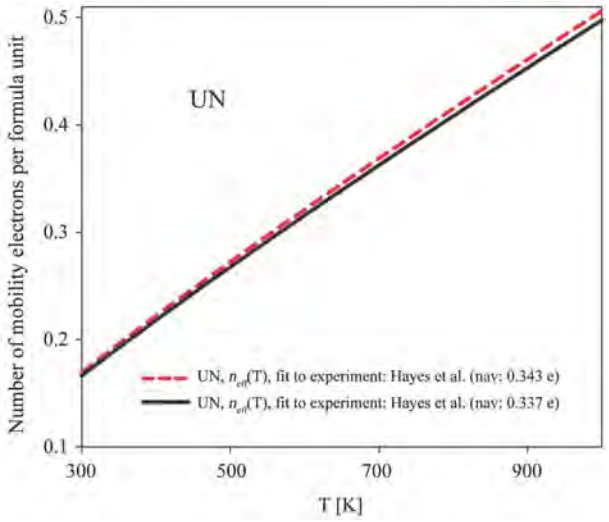

Figure 4. The evaluated temperature dependence of the number of mobility electrons of UN as a function of temperature, which reproduces the experimental resistivity [16] for Ziman's formula (Equation (2)).

3.3. Thermal Conductivity

In **Figure 5**, the electronic thermal conductivity of UN, as calculated from the experimental resistivity of UN [16], via Wiedemann-Franz law [13] Equation (5), is shown by a solid black line.

We also calculated the electronic thermal conductivity of UN, using Equation (5) and the calculated resistivity shown in **Figure 3** for the constant number of mobility electrons (n_{av}): 0.343 e and 0.337 e, respectively. They are indicated by the dashed red line and vertical, black marks, respectively.

It can be noted that the derived thermal conductivity for the assumed constant number of mobility electrons is almost independent of temperature and behaves similarly to that studied by us for Al [6]. Therefore, to reproduce the experimentally observed strong temperature dependence (indicated by black, solid line) of

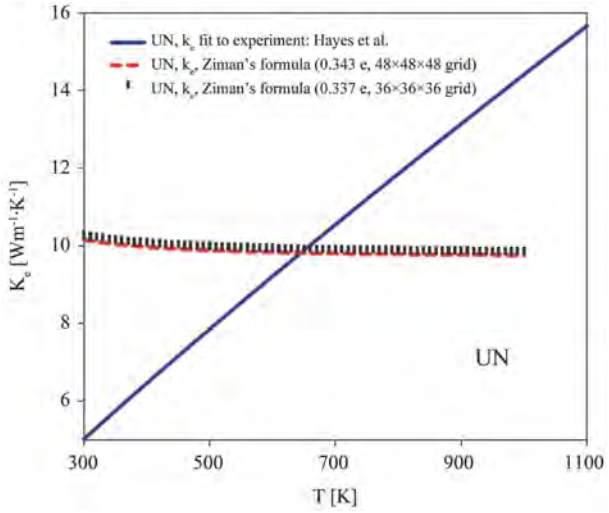

Figure 5. The calculated electronic thermal conductivities of UN, using Equation (5) and the calculated (presented above in **Figure 3**) resistivity for the constant number of mobility electrons (n_{av}): 0.343 e and 0.337 e are indicated by dashed red line and vertical, black marks, respectively. The black solid line represents the electronic thermal conductivity calculated from the experimental resistivity [16] and Equation (5) or alternatively using Equation (2) with the derived number of mobility electrons shown in **Figure 4**.

the electronic thermal conductivity of UN it is necessary to use the number of mobility electrons that increase with the increasing temperature, as presented in **Figure 4**. Further experimental investigation of the number of mobility electrons in UN as a function of temperature is of interest.

4. Summary

We have investigated the electronic heat capacity, thermal conductivity, and resistivity of UN using Quantum Espresso and EPW code. GGA, PBEsol functional, and non-local hybrid functional (B3LYP) were implemented. The calculated electronic heat coefficient was found to be significantly reduced (0.0176 J·mol^{-1}·K^{-2} versus 0.0006 J·mol^{-1}·K^{-2}) when the non-local hybrid functional (B3LYP) was used.

Furthermore, we found that the calculated electrical resistivity using Ziman's formula for metals with the Eliashberg transport coupling function as implemented in EPW code for non-spin-polarized calculations, would only reproduce the experimental results for UN when the derived number of mobility electrons, which increases with increasing temperature, was used. This also applies to the evaluated electronic thermal conductivity, which for any assumed constant number of carriers in UN would be not increasing with the increasing temperature but would remain almost independent of temperature, like Al for example.

Acknowledgements

The authors acknowledge access to high-performance supercomputers at Compute Canada (Calcul Quebec, West Grid and SHARCNET).

Free access to Quantum Espresso, EPW, with technical support is acknowl-

edged. The first author acknowledges a very constructive discussion with Dr. Samuel Poncé.

This work was supported by the Discovery grant from the National Sciences and Engineering Research Council of Canada.

Conflicts of Interest

The authors declare no conflicts of interest regarding the publication of this paper.

References

[1] Pioro, I.L., Khan, M., Hopps, V., *et al.* (2008) *Journal of Power and Energy Systems*, **2**, 874-888. https://doi.org/10.1299/jpes.2.874

[2] OECD (2018) Nuclear Science 2018, NEA No. 7317, ©, State-of-the-Art Report on Light Water Reactor Accident-Tolerant Fuels. 367.

[3] Brown, N.R., Gorton, J.P., Collins, B.S. and Nelson, A.T. (2019) *Nuclear Engineering and Design*, **355**, Article ID: 110317. https://doi.org/10.1016/j.nucengdes.2019.110317

[4] Szpunar, B. and Szpunar, J.A. (2014) *International Journal of Nuclear Energy*, **2014**, Article ID: 178360. https://doi.org/10.1155/2014/178360

[5] Szpunar, B., Ranasinghe, J.I., Malakkal, L. and Szpunar, J.A. (2020) *Journal of Physics and Chemistry of Solids*, **146**, Article ID: 109636. https://doi.org/10.1016/j.jpcs.2020.109636

[6] Ranasinghe, J.I., Szpunar, B., Jossou, E., Malakkal, L. and Szpunar, J.A. (2018) *The ASME Journal of Nuclear Engineering and Radiation Science*, **4**, Article ID: 031020. https://doi.org/10.1115/1.4039886

[7] Szpunar, B. and Szpunar, J.A. (2013) *Journal of Nuclear Materials*, **439**, 243-250. https://doi.org/10.1016/j.jnucmat.2012.10.009

[8] Becke, A.D. (1993) *The Journal of Chemical Physics*, **98**, 5648-5652. https://doi.org/10.1063/1.464913

[9] Giannozzi, P., *et al.* (2009) *Journal of Physics*: *Condensed Matter*, **21**, 395502-395521. https://doi.org/10.1088/0953-8984/21/39/395502

[10] Poncé, S., Margine, E.R., Verdia, C. and Giustinoa, F. (2016) *Computer Physics Communications*, **209**, 116-133. https://doi.org/10.1016/j.cpc.2016.07.028

[11] Perdew, J.P., Ruzsinszky, A., Csonka, G.I., Vydrov, O.A., Scuseria, G.E., Constantin, L.A., Zhou, X. and Burke, K. (2008) *Physical Review Letters*, **100**, Article ID: 136406. (Erratum: Physical Review Letters, 102 (2009) 039902 p. 1)

[12] Baroni, S., Giannozzi, P. and Testa, A. (1987) *Physical Review Letters*, **58**, 1861-1864. https://doi.org/10.1103/PhysRevLett.58.1861

[13] Wiedemann, F.R. (1853) *Annalen der Physik*, **165**, 497-531. (In German) https://doi.org/10.1002/andp.18531650802

[14] Knott, H.W., Lander, G.H., Mueller, M.H. and Vogt, O. (1980) *Physical Review B*, **21**, 4159-4165. https://doi.org/10.1103/PhysRevB.21.4159

[15] Parker, S.S., White, J.T., Hosemann, P. and Nelson, A.T. (2019) *Journal of Nuclear Materials*, **526**, Article ID: 151760. https://doi.org/10.1016/j.jnucmat.2019.151760

[16] Hayes, S.L., Thomas, J.K. and Peddicord, K.L. (1990) *Journal of Nuclear Materials*, **171**, 289-299. https://doi.org/10.1016/0022-3115(90)90376-X

Journal of Modern Physics, 2021, 12, 1418-1434
https://www.scirp.org/journal/jmp
ISSN Online: 2153-120X
ISSN Print: 2153-1196

Direct Relativistic Extension of the Madelung-de-Broglie-Bohm Reformulations of Quantum Mechanics and Quantum Hydrodynamics

Arquimedes Ruiz-Columbié[1], Hira Farooq[2], Luis Grave de Peralta[2,3*]

[1]Wind Energy Program, Texas Tech University, Lubbock, TX, USA
[2]Department of Physics and Astronomy, Texas Tech University, Lubbock, TX, USA
[3]Nano Tech Center, Texas Tech University, Lubbock, TX, USA
Email: *luis.grave-de-peralta@ttu.edu

How to cite this paper: Ruiz-Columbié, A., Farooq, H. and de Peralta, L.G. (2021) Direct Relativistic Extension of the Madelung-de-Broglie-Bohm Reformulations of Quantum Mechanics and Quantum Hydrodynamics. *Journal of Modern Physics*, **12**, 1418-1434.
https://doi.org/10.4236/jmp.2021.1210085

Received: July 18, 2021
Accepted: August 6, 2021
Published: August 9, 2021

Abstract

The basic equations of the non-relativistic quantum mechanics with trajectories and quantum hydrodynamics are extended to the relativistic domain. This is achieved by using a Schrödinger-like equation, which describes a particle with mass and spin-0 and with the correct relativistic relation between its linear momentum and kinetic energy. Some simple but instructive free particle examples are discussed.

Keywords

Quantum Mechanics, Bohm Quantum Mechanics, Quantum Hydrodynamics, Relativistic Quantum Mechanics

1. Introduction

In 1927, shortly after E. Schrödinger published a seminal paper containing his celebrated equation [1], E. Madelung dared an interpretation showing that the Schrödinger equation can be transformed into two equations that mimic the continuity and the Euler equations of hydrodynamics [2]. The Euler equation is a particular case of the Navier-Stokes equation [3]. Such hydrodynamic interpretation is now considered a forebear of the de Broglie-Bohm Pilot Wave Theory [4] [5] [6] [7], although germs of this theory were ventured in 1924 by L. de Broglie [8]. The process followed by Madelung consisted in expressing the Schrödinger solution in an exponential form which led to the two abovemen-

tioned equations, one for the amplitude and another for the phase. Those ideas were later retaken by D. Bohm [4] [5]. Consequently, most of the work related to the Madelung-de-Broglie-Bohm reformulation of quantum mechanics and quantum hydrodynamics applies to particles moving slowly respect to the speed of light. A fully relativistic quantum mechanics with trajectories was recently formulated [9]; however, it lacks the relative simplicity of the non-relativistic formulation. Other general approaches have been reported [10] [11], but we explore in this work an alternative methodology for extending, to the relativistic domain, the known non-relativistic quantum hydrodynamics and quantum theories with trajectories. Our approach, while having some points of contacts with previous reported approach [11], is based in a surprising wave equation which resembles the Schrödinger equation, but describes a particle with mass and spin-0 which moves through a potential V, and has the correct relativistic relation between the linear momentum p and the kinetic energy K [12]-[21]:

$$i\hbar\frac{\partial}{\partial t}\psi(x,t)=-\frac{\hbar^2}{(\gamma_v+1)m}\frac{\partial^2}{\partial x^2}\psi(x,t)+V(x)\psi(x,t). \tag{1}$$

In Equation (1), what we call the (one-dimensional) Grave de Peralta (GP) equation for a quantum particle with mass m, $\hbar$ is the Plank constant (h) divided by 2π, and γ_v is a factor commonly found in special theory of relativity formulas (the Lorentz factor), which depends on the ratio between the squares of the particle's speed (v^2) and the speed of the light in the vacuum (c^2) [22]:

$$\gamma_v=\frac{1}{\sqrt{1-\frac{v^2}{c^2}}}. \tag{2}$$

The basic properties of Equation (1) and its solutions, and detailed discussions of how to solve Equation (1) for some interesting potentials V, can be found in recently published works [12]-[21]. In a nutshell, solving Equation (1) requires simultaneously finding the wavefunction ψ and the square of the particle v^2, which determines the value of γ_v in Equation (2). This may look at first as an unmanageable problem; however, this is not the case in at least several interesting cases [12]-[17]. In general, Equation (1) is nonlinear; this has been discussed before [12] [16]. Nevertheless, due the formal similitude with the Schrödinger equation, Equation (1) is a useful and tractable equation. It is worth noting that Equation (1) can be rewritten in the following way [12] [14] [16]:

$$i\hbar\frac{\partial}{\partial t}\psi=\hat{H}\psi(x,t),\ \ \hat{H}=\hat{K}+V,\ \ \hat{K}=\frac{\hat{p}^2}{(\gamma_v+1)m},\ \ \hat{p}=-i\hbar\frac{\partial}{\partial x}. \tag{3}$$

The operator K corresponds to the (approximated) relativistic kinetic energy of the particle, thus [12] [14] [16] [19] [20]:

$$\hat{K}=\frac{\hat{p}^2}{(\gamma_v+1)m}\approx\sqrt{\hat{p}^2c^2+m^2c^4}-mc^2. \tag{4}$$

This means that Equation (1) is well-defined, but it is advantageous to write

the operator K as in Equation (1), because this results in an equation formally like the Schrödinger equation, which can then be exactly solved following similar procedures than the ones required for solving the Schrödinger equation [12]-[17] [19] [20]. It is also the striking similarity between Equation (1) and the Schrödinger equation what allowed us to extend, to the relativistic domain, the basic equations of the Madelung-de-Broglie-Bohm reformulation of quantum mechanics and quantum hydrodynamics [18]. It is worth noting that previous reports discussed the existing relationship between Equation (1) and the Klein-Gordon and Dirac equations for a free particle [12] [16] [19] [20]. From a pragmatic point of view, a Schrödinger-like equation appears to be very useful since Schrödinger-like solutions may apply. Investigating exact solutions using such an analogy might make more tractable some relativistic problems. In this work, we applied a methodology that extends already studied applications of the Schrödinger equation to the relativistic domain. This approach might become beneficial. From an epistemological point of view, the Schrödinger-like approach explored here should be considered as a "mathematical hypothesis" and the practical results must be examined as to its final test. We will assume in this work this procedural interpretation of Equation (1). Nevertheless, for self-reliance purpose, a summary of the fundamentals of the GP equation is presented in the Appendix. We hope that the scientific community, which is currently working on non-relativistic quantum mechanics theories with trajectories and quantum hydrodynamics, will recognize the simplicity of the theory presented in this work, and its potential for practical applications in relativistic quantum simulations. The rest of this work is organized in the following way. In the next Section, for the first time, a relativistic extension of the de Broglie-Bohm quantum mechanics is obtained from the relativistic but Schrödinger-like GP equation. Then, a relativistic extension of the Madelung quantum electrodynamics is presented. This is followed by five free particle examples in increasing order of complexity. Finally, the conclusions of this work are given in the Conclusions.

2. Madelung-Bohm-Like Reformulation of the GP Equation

The three-dimensional (3D) GP equation for a particle moving at relativistic speeds in a potential V is given by the following expression [14] [15] [16]:

$$i\hbar\frac{\partial}{\partial t}\psi = -\frac{\hbar^2}{\left(\gamma_v+1\right)m}\nabla^2\psi + V\psi. \tag{5}$$

In general, the wavefunction (ψ), the potential, and γ_v all depend on the three spatial coordinates and the time. Due to the formal similarity between Equation (5) and the Schrödinger equation, a Madelung-Bohm-like extension of Equation (5) can be done following the same procedure commonly used for reformulating the Schrödinger equation [2] [4] [5] [6] [7]. First, we look for a solution of Equation (5) of the following form:

$$\psi\left(\boldsymbol{r},t\right) = R\left(\boldsymbol{r},t\right)\mathrm{e}^{iS\left(\boldsymbol{r},t\right)/\hbar}. \tag{6}$$

In Equation (6), R and S are the amplitude and phase fields, respectively [2] [4] [7]. Inserting Equation (6) in Equation (5) and following step by step Ref. [6], we can obtain the following equations, which extend to the relativistic domain the basic equations of the Madelung-de Broglie-Bohm quantum mechanics [6]:

$$\frac{\partial}{\partial t}S+\frac{\nabla S^2}{\left(\gamma_v+1\right)m}+\left[V+Q\right]=0,\ \ Q=-\frac{\hbar^2}{\left(\gamma_v+1\right)m}\frac{\nabla^2 R}{R}. \tag{7}$$

$$\frac{\partial}{\partial t}R^2+\frac{2}{\left(\gamma_v+1\right)}\nabla\cdot\left[\gamma_v R^2\left(\frac{\nabla S}{\gamma_v m}\right)\right]=0. \tag{8}$$

In Equation (7), Q is the quantum potential [6]. Clearly, $\gamma_v\approx 1$ when $v^2\ll c^2$; therefore, as it should be expected when the particle moves at low speeds, Equations (7) and (8) coincide to the well-known equations of the Madelung-de Broglie-Bohm quantum mechanics [6]. At relativistic velocities, the velocity field should now be defined such that the relation between the velocity and the linear momentum (∇S) is the correct relativistic relationship [22]:

$$\gamma_v\boldsymbol{v}=\frac{\nabla S}{m}\Rightarrow\boldsymbol{v}=\frac{1}{\gamma_v}\frac{\nabla S}{m}. \tag{9}$$

Thus, the expression between parentheses in Equation (8) is the velocity field given by Equation (9). Again, when $v^2\ll c^2$, Equation (9) coincides with the non-relativistic equation [6]. However, in general [11]:

$$\boldsymbol{v}=\frac{c}{\sqrt{\left(mc\right)^2+\nabla S^2}}\nabla S\Rightarrow\gamma_v=\frac{\sqrt{\left(mc\right)^2+\nabla S^2}}{mc}. \tag{10}$$

Therefore, when ψ is known, Equation (10) determines the velocity field and γ_v. The direction of the velocity is then perpendicular to the surfaces of constant phase (S = constant). Bohm introduced a particle's trajectory as the solution of the following differential equation and initial conditions [4] [5] [6] [7]:

$$\frac{\partial}{\partial t}\boldsymbol{r}_p\left(t\right)=\boldsymbol{v}\left(\boldsymbol{r}=\boldsymbol{r}_p\left(t\right),t\right),\ \ \boldsymbol{r}_p\left(t=0\right)=\boldsymbol{r}_o. \tag{11}$$

Therefore, different trajectories correspond to different initial positions of the particle. The direction of the particle's velocity is always tangent to the particle's trajectory. The particle's velocity is given by the following equation:

$$\boldsymbol{v}_p\left(t\right)=\frac{\partial}{\partial t}\boldsymbol{r}_p\left(t\right). \tag{12}$$

Equations (11) and (12) related the velocity of the Bohmian particle with the velocity of the Madelung's fluid.

3. Relativistic Quantum Hydrodynamics

Madelung did not introduce particle trajectories in his reformulation of the Schrödinger equation [2]. This was done later by Bohm [4] [5]. Madelung interpreted Equations (7) and (8) as describing a fluid with density $\rho'=m\rho$ such that:

$$\rho(\mathbf{r},t) = R^2(\mathbf{r},t). \tag{13}$$

Then using Equation (9) with $\gamma_v = 1$ allowed him to directly rewrite Equation (8) with $\gamma_v = 1$ as a continuity equation [2] [6] [7]. Proceeding in a similar way, we obtained the following extension of the Madelung's continuity equation to the relativistic domain:

$$\frac{\partial}{\partial t}\rho + \frac{2}{(\gamma_v + 1)}\nabla\cdot\left[\rho(\gamma_v \mathbf{v})\right] = 0. \tag{14}$$

As it should be expected, at non-relativistic speeds, when $\gamma_v \approx 1$ because $v^2 \ll c^2$, Equation (14) coincides with the Madelung's continuity equation [2] [6] [7]. Equation (14) was obtained from Equation (8) by identifying $m\rho$ with the density of a fluid extending through space. Likewise, as it was done by Madelung [2] [6] [7], by identifying the velocity field of this fluid with the velocity field given by Equation (9), we can obtain from Equation (7) the following equation:

$$\frac{\partial}{\partial t}(\gamma_v \mathbf{v}) + \nabla\left[\frac{\gamma_v^2}{(\gamma_v + 1)}\mathbf{v}\cdot\mathbf{v}\right] + \frac{\nabla(V+Q)}{m} = 0,\ \ Q = -\frac{\hbar^2}{(\gamma_v+1)m}\frac{\nabla^2\sqrt{\rho}}{\sqrt{\rho}}. \tag{15}$$

If v and thus γ_v only depend on time but not on position, Equation (15) can be simplified in the following Euler-like equation:

$$\frac{\partial}{\partial t}(\gamma_v \mathbf{v}) + \frac{2}{(\gamma_v + 1)}\left[(\gamma_v \mathbf{v})\cdot\nabla(\gamma_v \mathbf{v})\right] = -\frac{\nabla(V+Q)}{m}. \tag{16}$$

As it should be expected, at non-relativistic speeds, when $\gamma_v \approx 1$, Equation (16) coincides with the Euler-like equation obtained by Madelung [2] [6] [7].

4. Plane Waves

The fluid dynamic of a classical ideal fluid flow supposes the fluid is non-viscous; the flow is steady, *i.e.*, the velocity is time independent; the fluid is incompressible, *i.e.*, the liquid density is constant; and assumes that the flow is irrotational [23]. The dynamic of an ideal fluid with density ρ', which is flowing close to the Earth's surface under the influence of the Earth gravitational potential, $U_g/m = gH$, where g is the gravitational acceleration and H is the high respect to the ocean's surface, it is given by the Bernoulli equation [23]:

$$\frac{1}{2}\rho' v^2 + \rho'\frac{U_g}{m} + P = \text{constant}. \tag{17}$$

In Equation (17), P is the pressure inside of the liquid. While Equation (17) is purely classical and has no connection with Madelung fluids, it is instructive to compare the Madelung liquid, associate to a free particle "guided" by a plane wave, to a classical ideal liquid under non-gravity conditions, which dynamics is described by the Bernoulli equation with $U_g = 0$. A simple solution of the GP equation for a free particle ($V = 0$) is the plane wave, normalized in a large cube of side L, given by the following equation [12] [14]:

$$\psi = \frac{1}{\sqrt{L^3}} \mathrm{e}^{\frac{i}{\hbar}\left(\boldsymbol{p}\cdot\boldsymbol{r} - \frac{p^2}{(\gamma_v+1)m}t\right)}. \tag{18}$$

In Equation (18), p is the magnitude of the particle's linear momentum, which can take any positive real value. Evaluating Equation (18) for $\gamma_v = 1$ gives the correct normalized plane wave when the free particle is traveling at non-relativistic speeds [6]. The surfaces of constant phase corresponding to Equation (18) are planes perpendicular to the particle's linear momentum. Note that for a given value of p, the value of γ_v get univocally determined by the equality of the following formulas for the relativistic kinetic energy [12] [14] [16]:

$$K = (\gamma_v - 1)mc^2 = \frac{p^2}{(\gamma_v+1)m} \Rightarrow \gamma_v = \frac{\sqrt{p^2 + m^2c^2}}{mc}. \tag{19}$$

Using Equations (6), (13) and (18), we can obtain:

$$R = \sqrt{\rho} = L^{-\frac{3}{2}} \Rightarrow Q \equiv 0,\ S(\boldsymbol{r},t) = \left(\boldsymbol{p}\cdot\boldsymbol{r} - \frac{p^2}{(\gamma_v+1)m}t\right). \tag{20}$$

From Equation (20) follows that the Madelung fluid associated to a free particle guided by a plane wave has constant density $\rho' = m\rho$; therefore, it is incompressible. It is also no viscous because the total force acting on it is $F = -\nabla(V+Q)/m = 0$. The velocity of this fluid and the corresponding value of γ_v can be obtained using Equations (10) and (20):

$$\boldsymbol{v} = \frac{c}{\sqrt{(mc)^2 + p^2}}\boldsymbol{p},\ \ \gamma_v = \frac{\sqrt{(mc)^2 + p^2}}{mc}. \tag{21}$$

The value of γ_v given by Equations (19) and (21) are identical in this case, but as it will be shown in the next Section, this is not a general feature of the theory. The maximum possible value of the fluid speed, $v \approx c$, occurs when $\nabla S = p \gg mc$. This corresponds to $\gamma_v \gg 1$. The fluid velocity is constant; thus, this Madelung fluid is irrotational. Equation (16) reduces now to:

$$\nabla\left[\frac{(\gamma_v v)^2}{(\gamma_v+1)}\right] = \frac{\nabla\left[\frac{p^2}{(\gamma_v+1)m}\right]}{m} = 0 \Rightarrow K = \text{constant}. \tag{22}$$

Evidently, Equations (21) and (22) also gives the correct results at the non-relativistic limit. A comparison between Equation (22), evaluated for $\gamma_v = 1$, and the Bernoulli equation (Equation (17) with $U_g = 0$) shows that there is not pressure in the Madelung fluid associated to a free quantum particle guided by a plane wave. From Equations (11), (12), and (21) follow that the Bohmian paths of a free quantum particle associated to a plane wave are given by the following equation [6] [11]:

$$\boldsymbol{r}_p(t) = \boldsymbol{r}_o + \frac{c}{\sqrt{(mc)^2 + p^2}}\boldsymbol{p}t. \tag{23}$$

Evidently, Equation (23) also gives the correct result for a particle moving at non-relativistic speeds. In Equation (23), the initial position of the particle lies everywhere in space. Like for free classical particles moving at non-relativistic speeds, these Bohmian paths are therefore uniform, rectilinear, and perpendicular to the planes of constant phase of the wave. This is because in this case the quantum potential is null, thus $\nabla Q = 0$ [6]. Also note that Equations (14) to (16) are fulfilled because both ρ and v are constant.

5. Standing Waves

A simple but interesting case, where Q is not null, occurs when a free quantum particle is in the superposition state formed by two plane waves, which are both solutions of Equation (5) with $V = 0$ but are traveling in opposite directions along the x-axis with the same value of p:

$$\begin{aligned} &\psi(x,t) = \frac{1}{\sqrt{2L^3}}\left[\mathrm{e}^{i(kx-w_k t)} + \mathrm{e}^{i(-kx-w_k t)}\right] = \frac{2}{\sqrt{2L^3}}\cos(kx)\mathrm{e}^{-iw_k t}, \\ &k = \frac{p}{\hbar},\ w_k = \frac{p^2}{(\gamma_v+1)m\hbar}. \end{aligned} \tag{24}$$

The speeds of the Madelung fluids associated to either one of these two plane waves are the same and given by Equation (23), but the corresponding velocities point to opposite directions; therefore, γ_v is also the same for each wave when individually considered. Consequently, the standing wave given by Equation (24) is also a solution of Equation (5) with $V = 0$, and with the same value of γ_v than for each of the plane waves components. For the standing wave:

$$\begin{aligned} &R(x) = \sqrt{\rho(x)} = \frac{2}{\sqrt{2L^3}}\cos(kx) \\ &\Rightarrow Q = -\frac{\hbar^2}{(\gamma_v+1)m}\frac{\frac{\mathrm{d}^2}{\mathrm{d}x^2}R(x)}{R(x)} = \frac{\hbar^2k^2}{(\gamma_v+1)m} = \frac{p^2}{(\gamma_v+1)m}, \\ &S(t) = -\frac{p^2}{(\gamma_v+1)m}t. \end{aligned} \tag{25}$$

From Equations (24) and (25) follows that the period of the $\cos^2(kx)$ density distribution is inverse proportional to p. The Madelung fluid associated to a free particle guided by a standing wave does not have a constant density; therefore, it is compressible, thus, it does not behave like a classical ideal fluid flow. The wavelength of the standing wave, λ, is inverse proportional to p. From Equation (25) also follows that $\nabla S = 0$; therefore, from Equation (10) follows that the velocity of this fluid is zero and $\gamma_v = 1$, which is different than the γ_v value corresponding to each superposing plane wave. Consequently, the Bohmian particle associated to a standing wave is at rest. In Equation (25), Q is equal to the relativistic kinetic energy of the free particle, which is constant; therefore, $\nabla S = 0$, thus this Madelung fluid is no viscous. Equations (14) to (16) are now fulfilled because ρ does not depend on time and $v = 0$. A comparison of the results obtained in this exam-

ple for a standing wave, to the results obtained in the previous Section for a plane wave, illustrates the well-known nonlocality properties of the theories resulting from the Madelung-de-Broglie-Bohm reformulation of the Schrödinger equation. The superposition of plane waves, which are solutions of the same GP equation for a free particle, modifies the properties of the corresponding Madelung fluid, and then the Bohmian trajectories of the guided particle.

6. Quasi-Standing Waves

In this Section we will consider a wavefunction of Equation (5) with $V = 0$, which is a slightly variation of Equation (24):

$$\begin{aligned} &\psi(x,t) = \frac{1}{\sqrt{2L^3}}\left[\mathrm{e}^{i(kx-w_k t)} + \mathrm{e}^{i(-k'x-w_{k'}t)}\right], \\ &k' = \frac{p+\Delta p}{\hbar},\ w_{k'} = \frac{(p+\Delta p)^2}{(\gamma_v+1)m\hbar},\ \Delta p \ll p. \end{aligned} \tag{26}$$

In Equation (26), k and w_k are given by Equation (24). Consequently, the first term of the wavefunction in Equation (26) is a solution of Equation (5) with $V = 0$. However, the second term is not because there is, in the denominator of $w_{k'}$, the same value of γ_v than for w_k. Nevertheless, from Equation (19) follows that the value of γ_v corresponding to $(p + \Delta p)$ is approximately equal to the value corresponding to p in two situations. First, $\gamma_v \approx 1$ at the non-relativistic limit when $p \ll mc$. Second, $\gamma_v \approx p/mc$ at the ultra-relativistic limit $p \gg mc$; therefore, $(p+\Delta p)/mc \approx p/mc$ when $\Delta p \ll mc$. Consequently, at these two limits ψ given by Equation (26) is approximately a solution of Equation (5) with $V = 0$. We will call here, a quasi-standing wave, to the wavefunction given by Equation (26) at these two limits. After some straightforward algebraic steps for transforming Equation (26) in a form like Equation (6), we obtained the following results:

$$\nabla S = \frac{-\Delta p}{2} \Rightarrow v = \frac{-c\Delta p}{\sqrt{4m^2c^2 + (\Delta p)^2}} \Rightarrow \gamma_v = \frac{1}{\sqrt{1 - \dfrac{(\Delta p)^2}{4m^2c^2 + (\Delta p)^2}}}. \tag{27}$$

And:

$$\begin{aligned} &\rho(x,t) = \frac{2}{L^3}\cos^2\left[k_b(x - v_b t)\right],\ k_b = \frac{\Delta p}{2\hbar},\ v_b = 2\frac{\frac{1}{2}\left[p - (p+\Delta p)\right]}{(\gamma_v+1)m} \\ &\Rightarrow Q = \frac{(\Delta p)^2}{4(\gamma_v+1)m}. \end{aligned} \tag{28}$$

In Equation (27), ΔS points to the negative direction of the axis x. As it should be expected, Equations (27) and (28) reduces to Equations (25) when $\Delta p = 0$. The density of the Madelung fluid associated to a free particle guided by a quasi-standing wave resembles a "standing wave" that is drifting without dispersion, in the direction of the plane wave associated with the linear momentum $p + \Delta p$, with speed $v_b \approx v \approx -\Delta p/2m$ when $\Delta p \ll mc$. It can be easily checked out that

the quasi-standing wave given by Equation (26) satisfies Equation (5) with $V = 0$, and with γ_v given by Equation (27). From Equations (27) and (28) also follows that Equations (7), (8), and (14) to (16) are satisfied. Note that $\gamma_v \approx 1$ for every p when $\Delta p \ll mc$; consequently, the Bohmian particle associated to a quasi-standing wave moves like a classical particle even at the ultra-relativistic limit.

7. Beats

In this Section we will consider another wavefunction of Equation (5) with $V = 0$, which can be obtained from Equation (26) after substituting $-k'$ by $+k'$. Equation (26) corresponds to the superposition of two plane waves with slightly different values of p traveling in opposite directions. Here we will consider what happens when the two waves travel in the same direction. In this case, we obtained the following results:

$$\nabla S = p + \frac{\Delta p}{2} \Rightarrow v = \frac{c\left(2p + \Delta p\right)}{\sqrt{4m^2c^2 + \left(2p + \Delta p\right)^2}} \Rightarrow \gamma_v = \frac{1}{2\sqrt{-\dfrac{m^2c^2}{4m^2c^2 + \left(2p + \Delta p\right)^2}}}. \quad (29)$$

And:

$$\rho\left(x,t\right) = \frac{2}{L^3}\cos^2\left[k_b\left(x - v_b t\right)\right],\ k_b = \frac{\Delta p}{2\hbar},\ v_b = 2\frac{\frac{1}{2}\left[p + \left(p + \Delta p\right)\right]}{\left(\gamma_v + 1\right)m}$$
$$\Rightarrow Q = \frac{\left(\Delta p\right)^2}{4\left(\gamma_v + 1\right)m}. \quad (30)$$

In Equation (29), ΔS points to the positive direction of the axis x. Note that k_b does not depend on p but is proportional to Δp. Therefore, as it should be expected, Equations (29) and (30) reduce when $\Delta p = 0$ to Equations (20) and (21), which correspond to the first example of a single plane wave discussed in Section 4. The Madelung fluid now flows without dispersion in the same direction than the plane waves, and at the average speed of both waves. The factor of 2 at the front of Equation (30) for v_b is because a $\cos^2\left(ax - bt\right)$ shaped wave travels at twice the speed than a $\cos\left(ax - bt\right)$ shaped one. The corresponding Bohmian paths are uniform and rectilinear at both non-relativistic and relativistic values of v_b. This result suggests the following very interesting possibility: a free ultra-relativistic quantum particle could be associated to a Gaussian pulse, which is formed by a superposition of plane waves traveling in the same direction with similar values of p, and thus could be a solution of Equation (5) with $V = 0$. Such a Gaussian pulse would travel with no dispersion at the average relativistic speed of all the plane waves forming the Gaussian pulse.

8. Ultra-Relativistic Gaussian Wave-Packets

Gaussian wave-packets are often considered the quantum entity that closest resemble a classical particle [24] [25]. A Gaussian pulse describes a quantum particle for which the uncertainty relation between its position (Δx) and linear mo-

mentum (Δp) has its minimum value $\Delta x \Delta p = 1/2\ \hbar$. Non-relativistic Gaussian wave-packets are formed by a superposition of plane waves which are solutions of the Schrödinger equation for a free particle [24]. There is a non-linear relationship between the angular frequency (w) and the wavenumber (k) of the plane waves which are solution of the Schrödinger equation [24] [26]:

$$w = \frac{K}{\hbar} = \frac{\frac{p^2}{2m}}{\hbar} = \frac{\hbar}{2m}k^2. \tag{31}$$

The non-lineal dispersion of the Schrödinger equation determines that the phase velocities $v_{ph} = w/k$ of different plane waves are different. Consequently, Gaussian wave-packets which are solution of the Schrödinger equation deform when propagate [24]. This differentiates a Gaussian pulse associated to a quantum particle from a free classical particle that travels without deforming. Relativistic Gaussian pulses corresponding to a free particle with mass and spin-0 can be formed by superposing plane waves, which are solutions of the Klein-Gordon equation [25] [27] [28]. The dispersion of the Klein-Gordon equation also is non-lineal [27] [28]:

$$w = \frac{E}{\hbar} = \frac{\pm\sqrt{p^2c^2 + m^2c^4}}{\hbar} = \frac{\pm\sqrt{\hbar^2k^2c^2 + m^2c^4}}{\hbar}. \tag{32}$$

The non-linearity of Equation (32) determines that Gaussian pulses which are solutions of the Klein-Gordon equation also deforms when propagate. Moreover, Equation (32) admits solutions with negative kinetic energy values, which results in additional difficulties when describing the propagation of these Gaussian wave-packets [25] [27] [28]. These difficulties disappear when using Equation (5) with $V = 0$ for describing a free particle. This is because Equation (4) implies the following dispersion relation:

$$w = \frac{K}{\hbar} = \frac{+\sqrt{p^2c^2 + m^2c^4} - mc^2}{\hbar} = \frac{mc^2\left[\sqrt{\left(\frac{\hbar k}{mc}\right)^2 + 1} - 1\right]}{\hbar}. \tag{33}$$

As it should be expected, in the non-relativistic limit $p = \hbar k \ll mc$, Equation (31) can be obtained from Equation (33) by approximating the square root in Equation (33) by the first two terms of the corresponding series in powers of k/mc. Moreover, in the ultra-relativistic limit $k \gg mc$, Equation (33) becomes:

$$w = \frac{K}{\hbar} \approx ck \Rightarrow v_{ph} = \frac{w}{k} \approx c. \tag{34}$$

Therefore, one should expect that all the ultra-relativistic plane waves which are solutions of Equation (5) with $V = 0$ propagates with the same phase velocity and thus, the ultra-relativistic Gaussian pulses formed by a superposition of these plane waves should propagate without deformation. This means that ultra-relativistic Gaussian wave-packets which are solutions of Equation (5) with $V = 0$ behave more like free classical particles than the non-relativistic ones. In the ul-

tra-relativistic limit, Equation (4) can be approximate by:

$$\hat{K} \approx \hat{p}c = -i\hbar c\nabla. \tag{35}$$

Consequently, the ultra-relativistic limit of Equation (5) with $V = 0$ is:

$$i\hbar\frac{\partial}{\partial t}\psi = -i\hbar c\nabla\psi. \tag{36}$$

A plane wave solution of Equation (36), which is a kind of Weyl equation for spin-0 particles, normalized in a large region of length L and traveling along the x-axis, is given by the following expression:

$$\psi(x,t) = \frac{1}{\sqrt{L}}\mathrm{e}^{i(kx-wt)} = \frac{1}{\sqrt{L}}\mathrm{e}^{\frac{i}{\hbar}(px-Kt)} = \frac{1}{\sqrt{L}}\mathrm{e}^{ik(x-ct)}. \tag{37}$$

The phase velocity of this plane wave is for any value of k, $v_{ph} = c$. Equation (36) is lineal, thus any wave-packet formed by a superposition of plane waves given by Equation (37) is a solution of Equation (36) and propagates without dispersion (deformation). Specifically, this occurs for the ultra-relativistic Gaussian pulse:

$$\psi(x,t) = \frac{1}{\sqrt{2\pi}}\int_{-\infty}^{+\infty}\varphi(k)\mathrm{e}^{ik(x-ct)}\mathrm{d}k,\ \ \varphi(k) \approx 0 \ \text{ when } |\hbar k| < mc. \tag{38}$$

In Equation (38):

$$\varphi(k) = \frac{1}{\sqrt{2\pi}}\int_{-\infty}^{+\infty}\psi(x,t=0)\mathrm{e}^{-ikx}\mathrm{d}x = \sqrt{\frac{\sigma}{\sqrt{\pi}}}\mathrm{e}^{-\frac{\sigma^2}{2}(k-\langle k\rangle)^2}. \tag{39}$$

For obtaining Equation (39), we assumed $\psi(x,t=0)$ is a Gaussian wave-packet that at $t = 0$ is peaked at $x = 0$, and it is moving along the x-axis with average momentum $\langle p\rangle = \hbar\langle k\rangle$:

$$\psi(x,t=0) = \left[\frac{1}{\sqrt{\sigma\sqrt{\pi}}}\mathrm{e}^{-\frac{1}{2\sigma^2}x^2}\right]\mathrm{e}^{i\langle k\rangle x}. \tag{40}$$

Using Equations (39) and (40), we found the expression corresponding to an ultra-relativistic Gaussian wave-packet that propagates along the x-axis at speed c without deformation:

$$\psi(x,t) = \frac{1}{\sqrt{\sigma\sqrt{\pi}}}\mathrm{e}^{-\frac{1}{2\sigma^2}(x-ct)^2}\mathrm{e}^{i\langle k\rangle(x-ct)}. \tag{41}$$

Therefore, for ultra-relativistic Gaussian pulses:

$$R(x,t) = \frac{1}{\sqrt{\sigma\sqrt{\pi}}}\mathrm{e}^{-\frac{1}{2\sigma^2}(x-ct)^2},\ \ S(x,t) = \hbar\langle k\rangle(x-ct). \tag{42}$$

From Equation (42), we can obtain the density of the Madelung's quantum fluid associated to an ultra-relativistic Gaussian pulse:

$$\rho(x,t) = R^2(x,t) = \frac{1}{\sigma\sqrt{\pi}}\mathrm{e}^{-\frac{1}{\sigma^2}(x-ct)^2}. \tag{43}$$

This means ultra-relativistic Gaussian wave-packets are density pulses in the

Madelung's quantum hydrodynamic description. Equation (43) describes a Gaussian density pulse propagating along the x-axis at speed c, and which peak is at any given time at $x = ct$. There is a characteristics quantum potential (Q) in the Madelung-de Broglie-Bohm reinterpretation of the Schrödinger equation and its relativistic extension, which can be evaluated using Equations (42) and (43):

$$\begin{aligned} Q(x,t) &= -\frac{\hbar^2}{(\gamma_v+1)m}\frac{\nabla^2 R}{R} = -\frac{\hbar^2}{(\gamma_v+1)m}\frac{\nabla^2\sqrt{\rho}}{\sqrt{\rho}} \\ &\approx -\frac{4\hbar^2}{\sigma^4 m}\frac{mc}{\langle p\rangle}(x-ct)^2 + \frac{2\hbar^2}{\sigma^2 m}\frac{mc}{\langle p\rangle}. \end{aligned} \tag{44}$$

The corresponding quantum force (F_Q) acting over the ultra-relativistic Gaussian wave-packet is:

$$F_Q(x,t) = -\frac{\partial Q(x,t)}{\partial x} = \frac{8\hbar^2}{\sigma^4}\frac{mc}{\langle p\rangle}(x-ct). \tag{45}$$

The quantum force is always null at the pulse's pick. The Gaussian density pulse is produced by the action of pairs of compressing quantum forces, which are equidistance from the peak and have the same magnitude but opposite directions. Note that the net quantum force over the Gaussian pulse is null, which corresponds with the propagation of the pulse with constant velocity. Particles have trajectories in the de Broglie-Bohm reinterpretation of the Schrödinger equation. The velocity of a particle associated to an ultra-relativistic Gaussian pulse can be computed from the phase field $S(x, t)$ using the following equation:

$$v = \frac{c}{\sqrt{(mc)^2 + \left(\frac{\partial S}{\partial x}\right)^2}}\frac{\partial S}{\partial x} \approx c. \tag{46}$$

I.e., a particle associated to an ultra-relativistic Gaussian pulse describes the same trajectory than the peak of the pulse.

9. Conclusion

Madelung, de Broglie, and Bohm reformulated the Schrödinger equation. In this way, they founded the non-relativistic quantum hydrodynamics and quantum mechanics with trajectories. Following a similar procedure, we reformulated the GP equation. In this way, we extended quantum hydrodynamics and quantum mechanics with trajectories to the relativistic domain. As it should be expected, we showed that at non-relativistic energies, the resulting equations coincide with the well-known non-relativistic equations. As a proof-of-concept demonstration of the potential practical value of the formulated theory, we discussed some simple but instructive free particle problems.

Conflicts of Interest

The authors declare no conflicts of interest regarding the publication of this paper.

References

[1] Schrodinger, E. (1926) *Annals of Physics*, **79**, 361-376, 489-527. https://doi.org/10.1002/andp.19263840602

[2] Madelung, E. and Zeit, F. (1927) *Zeitschrift für Physik*, **40**, 322-326. https://doi.org/10.1007/BF01400372

[3] Landau, L.D. and Lifshitz, E.M. (1987) Fluid Mechanics. Pergamon Press, Oxford.

[4] Bohm, D. (1952) *Physical Review*, **85**, 166-179. https://doi.org/10.1103/PhysRev.85.166

[5] Bohm, D. (1953) *Physical Review*, **89**, 319. https://doi.org/10.1103/PhysRev.89.319.2

[6] Holland, P.R. (1993) The Quantum Theory of Motion: An Account of the de Broglie-Bohm Causal Interpretation of Quantum Mechanics. Cambridge University Press, Cambridge. https://doi.org/10.1017/CBO9780511622687

[7] Wyatt, R.E. (2005) Quantum Dynamics with Trajectories: Introduction to Quantum Hydrodynamics. Springer, New York.

[8] de Broglie, L. (1924) *Philosophical Magazine*, **47**, 446-458. https://doi.org/10.1080/14786442408634378

[9] Poirier, B. (2016) *Journal of Physics*, **701**, Article ID: 012013. https://doi.org/10.1088/1742-6596/701/1/012013

[10] Struyve, W. and Valentine, A. (2008) *Journal of Physics A*: *Mathematical and Theoretical*, **42**, Article ID: 035301. https://doi.org/10.1088/1751-8113/42/3/035301

[11] Khodagholizadeh, J., Kazemi, J. and Babazadeh, A. (2014) Relativistic Bohmian Mechanics. https://arxiv.org/abs/1405.3822v2

[12] Grave de Peralta, L. (2020) *Journal of Modern Physics*, **11**, 196-213. https://doi.org/10.4236/jmp.2020.112012

[13] Grave de Peralta, L. (2020) *Journal of Modern Physics*, **11**, 788-802. https://doi.org/10.4236/jmp.2020.116051

[14] Grave de Peralta, L. (2020) *Results in Physics*, **18**, Article ID: 103318. https://doi.org/10.1016/j.rinp.2020.103318

[15] Grave de Peralta, L. (2020) *Scientific Reports*, **10**, Article No. 14925. https://doi.org/10.1038/s41598-020-71505-w

[16] Grave de Peralta, L. (2020) *European Journal of Physics*, **41**, Article ID: 065404. https://doi.org/10.1088/1361-6404/aba7dc

[17] Grave de Peralta, L., Poirier, B. and Poveda, L.A. (2021) Direct Relativistic Extension of the Schrödinger Equation. *APS March Meeting*, 15-19 March 2021, U71-00233.

[18] Columbié, R. and Grave de Peralta, L. (2021) Direct Relativistic Extension of the Madelung-de Broglie-Bohm Theories. *APS March Meeting*, 15-19 March 2021, U71-00234.

[19] Grave de Peralta, L. (2021) *European Journal of Physics*, **42**, Article ID: 055404. https://doi.org/10.1088/1361-6404/ac0ecc

[20] Grave de Peralta, L. and Farooq, H. (2021) *Journal of Modern Physics*, **12**, 1145-1159. https://doi.org/10.4236/jmp.2021.128068

[21] Poveda, L.A., Ruiz Columbié, A. and Grave de Peralta, L. (2021) Relativistic Corrections to the Diósi-Penrose Model. http://arxiv.org/abs/2103.00994

[22] Christodeulides, C. (2016) The Special Theory of Relativity. Springer, New York.

[23] Walker, J., Halliday, D. and Resnick, R. (2014) Fundamentals of Physics. 10th Edition, Wiley, Hoboken.

[24] Powell, J.L. and Crasemann, B. (1961) Quantum Mechanics. Addison-Wesley, Boston.

[25] Tsai, H.M. and Poirier, B. (2015) *Journal of Physics*: *Conference Series*, **701**, Article ID: 012013. https://doi.org/10.1088/1742-6596/701/1/012013

[26] Griffiths, D.J. (1995) Introduction to Quantum Mechanics. Prentice Hall, Englewood Cliffs.

[27] Strange, P. (1998) Relativistic Quantum Mechanics: With Applications in Condensed Matter and Atomic Physics. Cambridge University Press, New York. https://doi.org/10.1017/CBO9780511622755

[28] Greiner, W. (1990) Relativistic Quantum Mechanics: Wave Equations. Spring-Verlag, New York.

[29] Alberto, P., Fiolhais, C. and Gil, V.M.S. (1996) *European Journal of Physics*, **17**, 19. https://doi.org/10.1088/0143-0807/17/1/004

Appendix

In Special Theory of Relativity, the relevant Lorentz invariant magnitude is the four-component momentum given by the following equation [22] [27] [28]:

$$P^{\mu} = \left(\frac{E}{c}, p_x, p_y, p_z \right). \tag{A1}$$

The magnitude of the four-component vector is the relativistic invariant mc. Therefore, a relativistic quantum theory for a free spin-0 particle of mass m can be formally obtained from first quantization of the Lorentz-invariant relation between the particle's energy and the three-component momentum:

$$\sqrt{\frac{E^2}{c^2} - \boldsymbol{p}^2} = mc, \quad \boldsymbol{p}^2 = p_x^2 + p_y^2 + p_z^2. \tag{A2}$$

Equation (A.2) can be rewritten the following way:

$$E = mc^2 \sqrt{1 + \frac{\boldsymbol{p}^2}{m^2 c^2}} = \gamma_v mc^2, \quad \gamma_v = \sqrt{1 + \frac{\boldsymbol{p}^2}{m^2 c^2}}. \tag{A3}$$

Combining Equation (4) and (A.3), we obtain the Lorentz-covariant equation:

$$E = \frac{\boldsymbol{p}^2}{\left(\gamma_v + 1\right) m} + mc^2, \quad \gamma_v = \sqrt{1 + \frac{\boldsymbol{p}^2}{m^2 c^2}}. \tag{A4}$$

Making the following formal first-quantization substitutions in Equation (A.4):

$$E \to \hat{H} = i\hbar \frac{\partial}{\partial t}, \quad \boldsymbol{p} \to \hat{p} = -i\hbar \nabla. \tag{A5}$$

We can obtain the following Lorentz-covariant wave equation:

$$i\hbar \frac{\partial}{\partial t} \Omega = -\frac{\hbar^2}{\left(\hat{\gamma}_v + 1\right) m} \nabla^2 \Omega + mc^2 \Omega, \quad \hat{\gamma}_v = \sqrt{1 + \frac{\hat{p}^2}{m^2 c^2}}. \tag{A6}$$

Now, it is well known in quantum mechanics that applying a constant energy shift to the Hamiltonian gives rise to an immaterial time-evolving phase factor in the solution wavefunction. Therefore, in order to obtain a more Schrödinger-like result, we can remove the rest-energy contribution from Equation (10) above, by replacing Ω as follows:

$$\Omega = \psi \mathrm{e}^{-i\frac{mc^2}{\hbar}t}. \tag{A7}$$

Thus, obtaining the Poirier-Grave de Peralta (PGP) equation for a free spin-0 particle of mass m [19]:

$$i\hbar \frac{\partial}{\partial t} \psi = -\frac{\hbar^2}{\left(\hat{\gamma}_v + 1\right) m} \nabla^2 \psi, \quad \hat{\gamma}_v = \sqrt{1 + \frac{\hat{p}^2}{m^2 c^2}}. \tag{A8}$$

The Poveda's formalism consists in parametrizing Equation (A.8) by making [19] [21]:

$$\hat{\gamma}_v \to \gamma_v = \sqrt{1 + \frac{\langle \psi | \hat{p}^2 | \psi \rangle}{m^2 c^2}}. \tag{A9}$$

This formalizes the approach initially followed by Grave de Peralta for avoiding the use of the square root operator γ_v [12] [13] [14] [15] [16]. Equation (A.9) defines the parameter γ_v in terms of the average value, on the state ψ, of the square of the well-defined linear momentum operator. This allows for rewritten Equation (A.8) as the GP equation for a free spin-0 particle of mass:

$$i\hbar\frac{\partial}{\partial t}\psi = -\frac{\hbar^2}{(\gamma_v+1)m}\nabla^2\psi, \quad \gamma_v = \sqrt{1+\frac{\langle\psi|\hat{p}^2|\psi\rangle}{m^2c^2}}. \tag{A10}$$

In a similar way, we can obtain Equation (5). Therefore, when γ_v does not explicitly depend on the time, we can look for a solution of Equation (5) of the form:

$$\psi(\mathbf{r},t) = \chi(\mathbf{r})e^{-i\frac{E'}{\hbar}t}, \quad E' = E+V-mc^2 = K+V. \tag{A11}$$

Then obtaining the time-independent GP equation for a spin-0 particle of mass m which is moving through a time-independent potential V:

$$\left[\frac{\hat{p}^2}{(\gamma_v+1)m}+V\right]\chi = E'\chi, \quad \gamma_v = \sqrt{1+\frac{\langle\chi|\hat{p}^2|\chi\rangle}{m^2c^2}}. \tag{A12}$$

Equation (A.12) can be rewritten in the following way:

$$\hat{K}_{Sch}\chi = \frac{\gamma_v+1}{2}(E'-V)\chi, \ \hat{K}_{Sch} = \frac{\hat{p}^2}{2m}, \ \gamma_v = \sqrt{1+\frac{\langle\chi|\hat{p}^2|\chi\rangle}{m^2c^2}}. \tag{A13}$$

Clearly, when:

$$\langle\chi|\hat{p}^2|\chi\rangle \ll m^2c^2. \tag{A14}$$

The time-independent Schrödinger equation is obtained as a limit case of Equation (A.13):

$$\hat{K}_{Sch}\chi_{Sch} = (E'-V)\chi_{Sch}. \tag{A15}$$

For several important problems, solving Equation (A.13) reduces to solving an effective time-independent Schrödinger equation. For instance, this occurs for problems with stepwise constant potentials [12] [14] [16]. In each spatial region where V is constant ($V = V_o$), $\chi = \chi_{Sch}$. Consequently, solving the time-independent GP equation reduces to solving the following effective time-independent Schrödinger equation:

$$\hat{K}_{Sch}\chi_{Sch} = \varepsilon\chi_{Sch}. \tag{A16}$$

Equation (A.16) can be solved with no knowledge of the value of γ_v; therefore, after Equation (A.16) is solved, γ_v can then be calculated as:

$$\gamma_v = \sqrt{1+\frac{2}{mc^2}\langle\chi_{Sch}|\hat{K}_{Sch}|\chi_{Sch}\rangle} = \sqrt{1+\frac{2}{mc^2}\varepsilon}. \tag{A17}$$

Finally, the sum of the kinetic and potential energies of the particle is:

$$E' = (\gamma_v-1)mc^2+V_o = \left(\sqrt{1+\frac{2}{mc^2}\varepsilon}-1\right)mc^2+V_o. \tag{A18}$$

Alternatively, E' can be calculated as:

$$E' = \frac{2\varepsilon}{1+\sqrt{1+\frac{2}{mc^2}\varepsilon}} + V_o. \tag{A19}$$

It is worth noting the energy values calculated using Equations (A.18) and (A.19) are in excellent correspondence with the energies obtained using the Klein-Gordon and Dirac equations [20] [27] [28]. For instance, **Figure 1** shows a comparison of the energies calculated using the Grave de Peralta approach (continuous lines), the Schrödinger equation (dashed lines), and the Dirac equation (solid dots) [29], for a particle in a one-dimensional infinite well of width L [12] [14] [17] [21]. Even for relativistic energy values larger than 2 mc^2, there is an excellent correspondence between the energies calculated using the GP and the Dirac equations. More importantly, there is a large class of problems where $\chi \neq \chi_{Sch}$, but the formal similitude between Equation (A.13) and Equation (A.15) facilitates solving Equation (A.13) using similar procedures than the ones used for solving Equation (A.15). For instance, the energies of Hydrogen atom were calculated using the Grave de Peralta approach [13] [15] [20]. A good correspondence was obtained with the positive energies calculated using the Klein-Gordon and Dirac equations [13] [15] [20].

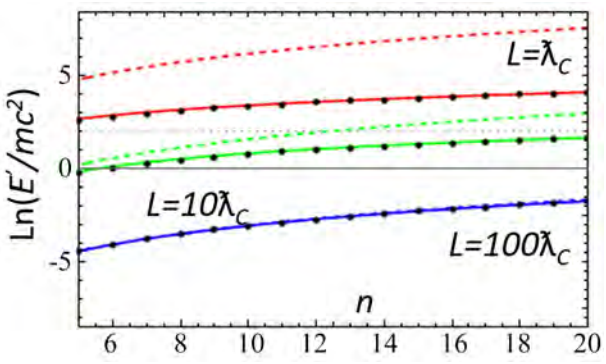

Figure 1. Comparison of the dependence on n (energy level) of the energies calculated using the GP approach (continuous line) [17] [21], the Schrödinger equation (dashed lines), and the Dirac equation [29] (solid dots) for three different widths (L) of a one-dimensional infinite well. $\lambda\!\!\!^{-}_C$ is the (reduced) Compton wavelength associated to a particle of mass m. The tenues horizontal dotted line corresponds to $E' = 2\ mc^2$.

Journal of Modern Physics, 2021, 12, 1435-1446
https://www.scirp.org/journal/jmp
ISSN Online: 2153-120X
ISSN Print: 2153-1196

Photoionization Study of the $2s^22p^2(^1D)ns(^2D)$, $2s^22p^2(^1D)nd(^2P)$, $2s^22p^2(^1D)nd(^2S)$, $2s^22p^2(^1S)nd^2D$, and $2s^22p^3(^3P)np(^2D)$ Rydberg Series of O+ Ions via the Modified Atomic Orbital Theory

Malick Sow*, Fatou Ndoye, Alassane Traoré, Abdou Diouf, Boubacar Sow, Youssou Gning, Papa Amadou Lamine Diagne

Department of Physics, Atoms Lasers Laboratory, Faculty of Sciences and Technologies, University Cheikh Anta Diop, Dakar, Senegal
Email: *malick711.sow@ucad.edu.sn

How to cite this paper: Sow, M., Ndoye, F., Traoré, A., Diouf, A., Sow, B., Gning, Y. and Diagne, P.A.L. (2021) Photoionization Study of the $2s^22p^2(^1D)ns(^2D)$, $2s^22p^2(^1D)nd(^2P)$, $2s^22p^2(^1D)nd(^2S)$, $2s^22p^2(^1S)nd^2D$, and $2s^22p^3(^3P)np(^2D)$ Rydberg Series of O+ Ions via the Modified Atomic Orbital Theory. *Journal of Modern Physics*, **12**, 1435-1446.
https://doi.org/10.4236/jmp.2021.1210086

Received: July 2, 2021
Accepted: August 15, 2021
Published: August 18, 2021

Abstract

We report in this paper energy positions of the $2P^\circ\_2s^22p^2(^1D)nd\ ^2P$, $2P^\circ\_2s^22p^2(^1D)nd\ ^2S$, $2P^\circ\_2s^22p^2(^1D)ns\ ^2D$, $2P^\circ\_2s^22p^2(^1S)nd\ ^2D$, and $2P^\circ\_2s^22p^3(^3P)np\ ^2D$ Rydberg series in the photoionization spectra originating from $2P^\circ$ metastable state of O+ ions. Calculations are performed up to n = 30 using the Modified Orbital Atomic Theory (MAOT). The present results are compared to the experimental data of Aguilar which are the only available values. The accurate data presented in this work may be a useful guideline for future experimental and other theoretical studies.

Keywords

Semiempirical Calculations, Modified Orbital Atomic Theory, Electron Correlation Calculations, Atoms and Ions, Rydberg Series, Quantum Defect

1. Introduction

The important role of studying Photoionization is a fundamental processes playing in laboratory and astrophysical systems such as nebulae plasmas [1], in inertial-confinement fusion experiments [2] and contributing to plasma opacity and radiation transfer inside plasmas. Thus, quantitative measurements of photoionization of ions provide precision data on ionic structure, and guidance to the development of theoretical approaches of multielectron interactions. Great-

est attention has been concentrated on studying Rydberg series of O+ ions for which photoabsorption from low-lying metastable states of open-shell ions has been shown to be important in the earth's upper atmosphere as well as in astrophysical plasmas. Formerly, studies on the O+ ion have been focused on ionization using the merged-beam technique. Thus, Aguilar *et al.* [3] performed the first experiment on the Absolute photoionization of O+ from 29.7 to 46.2 eV above the first ionization threshold, using a merged-beam line at the Advanced Light Source (ALS).

Therefore, it is an imperative task for physicists to provide accurate photoionization data for the modeling of astrophysical and laboratory plasmas.

The Opacity Project atomic database (at the Astronomic DataCenter of Strasbourg, France) was formed to re-estimate stellar envelope opacities in terms of atomic data computed by *ab initio* methods [4]. All these efforts led to the creation of several atomic databases widely used for astrophysical calculations [3].

In the present paper, we intend to provide accurate data on the photoionization of O+ ions that may be useful guideline for the physical atomic community. In addition, we aim to demonstrate the possibilities to use the Modified Atomic Orbital Theory of SOW *et al.* [5] [6] [7] [8] to reproduce excellently experimental data from merged beam facilities. For this purpose, we report calculations of energy resonances for the $2P^e\_2s^22p^2(^1D)nd\ ^2P$, $2P^e\_2s^22p^2(^1D)nd\ ^2S$, $2P^e\_2s^22p^2(^1D)ns\ ^2D$ $2P^e\_2s^22p^2(^1S)nd\ ^2D$, and $2P^e\_2s^22p^3(^3P)np\ ^2D$ Rydberg series of O+ ions up to $n = 30$, via the MAOT procedure along with the quantum defect theory.

Energy resonances and quantum-defect are compared to the only available experimental data of ALS [3].

Section 2 gives MAOT theory with a brief description of the formalism and the analytical expressions used in the calculations. In Section 3, we present and discuss the results obtained, compared to available experimental. In Section 4, we summarize our study and draw conclusions.

2. Theory

2.1. Brief Description of the MAOT Formalism

In the framework of Modified Atomic Orbital Theory (MAOT), total energy of $(\upsilon\ell)$-given orbital is expressed in the form [8] [9].

$$E(\upsilon\ell) = -\frac{\left[Z - \sigma(\ell)\right]^2}{\upsilon^2} \tag{1}$$

For an atomic system of several electrons M, the total energy is given by (in Rydbergs):

$$E = -\sum_{i=1}^{M} \frac{\left[Z - \sigma_i(\ell)\right]^2}{\upsilon_i^2}$$

With respect to the usual spectroscopic notation $(N\ell, N\ell')^{2S+1}L^{\pi}$, this equa-

tion becomes

$$E = -\sum_{i=1}^{M} \frac{\left[Z - \sigma_i \left({}^{2S+1}L^{\pi} \right) \right]^2}{\upsilon_i^2} \tag{2}$$

In this formula (2), L characterizes the considered quantum state (S, P, D …) and the symbol π is the parity of the system.

In the photoionisation study, energy resonances are generally measured relatively to the E∞ converging limit of a given $({}^{2S+1}L_J)$ nl-Rydberg series. For these states, the general expression of the energy resonances is given by the formula of Sakho presented previously [10] (in Rydberg units):

$$\begin{aligned} E_n = E_\infty - \frac{1}{n^2} \Bigg\{ & Z - \sigma_1 \left({}^{2S+1}L_J \right) - \sigma_2 \left({}^{2S+1}L_J \right) \times \frac{1}{n} \\ & - \sigma_2^{\mu} \left({}^{2S+1}L_J \right) \times (n-m) \times (n-q) \sum_k \frac{1}{f_k (n,m,q,s)} \Bigg\}^2 \end{aligned} \tag{3}$$

In this equation m and q $(m < q)$ denote the principal quantum numbers of the $({}^{2S+1}L_J)nl$-Rydberg series of the considered atomic system used in the empirical determination of the $\sigma_i({}^{2S+1}L_J)$-screening constants, s represents the spin of the nl-electron (s = 1/2), E_∞ is the energy value of the series limit generally determined from the NIST atomic database, E_n denotes the corresponding energy resonance, and Z represents the nuclear charge of the considered element. The only problem that one may face by using the MAOT formalism is linked to the determination of the $\sum_k \frac{1}{f_k (n,m,q,s)}$ term. The correct expression of this term is determined iteratively by imposing general Equation (3) to give accurate data with a constant quantum defect values along all the considered series. The value of μ is fixed to 1 and 2 during the iteration. The quantum defect is calculated from the standard formula below

$$E_n = E_\infty - \frac{RZ_{core}^2}{(n-\delta)^2} \quad \Rightarrow \delta = n - Z_{core} \sqrt{\frac{R}{(E_\infty - E_n)}} \tag{4}$$

In this equation, R is the Rydberg constant, E_∞ denotes the converging limit, Z_{core} represents the electric charge of the core ion, and δ means the quantum defect.

2.2. Energy Resonances of the $2P^\circ\_2s^2 2p^2(^1D)nd(^2P)$; $2P^\circ\_2s^2 2p^2(^1D)nd(^2S)$; $2P^\circ\_2s^2 2p^2(^1D)ns(^2D)$; $2P^\circ\_2s^2 2p^2(1S)nd(2D)$ and $2P^\circ\_2s^2 2p^3(^3P)np(^2D)$ Rydberg Series from $2P^\circ$ Metastable State of O+

In the framework of the MAOT formalism, the energy positions of the $2P^\circ\_2s^2 2p^2(^1D)nd(^2P)$; $2P^\circ\_2s^2 2p^2(^1D)nd(^2S)$; $2P^\circ\_2s^2 2p^2(^1D)ns(^2D)$; $2P^\circ\_2s^2 2p^2(1S)nd(2D)$ and $2P^\circ\_2s^2 2p^3(^3P)np(^2D)$ prominent Rydberg series from 2P° metastable state of O+ are given by (in Rydberg units)

- **For $2P^\circ\_2s^2 2p^2(^1D)nd(^2P)$ levels**

$$E_n = E_\infty - \frac{1}{n^2}\left\{Z - \sigma_1 - \frac{\sigma_2}{n} + \sigma_2 \times (n-m) \times (n-q) \times \left[\frac{1}{(n+q-s)^3} + \frac{1}{(n+m-s)^3} + \frac{1}{(n+m+s)^3} + \frac{1}{(n+m-s)^4} + \frac{1}{(n+q-m+s)^5}\right]\right\}^2 \quad (6)$$

Using the experimental data of ALS [3], we obtain (in eV) E_5 = 30.393 ± 0.15 (m = 5) and E_6 = 31.081 ± 0.15 (q = 6) respectively for the $2P^\circ\_2s^2 2p^2(^1D)5d\,^2P$ and $2P^\circ\_2s^2 2p^2(^1D)6d\,^2P$ levels. From NIST [11], we find E_∞ = 32.617 eV. Using these data, Equation (6) gives σ_1 = 6.012 ± 0.251 and σ_2 = −0.166 ± 0.009

- **For $2P^\circ\_2s^2 2p^2$ (^{1}D)nd(^{2}S) levels:**

$$E_n = E_\infty - \frac{1}{n^2}\left\{Z - \sigma_1 - \frac{\sigma_2}{n} + \sigma_2 \times (n-m) \times (n-q) \times \left[\frac{1}{(n+m-s)^3} + \frac{1}{(n-s)^4}\right]\right\}^2 \quad (7)$$

For the $2P^\circ\_2s^2 2p^2(^1D)5d\,^2S$ and $2P^\circ\_2s^2 2p^2(^1D)6d\,^2S$ levels, we find using the experimental data of ALS *et al.* [3], E_5 = 30.213 ± 0.150 (m = 5) and E_6 = 30. 905 ± 0.150 (q = 6). From NIST [11], we find E_∞ = 32.617 eV Equation (7) provides then σ_1 = 6.061 ± 0.185 and σ_2 = −0.367 ± 0.092

- **For $2P^\circ\_2s^2 2p^2$ (^{1}D) ns (^{2}D) levels**

$$E_n = E_\infty - \frac{1}{n^2}\left\{Z - \sigma_1 - \frac{\sigma_2}{n} + \sigma_2 \times (n-m) \times (n-q) \times \left[\frac{1}{(n+q-s)^3} + \frac{1}{(n+q+s-m)^4} + \frac{1}{(n+q-s)^4} + \frac{1}{(n+m-s)^4} + \frac{1}{(n+q-m+3s)^5}\right]\right\}^2 \quad (8)$$

For the $2P^\circ\_2s^2 2p^2$ (^1D) 6s (^2D) and $2P^\circ\_2s^2 2p^2$ (^1D) 7s (^2D) levels the experimental energy positions ALS *et al.* [3] are, E_6 = 30.578 ± 0.15 (m = 6) and E_7 = 31. 188 ± 0.15 (q = 7). From NIST [11], we find E_∞ = 32.617 eV. In that case, we find using Equation (8) σ_1 = 6.056 ± 0.322 and σ_2 = −2.274 ± 0.413

- **For $2P^\circ\_2s^2 2p^2$ (1S)nd(^{2}D) levels**

$$E_n = E_\infty - \frac{1}{n^2}\left\{Z - \sigma_1 - \frac{\sigma_2}{n} + \sigma_2 \times (n-m) \times (n-q) \times \left[\frac{1}{(n+q-m+s)(n-s)^2} + \frac{1}{(n+2m-q)^3} + \frac{1}{(n+q+s-m)^4}\right]\right\}^2 \quad (9)$$

From ALS of Aguilar *et al.* [3], we obtain for the $2P^\circ\_2s^2 2p^2$ (1S)4d(2D) and $2P^\circ\_2s^2 2p^2$ (1S)5d(^2D) E_4 = 31.924 ± 0.15 (m = 4) and E_5 = 33. 217 ± 0.15 (q = 5). From NIST [11], we find E_∞ = 35.458 eV. We find then using Equation (9) σ_1 = 6.008 ± 0.167 and σ_2 = −0.187 ± 0.05.

- **For $2s^2 2p^3$(^{3}P)np(^{2}D) levels**

$$E_n = E_\infty - \frac{1}{n^2}\left\{Z - \sigma_1 - \frac{\sigma_2}{n} + \sigma_2 \times (n-m) \times (n-q) \times \left[\frac{1}{(n-s)^2} + \frac{1}{(n+s-m)^2} - \frac{1}{(n+s-m)^3} + \frac{1}{(n+s-m)^4}\right]\right\}^2 \quad (10)$$

From ALS *et al.* [3], we obtain for the $2P^{o}\_2s^{2}2p^{3}(^{3}P)3p(^{2}D)$ *and* $2P^{o}\_2s^{2}2p^{3}(^{3}P)4p(^{2}D)$ $E_3 = 39.478 \pm 0.15$ ($m = 3$) and $E_4 = 43.115 \pm 0.15$ ($q = 4$). From NIST [11], we find $E_\infty = 47.527$eV. We find then using Equation (10) $\sigma_1 = 5.411 \pm 0.411$ and $\sigma_2 = -0.844 \pm 0.022$

3. Results and Discussions

The results obtained in the present paper are listed in **Tables 1-5** and compared with the Advanced Light Source experimental data of Aguilar *et al.* [3].

In **Table 1**, we quote the present MAOT results for energy resonances (E) and quantum defect (δ) of the $2P^{o}\_2s^{2}2p^{2}(^{1}D)nd(^{2}P)$ Rydberg series relatively to the 2P˚_metastable state of O+ ion. The current energy positions are calculated from equations (6) along with $Z = 8$, $m = 5$, and $q = 6$, $\sigma_1 = 6.012 \pm 0.251$ and $\sigma_2 = -0.166 \pm 0.009$. All these screening constant are evaluated using the Advanced Light Source (ALS) experimental results of Aguilar *et al.* [3], and take from NIST [11] the E_∞ energy limits which is 32.617 eV. Then our results are converted into eV for direct comparison by using the infinite Rydberg (1 Ry = 0.5 a.u = 13.605698 eV). It is seen that the data obtained compared very well to the experimental data of Aguilar *et al.* [3].

Up to $n = 11$, the maximum energy differences relative to the experimental data is less than 0.006 eV. In addition, the present quantum defect is almost constant up to $n = 30$. This may expect our results for $n > 11$ to be accurate.

In **Table 2**, we compare the present MAOT energy resonances (E) and quantum defect (δ) of the $2P^{o}\_2s^{2}2p^{2}(^{1}D)nd(^{2}S)$ Rydberg series relatively to the 2P˚_metastable state of O+ ion to experimental data [3]. All our energy values are obtained empirically using Equation (7) and converted into (eV) for direct comparison. Here again, the agreements are seen to be very good. Along the series, the present quantum defect is almost constant.

In **Table 3**, we show a comparison of the energy resonances (E) and quantum defect (δ) of the $2P^{o}\_2s^{2}2p^{2}(^{1}D)ns$ (^{2}D) Rydberg states relatively to the 2P˚_metastable state of O+ ion. The current energy positions are calculated from equations (8) along with $Z = 8$, $m = 6$, and $q = 7$, $\sigma_1 = 6.056 \pm 0.322$ and $\sigma_2 = -2.274 \pm 0.413$. The agreements between the studies are seen to be very good and the quantum defect is almost constant along the series. The agreements between the MOAT results and experimental data are seen to be very good. Along all the series investigated, the quantum defect is practically constant. This may expect our results up to $n = 30$ to be accurate.

In **Table 4**, we list the present energy resonances (E) and quantum defect (δ) for the $2P^{\circ}\_2s^{2}2p^{2}(^{1}S)nd$ (^{2}D) Rydberg states relatively to the 2P˚_metastable state of O+ ion compared to the experimental data [3]. The current energy positions are calculated from equations (9) along with $Z = 8$, $m = 4$, and $q = 5$, $E_\infty = 35.458\ eV$; $\sigma_1 = 6.008 \pm 0.167$ and $\sigma_2 = -0.187 \pm 0.05$. Comparison shows that the maximum energy deviation is at 0.006 up to $n = 14$. This indicates the very good accuracy between the results. For $n \geq 15$ it should be underlined that, since the MAOT formalism reproduces excellently the experimental measurements [3],

the present results quoted in Table 4 for the $2P^e\_2s^22p^2(^1S)nd\ (^2D)$ levels may be a very good representative of the nonexistent experimental data.

Table 1. Energy resonances (E) and quantum defect (δ) of the $2P^e\_2s^22p^2\ (^1D)nd\ (^2P)$ Rydberg series observed in the photoionization spectra originating from the $2P^e$ metastable states of O^+. The present results (MAOT) are compared to the Advanced Light Source (ALS) of Aguilar *et al.* [2]. The results are expressed in eV. The energy uncertainties in the present calculations and in the experimental data are indicated into parenthesis.

	$E(eV)$			δ	
n	MAOT	ALS	$\lvert\Delta E\rvert$	MAOT	ALS
5	30.393 (150)	30.393 (150)	0.000	0.054	0.054
6	31.081 (150)	31.081 (150)	0.000	0.048	0.048
7	31.496 (148)	31.496 (150)	0.000	0.032	0.033
8	31.763 (138)	31.762 (150)	0.001	0.018	0.023
9	31.955 (122)	31.948 (150)	0.005	0.004	−0.015
10	32.074 (106)	-----	---------	−0.008	− 0.092
11	32.170 (92)	32.169 (150)	0.001	−0.020	−0.018
12	32.241 (81)			−0.031	
13	32.297 (71)			−0.032	
14	32.341 (63)			−0.033	
15	32.377 (56)			−0.034	
16	32.406 (50)			−0.035	
17	32.431 (45)			−0.036	
18	32.451 (41)			−0.036	
19	32.468 (37)			−0.037	
20	32.483 (34)			−0.037	
21	32.495 (31)			−0.037	
22	32.506 (28)			−0.038	
23	32.515 (26)			−0.038	
24	32.524 (24)			−0.038	
25	32.531 (22)			−0.039	
26	32.538 (21)			−0.039	
27	32.543 (19)			−0.039	
28	32.549 (18)			−0039	
29	32.553 (17)			−0.038	
30	32.557 (16)			−0.039	
…					
∞[a]	32,617				

[a]NIST atomic database [11]. $\lvert\Delta E\rvert$: energy differences relative to the experimental data.

Table 2. Energy resonances (E) and quantum defect (δ) of the $2P^e\_2s^22p^2\ (^1D)nd\ (^2S)$ Rydberg series observed in the photoionization spectra originating from the $2P^e$ metastable states of O^+. The present results (MAOT) are compared to the Advanced Light Source (ALS) of Aguilar *et al.* [2]. The results are expressed in eV. The energy uncertainties in the present calculations and in the experimental data are indicated into parenthesis.

n	$E\,(eV)$			δ	
	MAOT	ALS	$\lvert\Delta E\rvert$	MAOT	ALS
5	30.413 (200)	30.413 (150)	0.000	0.031	0.031
6	31.105 (200)	31.105 (150)	0.000	0.001	0.001
7	31.517 (182)	--------		0.034	0.033
8	31.781 (161)	--------		0.020	0.023
9	31.961 (140)	--------		−0.016	−0.017
10	32.088 (122)	--------		−0.103	−0.092
11	32.182 (106)	--------		−0.018	−0.018
12	32.252 (93)			−0.026	
13	32.307 (82)			−0.023	
14	32.350 (73)			−0.029	
15	32.385 (65)			−0.022	
16	32.414 (58)			−0.022	
17	32.437 (52)			−0.027	
18	32.457 (47)			−0.023	
19	32.473 (43)			−0.028	
20	32.488 (39)			−0.024	
21	32.500 (36)			−0.029	
22	32.510 (33)			−0.024	
23	32.519 (30)			−0.028	
24	32.527 (28)			−0.023	
25	32/534 (26)			−0.027	
26	32.541 (24)			−0.021	
27	32.546 (23)			−0.025	
28	32.551 (21)			−0.029	
29	32.556 (20)			−0.023	
30	32.560 (19)			−0.027	
…					
∞[a]	32,617				

[a]NIST atomic database [11]. $\lvert\Delta E\rvert$: energy differences relative to the experimental data.

Table 3. Energy resonances (E) and quantum defect (δ) of the $2P^e\_2s^22p^2\ (^1D)ns\ (^2D)$ Rydberg series observed in the photoionization spectra originating from the $2P^e$ metastable states of O^+. The present results (MAOT) are compared to the Advanced Light Source (ALS) of Aguilar *et al.* [2]. The results are expressed in eV. The energy uncertainties in the present calculations and in the experimental data are indicated into parenthesis.

n	$E\,(eV)$			δ	
	MAOT	ALS	$\lvert\Delta E\rvert$	MAOT	ALS
6	30.578 (150)	30.578 (150)	0.000	0.834	0.834
7	31.188 (150)	31.188 (150)	0.000	0.829	0.829
8	31.562 (135)	31.561 (150)	0.002	0.826	0.822
9	31.803 (119)			0.824	
10	31.971 (104)			0.822	
11	32.092 (93)			0.820	
12	32.182 (79)			0.818	
13	32.250 (70)			0.817	
14	32.304 (62)			0.815	
15	32.347 (55)			0.814	
16	32.381 (49)			0.813	
17	32.409 (44)			0.811	
18	32.433 (40)			0.810	
19	32.453 (36)			0.809	
20	32.469 (33)			0.808	
21	32.484 (30)			0.807	
22	32.496 (29)			0.805	
23	32.507 (26)			0.804	
24	32.516 (24)			0.803	
25	32.524 (22)			0.802	
26	32.531 (20)			0.801	
27	32.538 (19)			0.800	
28	32.543 (18)			0.799	
29	32.549 (17)			0.799	
30	32.553 (16)			0.800	
…					
∞[a]	32,617				

[a]NIST atomic database [11]. $\lvert\Delta E\rvert$: energy differences relative to the experimental data.

Table 4. Energy resonances (E) and quantum defect (δ) of the $2P^e\_2s^22p^2\ (^1S)nd\ (^2D)$ Rydberg series observed in the photoionization spectra originating from the $2P^e$ metastable states of O^+. The present results (MAOT) are compared to the Advanced Light Source (ALS) of Aguilar *et al.* [2]. The results are expressed in eV. The energy uncertainties in the present calculations and in the experimental data are indicated into parenthesis.

n	$E\,(eV)$			δ	
	MAOT	ALS	$\lvert\Delta E\rvert$	MAOT	ALS
4	31.924 (150)	31.924 (150)	0.000	0.076	0.076
5	33.217 (150)	33.217 (150)	0.000	0.072	0.072
6	33.911 (125)	33.910 (150)	0.001	0.072	0.071
7	34.332 (103)	34.328 (150)	0.004	0.071	0.061
8	34.599 (85)	34.597 (150)	0,002	0.071	0.050
9	34.785 (70)	34.782 (150)	0.003	0.071	0.028
10	34.912 (59)	34.909 (150)	0.003	0.070	0.044
11	35.012 (51)	35.008 (150)	0.004	0.070	0.004
12	35.088 (44)	35.082 (150)	0.006	0.069	−0.030
13	35.147 (38)	35.145 (150)	0.002	0.069	−0.185
14	35.185 (33)	35.183 (150)	0.002	0.068	−0.066
15	35.222 (29)	35.219 (150)	0.003	0.068	−0.088
16	35.244 (26)			0.067	
17	35.268 (23)			0.067	
18	35.289 (21)			0.066	
19	35.306 (19)			0.066	
20	35.321 (17)			0.066	
21	35.334 (16)			0.067	
22	35.345 (14)			0.067	
23	35.355 (13)			0.067	
24	35.363 (12)			0.067	
25	35.370 (11)			0.067	
26	35.377 (11)			0.067	
27	35.383 (10)			0.067	
28	35.388 (09)			0.067	
29	35.393 (09)			0.067	
30	35.397 (08)			0.067	
…					
∞[a]	35,458				

[a]NIST atomic database [11]. $\lvert\Delta E\rvert$: energy differences relative to the experimental data.

Table 5. Energy resonances (E) and quantum defect (δ) of the $2P^e\_2s^22p^3\ (3P^e)nd\ (^2D)$ Rydberg series observed in the photoionization spectra originating from the $2P^e$ metastable states of O^+. The present results (MAOT) are compared to the Advanced Light Source (ALS) of Aguilar *et al.* [2]. The results are expressed in eV. The energy uncertainties in the present calculations and in the experimental data are indicated into parenthesis.

n	$E\,(eV)$			δ	
	MAOT	ALS	$\lvert\Delta E\rvert$	MAOT	ALS
3	39.478 (150)	39.478 (150)	0.000	0.436	0.436
4	43.115 (150)	43.115 (150)	0.000	0.576	0.576
5	45.092 (150)	45.093 (150)	0.001	0.485	0.480
6	46.009 (145)			0.483	
7	46.499 (138)			0.483	
8	46.788 (135)			0.483	
9	46.971 (133)			0.483	
10	47.095 (132)			0.482	
11	47.181 (131)			0.479	
12	47.244 (124)			0.479	
13	47.292 (116)			0.479	
14	47.328 (110)			0.480	
15	47.357 (106)			0.480	
16	47.380 (94)			0.480	
17	47.398 (84)			0.480	
18	47.412 (75)			0.480	
19	47.425 (68)			0.481	
20	47.436 (62)			0.481	
21	47.445 (56)			0.481	
22	47.453 (52)			0.481	
23	47.460 (47)			0.481	
24	47.466 (44)			0.481	
25	47.471 (40)			0.481	
26	47.475 (37)			0.481	
27	47.479 (35)			0.480	
28	47.483 (32)			0.480	
29	47.486 (30)			0.480	
30	47.489 (28)			0.480	
…					
∞[a]	47,527				

[a]NIST atomic database [11]. $\lvert\Delta E\rvert$: energy differences relative to the experimental data.

In Table 5, we compare the present MAOT energy resonances (E) and quantum defect (δ) of the $2P^{\circ}\_2s^2 2p^2(^1D)nd(^2S)$ Rydberg series relatively to the 2P°_metastable state of O+ ion to experimental data [3]. Our current energy positions are calculated from Equations (10) with $Z = 8$ along with $m = 3$, and $q = 4$, $E_\infty = 47.527\ eV$, $\sigma_1 = 5.411 \pm 0.411$ and $\sigma_2 = -0.844 \pm 0.022$. Here again, the agreements are seen to be very good. Along the series, the present quantum defect is almost constant. In a few series where discrepancies are observed, the maximum energy difference relative to the experimental data is at 0.001 eV. This indicates the excellent agreements between the present calculations and the experimental measurements for energy positions.

For all the Rydberg series investigated, the slight discrepancies between the present calculations and experiment may be explain by the simplicity of the MAOT formalism which does not include explicitly any relativistic corrections.

4. Summary and Conclusion

In this paper, energy resonances of the $2s^2 2p^2(^1D)ns(^2D)$, $2s^2 2p^2(^1D)nd(^2P)$, $2s^2 2p^2(^1D)nd(^2S)$, $2s^2 2p^2(^1S)nd\ (^2D)$, and $2s^2 2p^3(^3P)np\ (^2D)$ Rydberg series in the photoionization spectra originating from 2P metastable state of O+ ions are reported in this paper using the Modified Orbital Atomic Theory (MAOT). Over the entire Rydberg series investigated, it is shown that the present MOAT results agree very well with the only available experimental data of ALS [3]. A host of accurate data up to $n = 30$ are quoted in the recent work. The very good result obtained is this work points out the possibilities to use the MAOT formalism in the investigation of high lying Rydberg series of ions containing several electrons in the framework of a soft procedure. This work may be of interest for future experimental and theoretical studies in the photoabsorption spectrum of O^+.

Acknowledgements

The authors are grateful to the Orsay Institute of Molecular Sciences (OIMS), Paris, France and the Abdus Salam International Center for Theoretical Physics (ICTP), Trieste, Italy.

Conflicts of Interest

The authors declare no conflicts of interest regarding the publication of this paper.

References

[1] Bregman, J.N. and Harrington, J.P. (1986) *The Astrophysical Journal*, **309**, 833. https://doi.org/10.1086/164652

[2] Hofmann, I. (1990) *Laser and Particle Beams*, **8**, 527-539. https://doi.org/10.1017/S026303460000896X

[3] Aguilar, A., Covington, A.M., Hinojosa, G. and Phaneuf, A.R. (2003) *The Astrophysical Journal Supplement Series*, **146**, 467-477. https://doi.org/10.1086/368077

[4] Burke, P.G. and Berrington, K.A. (1993) Atomic and Molecular Processes: An Rmatrix Approach. Institute of Physics, Bristol.

[5] Sow, M., Diallo, A., Ba, A.D., Badiane, J.K., Diallo, S., Gning, M.T., Sakho, I. and Wagué, A. (2017) *International Journal of Atomic and Nuclear Physics*, **2**, 006. https://doi.org/10.35840/2631-5017/2506

[6] Sow, M., Sakho, I., Sow, B., Diouf, A., Gning, Y., Diop, B., Dieng, M., Diallo, A., Ba, M.D. and Kouhis, J. (2020) *Journal of Applied Mathematics and Physics*, **8**, 85-99. https://doi.org/10.46411/jpsoaphys.2020.02.16

[7] Faye, M., Diop, B., Sow, M., Sakho, I., Ndao, A.S., Biaye, M. and Wague, A. (2015) *Chinese Journal of Physics*, **53**, No. 5.

[8] Sow, M., Dieng, M., Faye, M., Diop, B., Gueye, M., Sakho, I., Biaye, M. and Wague, A. (2014) *Chinese Journal of Physics*, **52**, 1459.

[9] Sakho, I. (2013) *Chinese Journal of Physics*, **51**, 209.

[10] Diop, B., Faye, M., Dieng, M., Sow, M., Gueye, M., Sakho, I., Biaye, M. and Wague, A. (2014) *Chinese Journal of Physics*, **52**, 1227.

[11] Ralchenko, Y., Kramida, A.E., Reader, J. and NIST ASD Team (2011) NIST Atomic Spectra Database (version 4.0.1). National Institute of Standards and Technology, Gaithersburg, MD, USA. http://physics.nist.gov/asd3

Journal of Modern Physics, 2021, 12, 1447-1463
https://www.scirp.org/journal/jmp
ISSN Online: 2153-120X
ISSN Print: 2153-1196

Quantum Gravity

Konstantinos Patrinos

National Technical University of Athens, Athens, Greece
Email: kpatr@central.ntua.gr

How to cite this paper: Patrinos, K. (2021) Quantum Gravity. *Journal of Modern Physics*, **12**, 1447-1463.
https://doi.org/10.4236/jmp.2021.1210087

Received: July 29, 2021
Accepted: August 21, 2021
Published: August 24, 2021

Abstract

Quantum gravitational theory, based on the hypothesis of the absolute reference system, reveals the function of the effects of the gravitational field at the microscopic and macroscopic scale. The quantum nature of gravitational potential, and the dynamics and kinetic energy of photons and elementary particles under the influence of the gravitational field are studied, and a quantum interpretation of gravitational redshift is given. There is also a complete agreement of this quantum gravitational theory with the existing experimental data.

Keywords

Quantum Gravity, Gravitational Time Dilation, Gravitational Redshift, Perihelion of Mercury, Gravitational Deflection of Light, Time Delay of Light

1. Introduction

Quantum gravitational theory based on hypothesis of the absolute reference system is fully compatible with quantum mechanics and quantum field theory, for the following reasons:

1) Quantum gravity based on the hypothesis of the absolute reference system does not need the possibility of renormalization, since there are no infinities arising in calculated quantities. There is also no point-particle, since the elementary particles of matter have a specific structure, consisting of bound photons.

2) Changes in the operating rate of clocks under the influence of a gravitational field or due to motion at high speeds comparable to the speed of light in vacuum, based on the hypothesis of an absolute reference system, are not related to the concept of spacetime, but are related to the influences exerted on the structural elements of the particles, such as the effect of a gravitational field on bound photons, as well as Lorentz contraction.

3) Spacetime is not dynamic as in the general theory of relativity. The space of the hypothesis of the absolute reference system is a Euclidean space, and there is the possibility of an unambiguous description of all the cosmic events observed in the absolute reference system.

The study of inertial systems based on the hypothesis of the absolute reference system is stated in [1] [2] [3]. In the present work, the quantum nature of the gravitational field is studied and in addition the effects of the gravitational field on physical phenomena are studied by supplementing what is already stated in [4].

Some references related to the general theory of relativity, in which are presented the principles of this gravitational theory by its author himself, are in [5]-[10].

2. Quantum Description of the Gravitational Field

Based on the hypothesis of the absolute reference system, the elementary photonic wave is considered to be an oscillator whose mean value of kinetic energy is equal to $(1/2)h\nu$, where h is Plank's constant and ν is the frequency, and mean value of dynamic energy is also equal to $(1/2)h\nu$ ([2], subsection 3.3. **Harmonic Oscillator**). The total energy of a photon is equal to $h\nu$. Also according to the section "**Introduction to Particle Mechanics**" in [1], we have the relation $h\nu = m_{ph}c^2$, where m_{ph} is the photonic mass and c is the speed of light in vacuum. We must then consider the effect of the gravitational field on a photon coming from a space in which there is no gravitational field, and then propagates in a gravitational field, that is, on the already disturbed ether.

We consider that outside the gravitational field is a body or a measuring instrument, when it is included in the natural reference frame of the celestial body to which the gravitational field is due, but it is very far from this celestial body, so that the effect of the gravitational field is considered practically zero. Also, we denote by m_{ph_o}, c_o *and* ν_o *the mass, velocity and frequency of a photon, when it is outside the gravitational field, while these physical quantities will be denoted by* m_{ph}, c *and* ν *respectively, when the same photon is inside the gravitational field.*

The momentum of the photon, without the presence of a gravitational field, making use of the clock which is outside the gravitational field, is given by the relation $p_{ph_o} = m_{ph_o}c_o$ ([1] section 4. **Introduction to Particle Mechanics**). The corresponding relation for a photon propagating in a gravitational field and resulting from the use of the aforementioned clock, in vector form, is:

$$\boldsymbol{p}_{ph} = m_{ph}\boldsymbol{c} \tag{1}$$

where m_{ph}, $\boldsymbol{c}$ are functions dependent on the radius r ([4] section 2. **Mass and velocity of a photon in the gravitational field**). We consider that the photon propagates in space with the simultaneous presence of a gravitational field derived from the spherical body of mass M.

Therefore, the momentum - energy relation of a photon that is a force carrier

of the gravitational field is:

$$\frac{\boldsymbol{p}_{ph}^2}{m_{ph}} = \mathcal{E}_{ph} \tag{2}$$

Suppose that in a small volume δV, at a radial distance r, a set of N force carriers of the gravitational field is an elementary part of the whole spherical wave of all force carriers of the gravitational field of a celestial spherical body of mass M. The wavefunction Ψ of this system of N photons of different frequencies will obey the classical differential equation of a spherical electromagnetic wave. Specifically, the action of the kinetic energy operator[1] on the wavefunction Ψ is given by the equation:

$$\hat{\mathcal{E}}_{ph,kin}\Psi = \frac{i\hbar}{2}\frac{\partial\Psi}{\partial t} \tag{3}$$

and gives us the equation of action of the total energy operator on the wavefunction Ψ of the photon:

$$\hat{\mathcal{E}}_{ph}\Psi = 2\hat{\mathcal{E}}_{ph,kin}\Psi = i\hbar\frac{\partial\Psi}{\partial t} \tag{4}$$

The momentum operator is $\hat{\boldsymbol{p}}_{ph} = -i\hbar\nabla$. From Equations (1) and (2) we get the equation:

$$\boldsymbol{p}_{ph}^2 = \frac{1}{c^2}\mathcal{E}_{ph}^2 \tag{5}$$

from which we get the classical electromagnetic wave equation:

$$\left(\nabla^2 - \frac{1}{c^2}\frac{\partial^2}{\partial t^2}\right)\Psi(r,t) = 0 \tag{6}$$

where the wavefunction Ψ depends on the radial distance r and not on the vector position $\boldsymbol{r}$, since this wave is spherical. Under these conditions the action of the operator ∇^2 on the wavefunction Ψ is expressed by the equation:

$$\nabla^2\Psi = \frac{1}{r^2}\frac{\partial}{\partial r}\left(r^2\frac{\partial\Psi}{\partial r}\right)$$

so, Equation (6) can take the form:

$$\frac{\partial^2(r\Psi)}{\partial r^2} - \frac{1}{c^2}\frac{\partial^2(r\Psi)}{\partial t^2} = 0 \tag{7}$$

The solution of this differential equation, for N photons, which are force carriers in the elementary volume δV, is given by the relation:

$$\Psi(r,t) = \frac{1}{r}\sum_{i=1}^{N} A_i \mathrm{e}^{i(k_i r - \omega_i t)} \tag{8}$$

where A_i, for $i = 1,2,\cdots,N$, is constant. The gravitational potential, $U(r)$, is proportional to the time-averaged absolute value of $\Psi(r,t)$, so it is in a form given by the relation:

[1]The momentum and kinetic energy operators are described in the literature reference [2], subsection 2.2, **Wave Function of a Free Particle**, Equations (2.9) and (2.10).

$$U(r) \sim \overline{|\Psi|} = \overline{\sqrt{\Psi\Psi^*}} = \frac{A}{r} \tag{9}$$

where $A = \sqrt{\sum_{i=1}^{N} |A_i|^2}$. If we denote by $\boldsymbol{E}$ the intensity of the gravitational field (something analogous to the intensity of the electric field in electromagnetism), then this is given by the relation:

$$\boldsymbol{E}(r) = -\nabla U(r) \tag{10}$$

On a photon located in the above elementary volume δV and having mass m_{ph} a gravitational force is exerted, determined by the equation:

$$\boldsymbol{F} = m_{ph}\boldsymbol{E} = -m_{ph}\nabla U = -\frac{GMm_{ph}}{r^2}\hat{u}_r \tag{11}$$

where $\hat{u}_r$ is the unit radial vector. Therefore, the expression for gravitational potential, $U(r)$, is:

$$U(r) = -\frac{GM}{r} \tag{12}$$

We must also summarize the findings of the study regarding the dependence of the mass and velocity of a photon under the influence of a gravitational field, as stated in [4] (section 3, **Mass and Velocity of a Photon in the Gravitational Field**). This dependence of the velocity and mass of a photon on the radial distance *r*, which is the distance of the photon from the center of the spherical celestial body of mass *M*, is determined by the relations:

$$c = c_o\left(1 - \frac{4GM}{rc_o^2}\right)^{1/2} \tag{13}$$

$$m_{ph} = m_{ph_o}\left(1 - \frac{4GM}{rc_o^2}\right)^{-3/4} \tag{14}$$

Since the elementary particles have as structural elements the bound photons, the function of the photonic mass, which is due to the dependency on the radial distance, will be analogous to the corresponding function of the mass of a body located inside the gravitational field. If m and m_o are the masses of a spherical body inside and outside the gravitational field respectively, and r is the radial distance, the mass function m is given by the relation:

$$m = m_o\left(1 - \frac{4GM}{rc_o^2}\right)^{-3/4} \tag{15}$$

The dynamic energy of a photon, due to the effect of the gravitational field when moving from a position outside the gravitational field (*i.e.* theoretically from infinite distance) to a radial distance *R*, is calculated by the integral:

$$V_{ph}(R) = \int_{\infty}^{R} \boldsymbol{F} \cdot \mathrm{d}\boldsymbol{r} = -\int_{R}^{\infty} \left(-m_{ph}\nabla U(r)\right) \cdot \mathrm{d}\boldsymbol{r} \tag{16}$$

With the help of the relation (11) and the relation (12) for the gravitational potential, we get:

$$V_{ph}(R)=\int_R^{\infty}\frac{GM}{r^2}m_{ph_o}\left(1-\frac{4GM}{rc_o^2}\right)^{-3/4}\mathrm{d}r$$
$$=-m_{ph_o}c_o^2+m_{ph_o}c_o^2\left(1-\frac{4GM}{Rc_o^2}\right)^{1/4} \quad (17)$$
$$=-m_{ph_o}c_o^2+m_{ph}c^2$$

The first-order approximation of this photon gravitational dynamic energy is calculated according to relation:

$$V_{ph}(R)\simeq-\frac{GMm_{ph_o}}{R}$$

and respectively for a particle, which had mass m_o when it was outside the gravitational field, and now it is inside the gravitational field at a radial distance R, the gravitational dynamic energy is calculated approximately according to relation:

$$V(R)\simeq-\frac{GMm_o}{R}$$

The nature of this dynamic energy is studied in [4], section 2, **The Origin of Attractive Force in a Gravitational Field**, and we observe that the energy E_{ph}, which is also stated in [4] (section 2), at a radial distance r is equal to $-V_{ph}(r)$. Indeed, by putting $\boldsymbol{F}=f(r)\hat{u}_r$, as stated in [4] (section 2, Equation (2)), we get the relation:

$$\boldsymbol{F}=f(r)\hat{u}_r=\frac{\mathrm{d}E_{ph}}{\mathrm{d}r}\hat{u}_r=-\nabla V_{ph}(r) \quad (18)$$

which is easily confirmed according to relation (17).

The total energy of a photon propagating inside a gravitational field at a radial distance R, using the measuring instruments of a laboratory located outside the gravitational field, according to relation (17) is:

$$m_{ph}c^2=m_{ph_o}c_o^2+V_{ph}(R) \quad (19)$$

where $m_{ph}c^2=h\nu$, $m_{ph_o}c_o^2=h\nu_o$, and the frequencies ν and ν_o are the frequencies of the same photon when it is inside the gravitational field or outside it respectively, measured by a clock located outside the gravitational field. As already mentioned at the beginning of this section, there is a term for the kinetic energy of this photon, which is $\frac{1}{2}h\nu_o=\frac{1}{2}m_{ph_o}c_o^2$, and two terms of dynamic energy, one of which is that of the elementary photonic harmonic oscillator equal to the kinetic energy term, and the other term of dynamic energy, $V_{ph}(R)$, is due to the effect of the gravitational field on the photon. Due to this effect of the gravitational field, a physical system located within a gravitational field becomes non-inertial. Therefore, in order to estimate the kinetic energy of the photon using the above-mentioned clock, one must calculate the quantity $\frac{1}{2}h\nu_o$, which is equal to the kinetic energy of the same photon, when this photon is outside the gravitational field.

The spherical electromagnetic wave, which consists of free photons of gravitational field force carriers, comes from the continuous conversion of bound photons into free photons (and vice versa), and their frequency spectrum is the spectrum of the "mass frequency" of bound photons[2] from which they originate. The density of these force carriers at a radial distance of r is proportional to the time-averaged value of the quantity $\Psi\Psi^*$ (as mentioned in [2], subsection 2.2, **Wave Function of a Free Particle**), and is also proportional to the mass of the spherical homogeneous body from which the gravitational field originates. But the mass of the spherical homogeneous celestial body is affected by the gravitational field created by the body itself. Suppose that the whole mass of the spherical body is converted to free photons in a space in which there is no gravitational field and that this measured mass of free photons is equal to M_o. This mass, M_o, is called *non-gravitational mass*. Therefore the mass of the spherical body before this conversion, that is, when it was in a solid state, must have been slightly greater than the measured mass of free photons, due to the existence of the gravitational field created by the body itself. This mass, which we consider equal to *M*, is called *gravitational mass*.

If we want to calculate the gravitational mass, *M*, of this body we can do it with a good approximation ignoring terms of very small order of magnitude. Suppose first that a concentric spherical part of this body of radius r and gravitational mass $\mathcal{M}(r)$ is surrounded by a spherical shell of differential thickness $\mathrm{d}r$ and differential gravitational mass $\mathrm{d}\mathcal{M}(r)$, as shown in **Figure 1**, and that the density ρ of the non-gravitational mass is constant throughout the body. The differential gravitational mass of the spherical shell is given by the relation:

$$\mathrm{d}\mathcal{M}(r)=\mathrm{d}\mathcal{M}_o(r)\left(1-\frac{4G\mathcal{M}(r)}{rc_o^2}\right)^{-3/4}$$

where $\mathrm{d}\mathcal{M}_o(r)$ is the non-gravitational differential mass of the spherical shell. By setting $\mathcal{M}(r)-\mathcal{M}_o(r)=\Delta\mathcal{M}$ we get the approximate relation:

$$\frac{G\mathcal{M}(r)}{rc_o^2}=\frac{G\mathcal{M}_o(r)}{rc_o^2}+\frac{G\Delta\mathcal{M}}{rc_o^2}\simeq\frac{G\mathcal{M}_o(r)}{rc_o^2}$$

since the quantity $G\mathcal{M}_o(r)\big/\left(rc_o^2\right)$ is quite small (of the order of 10^{-5} for the solar system). If we denote by R the radius of the spherical body, the approximate calculation of the gravitational mass of the body gives us:

$$M=\int_0^R\mathrm{d}\mathcal{M}(r)\simeq\int_0^R\left(1+\frac{3G\mathcal{M}_o(r)}{rc_o^2}\right)\mathrm{d}\mathcal{M}_o(r) \tag{20}$$

Since the above density, ρ, is constant, it follows that the non-gravitational mass in the spherical part of radius r is $\mathcal{M}_o(r)=\frac{4}{3}\pi\rho r^3$, and also $\mathrm{d}\mathcal{M}_o(r)=4\pi\rho r^2\mathrm{d}r$, so, it follows that using the previous integration, the gravitational mass of the body is determined by the following relation:

[2]The concept of mass frequency is described in [1], subsection 4.1, **The Structure of the Smallest Elementary Particle**.

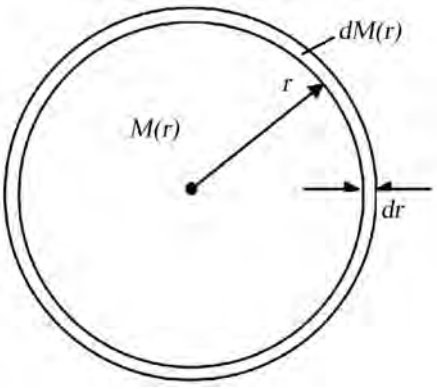

Figure 1. A concentric spherical part of the body of radius r and gravitational mass $\mathcal{M}(r)$ is surrounded by a spherical shell of differential thickness $\mathrm{d}r$ and differential gravitational mass $\mathrm{d}\mathcal{M}(r)$.

$$M = M_o\left(1+\frac{9}{5}\frac{GM_o}{Rc_o^2}\right) \tag{21}$$

where $M_o = \frac{4}{3}\pi\rho R^3$.

3. Additional Effects of the Influence Exerted by the Gravitational Field on Matter

As mentioned in the previous section, the kinetic energy of a photon propagating inside a gravitational field is equal to the kinetic energy of the same photon when it is outside the gravitational field. Also, the physical reference system of a massive celestial body M is not an inertial reference system, since it dynamically affects all the structural elements of all the elementary particles of matter. According to the hypothesis of the absolute reference system, these structural elements are the bound photons.

Although all the internal dynamic energies of an elementary particle have a sum equal to zero in order for the particle to be in a stable state, the state of the particle due to the gravitational field remains as an exogenous non-inertial state of the particle. For example the effect on the velocity and mass of a captive photon, according to relations (13) and (14), gives us the total energy of the bound photon, but its kinetic energy is maintained equal to the kinetic energy estimated when this captive photon is outside the gravitational field. Therefore the kinetic energy of a particle is that which the particle had when it was outside the gravitational field, moving in an inertial system at a speed measured by the measuring instruments of the same inertial system equal to the velocity of the particle inside the gravitational field that measured by same measuring instruments. The kinetic energy of a particle which is at a radial distance r and moves with speed u measured by the measuring instruments of a laboratory located outside the gravitational field, according to the hypothesis of the absolute reference system, is

given by the equation:

$$E_{kin} = \frac{1}{2} m_o \gamma^2 c_o^2 - \frac{1}{2} m_o c_o^2 = \frac{1}{2} m_o \gamma^2 u^2$$

where $\gamma = \left(1 - u^2 / c_o^2\right)^{-1/2}$.

A notable change, due to the effect of the gravitational field, is the change in the quantitative estimation of the electric charge of an elementary charged particle. As has already been proved by the principles of the hypothesis of the absolute reference system (in [1], subsection 2.4.2, **The Charge and the Force Carrier of Electromagnetic Interactions**, Equation (2.60)), a charged particle initially accelerated by electromagnetic interactions in the inertial reference system of the laboratory, then moving at a constant velocity $\boldsymbol{v}$ with respect to it measured by the instruments of the laboratory, has an electric charge equal to q_v, while before acceleration, practically stationary in the laboratory, it had an electric charge equal to q. The corresponding relation is:

$$q_v = \frac{q}{\gamma_v} \tag{22}$$

A charged particle under the influence of a gravitational field, considered as stationary at a radial distance r, undergoes a change in the quantitative estimation of its charge due to the expression of the estimated time[3], obtained by using a clock that is at the same radial distance, r, as that of the electric charge, according to relation:

$$t_g = t\left(1 - \frac{4GM}{rc_o^2}\right)^{1/4} \tag{23}$$

because this estimated time causes a change in the estimation of the emission rate of the force carriers in relation to the estimation of the emission rate of the force carriers resulting from a clock outside the gravitational field, as in the case of the aforementioned moving charged particle.

We denote by q the electric charge of a particle located at a radial distance R within the gravitational field, which is measured by the measuring instruments of a laboratory located outside the gravitational field. Also, we denote by q_o the electric charge of the same particle when this particle is outside the gravitational field, measured by the aforementioned laboratory. The functional relation between the quantities q and q_o is:

$$q = q_o\left(1 - \frac{4GM}{Rc_o^2}\right)^{1/4} \tag{24}$$

If the measuring instruments and the aforementioned charged particle are located inside the gravitational field, at a radial distance R, then the electric charge is evaluated as equal to q_o.

[3]The relation between the estimated time inside the gravitational field and the measured time with a clock outside the gravitational field, and the discussion regarding this relationship is in [4], section 4, **Gravitational time dilation and redshift**, Equation (21).

4. The Quantum Interpretation of Gravitational Redshift

In order to study the phenomenon of gravitational redshift, we will study the energy emission spectrum derived from a hydrogen atom under the influence of a gravitational field, using the principles of quantum mechanics based on the absolute reference system hypothesis.

We consider a hydrogen atom affected by the gravitational field of a spherical and homogeneous celestial body of mass M, and located at a constant radial distance R from the center of this spherical body. In order to study this phenomenon according to the principles of hypothesis of the absolute reference system, the energy of this atomic electron should be estimated using the clock of the particle under study, *i.e.* the clock of the electron of the hydrogen atom.

According to the relevant example in [2] (subsection 3.4, **Hydrogen Atom**, Equation (3.29)), if we use the subscript o for frequencies, measured with the instruments of a laboratory which is outside the gravitational field, where the phenomenon we are considering takes place, the average value of kinetic energy at the energy level of quantum number n, is given by the equation:

$$\overline{E_{kin,n}} = \frac{1}{2} h n \nu_{n_o} \tag{25}$$

In the same example (in [2], subsection 3.4, **Hydrogen Atom**, Equations (3.31), (3.33)), if we use the subscript o for mass and electric charge measured with the instruments of the above laboratory, it appears that:

$$\overline{E_{kin,n}} = \frac{m_o e_o^4}{2\hbar^2} \frac{1}{n^2} \tag{26}$$

Therefore:

$$\frac{1}{2} h n \nu_{n_o} = \frac{m_o e_o^4}{2\hbar^2} \frac{1}{n^2} \tag{27}$$

But we need to understand the origin of the first member of the Equation (27). The definition of particle frequency is given in [2] (subsection 2.1, **Particle-Frequency and Wavelength**, Equation (2.3)) by the relation $\nu_{q_o} = \sum_{i=1}^{N} \nu_{u_{i_o}}$, where $\nu_{u_{i_o}}$ is the frequency that comes from the kinetic energy of the i bound photon. The kinetic energy of the particle is:

$$E_{kin} = \frac{1}{2} m_o \gamma^2 u^2 = \frac{1}{2} h \sum_{i=1}^{N} \nu_{u_{i_o}} \tag{28}$$

Therefore the kinetic energy in relation to the particle frequency is:

$$E_{kin} = \frac{1}{2} m_o \gamma^2 u^2 = \frac{1}{2} h \nu_{q_o} \tag{29}$$

Therefore the average value of kinetic energy, when $\gamma \simeq 1$, is given by the relation:

$$\overline{E_{kin}} = \frac{1}{2} m_o \overline{u^2} = \frac{1}{2} h \overline{\nu_{q_o}} \tag{30}$$

where $\overline{\nu_{q_o}} = n \nu_{n_o}$, as formulated in [2] (subsection 2.4, **Particle Motion in**

Closed Orbits, Equation (2.23)), and finally a general equation is:

$$\overline{E_{kin}} = \frac{1}{2} m_o \overline{u^2} = \frac{1}{2} h n \nu_{n_o} \tag{31}$$

Suppose that the hydrogen atom moves slowly from a region outside the gravitational field to the celestial spherical body, that is, it gradually enters the gravitational field, and finally immobilizes at a radial distance R within the gravitational field. Then according to the measurements of the laboratory instruments located outside the gravitational field, the Equation (27) is modified according to relation:

$$\frac{1}{2} h n \nu_n = \frac{m e^4}{2\hbar^2} \frac{1}{n^2} \tag{32}$$

According to the clock of the above laboratory, following the relevant wording in [4] (section 4, **Gravitational Time Dilation and Redshift**, Equation (18)), the frequency ν_n is given by the equation:

$$\nu_n = \nu_{n_o} \left(1 - \frac{4GM}{R c_o^2} \right)^{1/4} \tag{33}$$

It is obvious that the first member of the Equation (32), is not equal to the average kinetic energy, according to the definition of kinetic energy given in the previous section, hence the Equation (32) no longer gives us the average kinetic energy. However, since the hydrogen atom is at a radial distance R inside the gravitational field, using a clock located at the same radial distance, according to the estimated time given by the relation (23), the estimated frequency, ν_{n_g}, is calculated according to the equation:

$$\nu_{n_g} = \nu_n \left(1 - \frac{4GM}{R c_o^2} \right)^{-1/4} \tag{34}$$

This estimated frequency is equal to the frequency ν_{n_o}, measured when the effect occurs outside the gravitational field[4]. Therefore the mean value of kinetic energy is given by the equation:

$$\overline{E_{kin,n}} = \frac{1}{2} h n \nu_{n_g} = \frac{m e^4}{2\hbar^2} \frac{1}{n^2} \left(1 - \frac{4GM}{R c_o^2} \right)^{-1/4} \tag{35}$$

From the relations (15) and (24) the following equality results:

$$m e^4 = m_o e_o^4 \left(1 - \frac{4GM}{R c_o^2} \right)^{1/4} \tag{36}$$

therefore the average kinetic energy of the electron of the hydrogen atom at the energy level n is:

$$\overline{E_{kin,n}} = \frac{m_o e_o^4}{2\hbar^2} \frac{1}{n^2} \tag{37}$$

[4]A similar description of this estimated frequency can be found in [4], section 4, **Gravitational Time Dilation and Redshift**, Equation (23).

The total energy of the electron is the sum of the time average value of kinetic energy, time average value of Coulomb energy, and gravitational potential energy. The time average of Coulomb energy is denoted by $\overline{E_{dyn}}$. Since the gravitational dynamic energy is constant, given that the radial distance R is constant, does not contribute to the energy difference of an energy transition of the electron, and, based on the virial theorem, $2\overline{E_{kin}} + \overline{E_{dyn}} = 0$ ([11], paragraph **3-4**, **THE VIRIAL THEOREM**), it follows that the energy of the electron, which actually contributes to the energy of an emitted or absorbed photon, is given by the relation:

$$E_n = -\frac{m_o e_o^4}{2\hbar^2}\frac{1}{n^2} \tag{38}$$

that is, it is equal to the energy of the electron when the phenomenon takes place outside the gravitational field.

We now assume an energy transition of the electron of the hydrogen atom, from the initial energy level, E_{n_1}, with quantum number n_1 to the final energy level, E_{n_2}, with quantum number n_2, so, for the emission of a photon the inequality $n_1 > n_2$ must apply.

The energy difference is calculated according to the known relation:

$$\Delta E = E_{n_2} - E_{n_1} = -\frac{m_o e_o^4}{2\hbar^2}\left(\frac{1}{n_2^2} - \frac{1}{n_1^2}\right) \tag{39}$$

The estimated, by the clock of the electron, energy of the emitted photon, as stated in [4] (section 4, **Gravitational Time Dilation and Redshift**, Equation (25)), is given by the relation:

$$\mathcal{E}_{ph_g} = h\nu_o\left(1 - \frac{4GM}{Rc_o^2}\right)^{-1/4} \tag{40}$$

where $h\nu_o = m_{ph_o}c_o^2$, and ν_o is the frequency of the emitted photon within the gravitational field, estimated by the clock of the electron. This frequency is equal to the frequency which is measured by a clock outside the gravitational field, when the emitted photon has come out of the gravitational field. Given that $\mathcal{E}_{ph_g} = -\Delta E$, the relations (39) and (40) give us:

$$\frac{m_o e_o^4}{2\hbar^2}\left(\frac{1}{n_2^2} - \frac{1}{n_1^2}\right) = h\nu_o\left(1 - \frac{4GM}{Rc_o^2}\right)^{-1/4} \tag{41}$$

If this phenomenon had taken place outside the gravitational field, then the energy of the emitted photon, estimated by a clock outside the gravitational field, would had been equal to:

$$\frac{m_o e_o^4}{2\hbar^2}\left(\frac{1}{n_2^2} - \frac{1}{n_1^2}\right) = h\nu_{o,n_1\to n_2} \tag{42}$$

where $\nu_{o,n_1\to n_2}$ is the frequency of the emitted photon, estimated by a clock outside the gravitational field. From the relations (41) and (42) it appears that the photon whose emission takes place inside the gravitational field, when it has

come out of the gravitational field, it has shifted toward the red in relation to the photon emitted outside the gravitational field, according to the following relation:

$$\nu_o = \nu_{o,n_1\to n_2}\left(1-\frac{4GM}{Rc_o^2}\right)^{1/4} \simeq \nu_{o,n_1\to n_2}\left(1-\frac{GM}{Rc_o^2}\right) \tag{43}$$

5. Experimental Confirmation of the Hypothesis of the Absolute Reference System

In this section we examine the known experimental tests of the general theory of relativity, in order to determine whether the experimental results confirm the hypothesis of the absolute reference system.

Everything in this section is a brief description of what is stated in [4], section 4, and section 5.

5.1. Gravitational Time Dilation

According to the hypothesis of the absolute reference system, the bound photons, which are the building elements of the elementary particles of matter, will undergo these changes in frequency and wavelength. If the closed orbit of a bound photon has a length equal to $n\lambda$, where $n=1,2,\cdots$, then the time of a period is $T=n\lambda/c$, while, outside the gravitational field, the corresponding time is $T_o=n\lambda_o/c_o$. Therefore:

$$T = T_o\frac{c_o\lambda}{c\lambda_o} = T_o\left(1-\frac{4GM}{rc_o^2}\right)^{-1/4} \tag{44}$$

According to the hypothesis of the absolute reference system, the estimated time is inversely proportional to the time of the aforementioned period ([1], **2.4.1. Contraction of Length and Time**, p. 440-441). Assuming that t_g is the estimated time recorded between two events occurring inside the gravitational field using a clock at a fixed position $\boldsymbol{r}$ also inside the gravitational field, and t is the corresponding estimated time using a clock outside the gravitational field, then the correlation of these times is given by the equation:

$$\frac{t_g}{t}=\frac{T_o}{T} \quad\Leftrightarrow\quad t_g = t\left(1-\frac{4GM}{rc_o^2}\right)^{1/4} \simeq t\left(1-\frac{GM}{rc_o^2}\right) \tag{45}$$

The corresponding result of the general theory of relativity is:

$$t_g = t\left(1-\frac{2GM}{rc_o^2}\right)^{1/2} \simeq t\left(1-\frac{GM}{rc_o^2}\right) \tag{46}$$

Therefore the estimated time, based on the hypothesis of the absolute reference system, with a very good approximation is the same as that of the general theory of relativity. This estimated time value has been experimentally confirmed ([12] [13]).

5.2. The Advance of the Perihelion of Mercury

Denoting the mass of the Sun by M and the mass of Mercury by m, according to the Equation (15) and the relevant study in [4] (section 3, **Mass and Velocity of a Photon in the Gravitational Field**, Equation (15)), we get the equation:

$$\frac{\mathrm{d}^2u}{\mathrm{d}\theta^2}+u=\frac{GMm_o^2}{L^2}\left(1-\frac{4GM}{rc_o^2}\right)^{-3/2} \tag{47}$$

Given that $u=1/r$, and $\left(1-4GM/\left(rc_o^2\right)\right)^{-3/2}\simeq 1+6GM/\left(rc_o^2\right)$, the first order approach is given by the differential equation:

$$\frac{\mathrm{d}^2u}{\mathrm{d}\theta^2}+\left(1-\frac{6G^2M^2m_o^2}{c_o^2L^2}\right)u=\frac{GMm_o^2}{L^2} \tag{48}$$

We define the constants:

$$A=1-\frac{6G^2M^2m_o^2}{c_o^2L^2}$$

$$B=\frac{GMm_o^2}{L^2}$$

The solution of the differential Equation (48) has the form:

$$u=\frac{1}{r}=\frac{B}{A}+K\cos\left(\sqrt{A}\theta\right) \tag{49}$$

where K is constant.

Two consecutive minimizations of the distance r are performed for $\sqrt{A}\theta=0$ and for $\sqrt{A}\theta=2\pi$. For $\sqrt{A}\theta=0$ the angle θ is zero, while for $\sqrt{A}\theta=2\pi$ the angle θ is given by the relation:

$$\theta=\frac{2\pi}{\sqrt{A}}\simeq 2\pi+\frac{6\pi G^2M^2m_o^2}{c_o^2L^2} \tag{50}$$

This result is the same as that of the general theory of relativity ([14], §101. **Motion in a centrally symmetric gravitational field**) and is confirmed by observations already announced in the 19th century.

More details on this topic are given in [4], subsection 5.1, **The Advance of the Perihelion of Mercury**.

5.3. The Deflection of Light in the Gravitational Field of the Sun

When a photon enters the gravitational field of the sun, its energy changes from the value $m_{ph_o}c_o^2$ to the value $m_{ph}c^2$, when it leaves the gravitational field, it takes again the value $m_{ph_o}c_o^2$. Also the motion of said photon at a great distance from the sun, where it can be considered to be outside the gravitational field, tends to be asymptotically a straight line, while inside the gravitational field it is curvilinear, due to the effect of the gravitational force of the Sun. Since the force is central, the trajectory equation has the geometric shape of the hyperbola, so, in polar coordinates r, Φ, obeys the equation:

$$\frac{1}{r}=\frac{1}{a\left(\varepsilon^2-1\right)}+\frac{\varepsilon}{a\left(\varepsilon^2-1\right)}\cos\Phi \tag{51}$$

where ε is the eccentricity, which is greater than unit, and a is the distance from the center C to the vertex V called the semi-major axis (Figure 2).

Holding only the first order terms, the approximate solution of the following differential equation:

$$\frac{\mathrm{d}^2u}{\mathrm{d}\theta^2}+u=\frac{GMm_{ph_o}^2}{L^2}\left(1-\frac{4GM}{rc_o^2}\right)^{-3/2} \tag{52}$$

as stated in [4] (subsection 5.2, **The Deflection of Light in the Gravitational Field of the Sun**, Equation (43)), is given by the equation:

$$u=\frac{1}{r}=\frac{B'}{A'}+K'\cos\left(\sqrt{A'}\theta\right) \tag{53}$$

where A', B' are the constants given by the equations:

$$A'=1-\frac{6G^2M^2m_{ph_o}^2}{c_o^2L^2}$$

$$B'=\frac{GMm_{ph_o}^2}{L^2}$$

The deflection angle is given by the equation:

$$\delta\simeq\frac{2}{\varepsilon} \tag{54}$$

We get the result:

$$\delta\simeq 2''.13$$

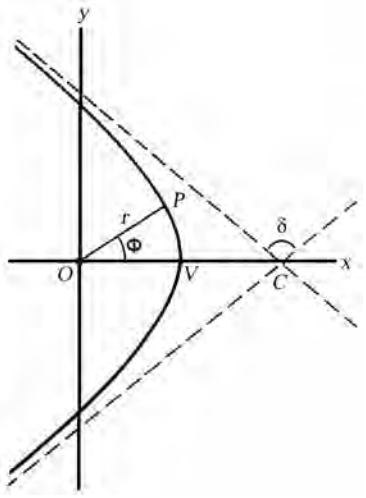

Figure 2. The continuous curved line is the elliptical orbit of the photon within a gravitational field. The hyperbolic orbit asymptotically approaches the dashed lines which are the directions of motion of the photon at a great distance from the spherical body of mass M. The angle δ is the angle of deflection of the photon.

The corresponding value derived from the general theory of relativity is:

$$\delta_{\mathrm{GR}} = \frac{4GM}{R_e c_o^2} \simeq 1''.75$$

The result of calculating the deviation angle based on the hypothesis of the absolute reference system, which is 2 ″.13, is closer to the experimental value than the result of the general theory of relativity. This experimental value was obtained from measurements at the Sobral in 1919 ([15], V. General Conclusions. p. 330), which were:

From declinations 1 ″.94

From right ascensions 2 ″.06

More details on this topic can be found in [4], subsection 5.2, **The Deflection of Light in the Gravitational Field of the Sun**.

5.4. The Time Delay of Light

We will now study the test proposed by Irwin I. Shapiro in order to measure a time delay (Shapiro delay) in the round-trip travel time for radar signals reflecting off other planets ([16]), sometimes called the fourth "classical test" of general relativity.

We consider that an electromagnetic signal is emitted from Earth, reflected on a planet (or spacecraft) and returned to Earth, but under the influence of the Sun's gravitational field during its motion towards the planet and during its return to the Earth. We will calculate the time delay due to the effect of the solar gravitational field on an elementary photonic signal, *i.e.* a photon. The path of the examined photon is the path CBABC, of the axis x shown in **Figure 3**. Of course the deflection angle, which was calculated in the previous section, is very small, so the above-mentioned orbit is considered straight. Here we have ignored the motion of the Earth and planets during the round trip of the signal, because the corresponding velocities, estimated in the reference frame of the solar system, are much slower than the speed of light in vacuum.

The total time of the round trip path is calculated according to relation:

$$\Delta t = \frac{2\left(x_e + x_p\right)}{c_o} + \frac{4GM}{c_o^3} \ln\left(\frac{\left(r_e + x_e\right)\left(r_p + x_p\right)}{d^2}\right) \tag{55}$$

This result agrees with the corresponding result of the general theory of relativity ([17], **7.2 The Time Delay of Light**, Equation (7.31)).

More details on this topic can be found in [4], subsection 5.3, **The Time Delay of Light**.

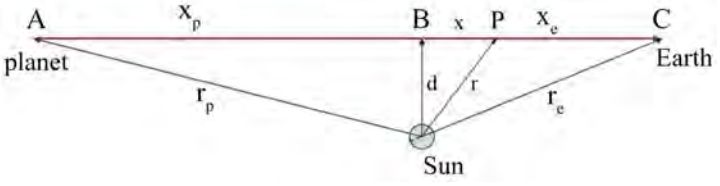

Figure 3. Geometry of light deflection measurements.

5.5. The Gravitational Redshift

We will first study the redshift due to the Earth's gravitational field for example, which is observed if two measurements of the estimated energy of a photon are taken at two different radial distances r_1 and r_2 that differ only slightly, and $r_1 < r_2$. Also we consider that r_1 is equal to the distance of the earth ground of the experiment from the center of the Earth. The ratio of the two estimated energies is calculated as follows:

$$\frac{\mathcal{E}_{ph_g}(r_2)}{\mathcal{E}_{ph_g}(r_1)} = \frac{m_{ph_o}c_o^2\left(1-\frac{4GM}{r_2c_o^2}\right)^{-1/4}}{m_{ph_o}c_o^2\left(1-\frac{4GM}{r_1c_o^2}\right)^{-1/4}} \simeq 1-\frac{GM}{c_o^2}\frac{r_1-r_2}{r_1r_2} \tag{56}$$

If $h = r_2 - r_1$ is the height, R is the radius of the Earth, $g = GM/R^2$, and $r_1r_2 \simeq R^2$, then the previous relation becomes:

$$\frac{\mathcal{E}_{ph_g}(r_2)}{\mathcal{E}_{ph_g}(r_1)} \simeq 1-\frac{gh}{c_o^2} \tag{57}$$

This result agrees with the corresponding prediction of the general theory of relativity and has been experimentally confirmed ([18]).

More details on this topic can be found in [4], subsection 5.4, **The Gravitational Redshift**.

6. Conclusion

The physics of an absolute reference system is a comprehensive and self-contained view of physical reality, extending to all areas of the physical sciences, and confirmed by a wide range of scientific observations and experiments, including all experiments performed from time to time in order to confirm the special and general theory of relativity. In this article, the quantum gravitational phenomena are studied, and it is proved that the gravitational redshift is fully interpreted based on the principles of the absolute reference system hypothesis. Also, the calculations are confirmed by the experimental results, and it is also found that the prediction for the experiment on the deflection of light in the gravitational field of the Sun on the basis of the hypothesis of the absolute reference system, is in better agreement with the experimental data compared to the corresponding prediction of the general theory of relativity. It is therefore necessary to carry out an experiment in order to take high-precision measurements of light deflection, in the special case of the effect of the gravitational field of the Sun.

Conflicts of Interest

The author declares no conflicts of interest regarding the publication of this paper.

References

[1] Patrinos, K. (2019) *Journal of Applied Mathematics and Physics*, **7**, 431-475. https://doi.org/10.4236/jamp.2019.73033

[2] Patrinos, K. (2019) *Journal of Applied Mathematics and Physics*, **7**, 747-780. https://doi.org/10.4236/jamp.2019.74052

[3] Patrinos, K. (2020) *Journal of Applied Mathematics and Physics*, **8**, 999-1015. https://doi.org/10.4236/jamp.2020.86078

[4] Patrinos, K. (2021) *Journal of Applied Mathematics and Physics*, **9**, 1194-1214. https://doi.org/10.4236/jamp.2021.96082

[5] Einstein, A. (1907) *Jahrbuch der Radioaktivität und Elektronik*, **4**, 411.

[6] Einstein, A. (1915) Die Feldgleichungen der Gravitation. Sitzungsberichte der Preußischen Akademie der Wissenschaften zu Berlin. 844-847.

[7] Einstein, A. (1916) *Annalen der Physik*, **354**, 769-822. https://doi.org/10.1002/andp.19163540702

[8] Einstein, A. (1916) Näherungsweise Integration der Feldgleichungen der Gravitation. Sitzungsberichte der Königlich Preußischen Akademie der Wissenschaften Berlin (Part 1). 688-696.

[9] Einstein, A. (1917) Kosmologische Betrachtungen zur allgemeinen Relativitätstheorie. Sitzungsberichte der Preußischen Akademie der Wissenschaften. 142.

[10] Einstein, A. (1918) Über Gravitationswellen. Sitzungsberichte der Königlich Preußischen Akademie der Wissenschaften Berlin (Part 1). 154-167.

[11] Goldstein, H. (1980) Classical Mechanics. Second Edition, Addison-Wesley Publishing Company, Boston.

[12] Hafele, J.C. and Keating, R.E. (1972) *Science*, **177**, 166-168. https://doi.org/10.1126/science.177.4044.166

[13] Hafele, J.C. and Keating, R.E. (1972) *Science*, **177**, 168-170. https://doi.org/10.1126/science.177.4044.168

[14] Landau, L. and Lifshitz, E. (1975) The Classical Theory of Fields. Pergamon Press Ltd., Oxford.

[15] Dyson, F.W., Eddington, A.S. and Davidson, C. (1920) *Philosophical Transactions of the Royal Society of London. Series A, Containing Papers of a Mathematical or Physical Character*, **220**, 291-333. https://doi.org/10.1098/rsta.1920.0009

[16] Shapiro, I.I. (1964) *Physical Review Letters*, **13**, 789-791. https://doi.org/10.1103/PhysRevLett.13.789

[17] Will, C.M. (1993) Theory and Experiment in Gravitational Physics. Cambridge University Press, Cambridge.

[18] Pound, R.V. and Snider, J.L. (1965) *Physical Review*, **140**, B788. https://doi.org/10.1103/PhysRev.140.B788

Journal of Modern Physics, 2021, 12, 1464-1474
https://www.scirp.org/journal/jmp
ISSN Online: 2153-120X
ISSN Print: 2153-1196

Quantum Charged Particle in a Flat Box under Static Electromagnetic Field with Landau's Gauge and Special Case with Symmetric Gauge

Gustavo V. López, Jorge A. Lizarraga, Omar J. P. Bravo

Departamento de Física, Universidad de Guadalajara, Guadalajara, México
Email: gulopez@cencar.udg.mx, yjorge.a.lizarraga.b@gmail.com, zomarbravomac@icloud.com

How to cite this paper: López, G.V., Lizarraga, J.A. and Bravo, O.J.P. (2021) Quantum Charged Particle in a Flat Box under Static Electromagnetic Field with Landau's Gauge and Special Case with Symmetric Gauge. *Journal of Modern Physics*, **12**, 1464-1474.
https://doi.org/10.4236/jmp.2021.1210088

Received: July 25, 2021
Accepted: August 21, 2021
Published: August 24, 2021

Abstract

We summarize our results about the quantization of a charged particle motion without spin inside a flat box under a static electromagnetic field with Landau's gauge for the magnetic field, where Fourier's transformation was used to analyze the problem, to point out that there exists a wave function which is different to that one given by Landau with the same Landau's levels. The quantization of the magnetic flux is deduced differently to previous one, and a new solution is presented for the case of symmetric gauge of the magnetic field, and having the same Landau's levels.

Keywords

Landau's Gauge, Symmetric Gauge, Quantum Hall Effect, Flat Box

1. Introduction

The work of Klitzing, Dora and Pepper [1] presented a breakthrough in experimental physics due to its success in measuring the Hall voltage of a two-dimensional electron gas realized in a MOSFET. The important fact discovered in this experiment was that the Hall resistance is quantized, and Landau's eigenvalues solution [2] (Landau's levels) of a charged particle in a flat surface with magnetic field has become of great importance in trying to understand integer Hall effect [1] [3] [4] [5] [6], fractional Hall effect [6] [7] [8] [9], and topological insulators [10]-[14]. This last elements promise to become essential for future nanotechnology devices [15] [16] [17]. Therefore, it is worth to re-take this problem and to consider in detail the characteristics that it presents. In our previous paper [18], we considered the static magnetic field given through the Lan-

dau's gauge and obtained, by using the Fourier transformation, a different solution for the eigenfunction to those given by Landau. We summarize those results here and make a different approach to obtain the quantization of the magnetic flux or the density of states between two Landau's levels. We continue considering that this result could be relevant, because Landau's solution is kept using in different works like Prange's [19], Laughling's [20], solid state and quantum transport books as well [3] [7] [21] [22]. In addition, for the especial case where the charged particle is moving on the plane x-y under the same static transversal magnetic field but defined by the symmetric gauge, we present a new solution, which matches the characteristics mentioned in [18] and on this paper, we have the same Landau's Levels as solution of the eigenvalue problem.

2. Analytical Approach with Landau's Gauge

Let us consider a charged particle "q" with mass "m" in the box with a constant magnetic field orthogonal to the flat surface x-y, $\boldsymbol{B}=(0,0,B)$, where the magnetic field is given in terms of the vector potential $\boldsymbol{A}$, $\boldsymbol{B}=\nabla\times\boldsymbol{A}$, and let us choose the Landau's gauge $\boldsymbol{A}=(-By,0,0)$ to represents this magnetic field.

2.1. Analytical Approach for the Case $B=(0,0,B)$

For a nonrelativistic charged particle, the Hamiltonian of the system (units CGS) is

$$H=\frac{\left(\boldsymbol{p}-q\boldsymbol{A}/c\right)^2}{2m}, \tag{1}$$

where $\boldsymbol{p}$ is the generalized linear momentum, $\boldsymbol{A}$ is the magnetic potential, and "c" is the speed of light. Therefore, the Hamiltonian has the following form $H=\frac{\left(p_x+qBy/c\right)^2}{2m}+\frac{p_y^2}{2m}+\frac{p_z^2}{2m}$, which does not depend explicitly on time and the eigenvalue problem, $\hat{H}\Phi=E\Phi$, for the Schrödinger's equation [23] is

$$\left\{\frac{1}{2m}\left(\hat{p}_x^2+\frac{2qB}{c}y\hat{p}_x+\frac{q^2B^2}{c^2}y^2\right)+\frac{\hat{p}_y^2}{2m}+\frac{\hat{p}_z^2}{2m}\right\}\Phi=E\Phi. \tag{2}$$

The variable "z" is separable through the proposition $\Phi(\boldsymbol{x})=\phi(x,y)\mathrm{e}^{-ik_z z}, k_z\in\Re$, resulting in the following equation

$$\left\{\frac{1}{2m}\left(\hat{p}_x^2+\frac{2qB}{c}y\hat{p}_x+\frac{q^2B^2}{c^2}y^2\right)+\frac{\hat{p}_y^2}{2m}\right\}\phi=E'\phi, \tag{3}$$

where E' is

$$E'=E-\frac{\hbar^2k_z^2}{2m}. \tag{4}$$

Solving this equation through Fourier transformation [24] on the variable "x", $\hat{\phi}(k,y)=\mathcal{F}[\phi]=\frac{1}{\sqrt{2\pi}}\int_{\Re}\mathrm{e}^{ikx}\phi(x,y)\mathrm{d}x$, it is known [18] (Equation (18)) that one

gets the solution

$$\Phi_{n,k_z}(\boldsymbol{x}) = \frac{1}{\sqrt{L_y L_z}}\left(\frac{m\omega_c}{\hbar}\right)^{1/4} \mathrm{e}^{-i\left(\frac{m\omega_c}{\hbar}xy + k_z z\right)} \psi_n\left(\sqrt{\frac{m\omega_c}{\hbar}}\, x\right). \tag{5}$$

and

$$E_{n,k_z} = \hbar\omega_c\left(n + \frac{1}{2}\right) + \frac{\hbar^2 k_z^2}{2m}. \tag{6}$$

where ψ_n represents the solution of the quantum harmonic oscillator, and ω_c is the so called cyclotron frequency

$$\omega_c = \frac{qB}{mc} \tag{7}$$

These eigenvalues represent just the Landau's levels, but its solution (5) is different to that given by Landau on the variables "*x*" and "*y*". Note that there is not displacement at all in the harmonic oscillation solution. Now, assuming a periodicity in the *z*-direction, $\Phi_{n,k_z}(\boldsymbol{x},t) = \Phi_{n,k_z}(x,y,z+L_z,t)$, the usual condition $k_z L_z = 2\pi n', n' \in \mathcal{Z}$ makes the eigenvalues to be written as and the general solution of Schrödinger's equation can be written as[1]

$$\Phi_{n,n'}(\boldsymbol{x}) = \frac{1}{\sqrt{L_y L_z}}\left(\frac{m\omega_c}{\hbar}\right)^{1/4} \mathrm{e}^{-i\left(\frac{m\omega_c}{\hbar}xy + \frac{2\pi n'}{L_z}z\right)} \psi_n\left(\sqrt{\frac{m\omega_c}{\hbar}}\, x\right). \tag{8}$$

and

$$E_{n,n'} = \hbar\omega_c\left(n + 1/2\right) + \frac{\hbar^2 2\pi^2}{mL_z^2} n'^2, \tag{9}$$

On the other hand, we could have used the boundary conditions $\Phi_{n,k_z}(x,y,0) = \Phi_{n,k_z}(x,y,L_z) = 0$ to obtain the same expression (9) but with the following eigenfunction

$$\Phi_{n,n'}(\boldsymbol{x}) = \frac{1}{\sqrt{L_y L_z}}\left(\frac{m\omega_c}{\hbar}\right)^{1/4} \mathrm{e}^{-i\left(\frac{m\omega_c}{\hbar}xy\right)} \sin\left(\frac{2\pi n'}{L_z}z\right) \psi_n\left(\sqrt{\frac{m\omega_c}{\hbar}}\, x\right). \tag{10}$$

It is necessary to point out that the solution (10) is not separable solution type on the variables *x* and *y*, contrary to Landau's solution. In addition, harmonic oscillator is on the variable *x* without displacement, contrary to Landau's solution which the harmonic oscillator is on the variable y with a displacement. Now, the area of the surface of a circular ring of radius r_1 and r_2 is given classically by $\Delta A = \pi\left(r_2^2 - r_1^2\right)$, where $r^2 = x^2 + y^2$ and $r_2 > r_1$. For the quantum case and using (8), one has

[1]In fact, our Hamiltonian is invariant under translation in the x-direction, and this fact is represented by $\left[\hat{p}_x, \hat{H}\right] = 0$, where $\hat{p}_x$ is the infinitesimal generator of the element of the group of symmetry, it is not difficult to see that $\hat{p}_x\Phi_{n,k_z} = m\omega_c(ix - y)\Phi_{n,k_z} - 2ni\hbar\sqrt{\frac{m\omega_c}{\hbar}}\Phi_{n-1,k_z}$ is another eigenfunction of our Hamiltonian, $\hat{H}\left(\hat{p}_x\Phi_{n,k_z}\right) = E_{n,n'}\left(\hat{p}_x\Phi_{n,k_z}\right)$. In this way, one has that the energy being double degenerated by this symmetry. The same will happen with the next cases.

$$\Delta A = \pi\left[\left\langle \Phi_{n_2,n_2'} \left| r^2 \right| \Phi_{n_2,n_2'} \right\rangle - \left\langle \Phi_{n_1,n_1'} \left| r^2 \right| \Phi_{n_1,n_1'} \right\rangle\right] = \frac{2\pi\hbar}{m\omega_c}\left(n_2 - n_1\right), \tag{11}$$

where the integration has been carried out on the region $z \in [0, L_z]$, $y \in [-L_y, L_y]$ and $x \in (-\infty, +\infty)$. Now, since $\omega_c = qB/mc$, the above expression brings about the relation

$$\frac{qB(\Delta A)}{2\pi\hbar c} = n_2 - n_1 = j \in \mathcal{Z}, \tag{12}$$

which represents the quatization of the magnetic flux [18] (expression (20)), and it is related with the density of states between two Landau's levels [2]. If $\Phi = B(\Delta A)$ is the magnetic flux, and $\Phi_0 = 2\pi\hbar c/2q$ is the so called *quantum magnetic flux* [25] [26], this expression can be written as

$$\frac{\Phi}{\Phi_0} = 2j, \quad j \in \mathcal{Z}. \tag{13}$$

Thus, the general solution (absorbing the sign in the constants) is

$$\Psi(\boldsymbol{x},t) = \frac{1}{\sqrt{L_y L_z}}\left(\frac{m\omega_c}{\hbar}\right)^{1/4} \mathrm{e}^{-i\frac{m\omega_c}{\hbar}xy} \sum_{n,n'} C_{nn'} \mathrm{e}^{i\frac{2\pi n'}{L_z}z} \mathrm{e}^{-i\frac{E_{n,n'}}{\hbar}t} \psi_n\left(\sqrt{\frac{m\omega_c}{\hbar}}\, x\right). \tag{14}$$

where the constants $C_{nn'}$ must satisfy that $\sum_{n,n'} |C_{nn'}|^2 = 1$. The Landau's levels $E_{n,n'}$ are given by expression (9).

2.2. The Analytical Approach for Case $B \perp E$

The magnetic is given as before and electric constant fields is given by $\boldsymbol{E} = (0, \mathcal{E}, 0)$, and $\phi = -\mathcal{E}y$. Then, our Hamiltonian is [20] [21] [22]

$$\hat{H} = \frac{\left(\hat{\boldsymbol{p}} - \frac{q}{c}\boldsymbol{A}\right)^2}{2m} + q\phi(\boldsymbol{x}), \tag{15}$$

and using again the Fourier transformation on the Schrödinger's equation, $i\hbar\frac{\partial\Psi}{\partial t} = \hat{H}\Psi$, it is known [18] (Equation (39)) that a solution is given by

$$\Psi_{n,k_z}(\boldsymbol{x},t) = \frac{1}{\sqrt{L_y L_z}}\left(\frac{m\omega_c}{\hbar}\right)^{1/4} \mathrm{e}^{-i\phi_{n,k_z}(\boldsymbol{x},t)} \psi_n\left(\sqrt{\frac{m\omega_c}{\hbar}}\left(x - \frac{c\mathcal{E}t}{B}\right)\right), \tag{16}$$

where the phase $\phi_{n,k_z}(\boldsymbol{x},t)$ has been defined as

$$\begin{aligned}\phi_{n,k_z}(\boldsymbol{x},t) = &\left[\hbar\omega_c\left(n + 1/2\right) + \frac{\hbar^2 k_z^2}{2m} - \frac{mc^2\mathcal{E}^2}{2B^2}\right]\frac{t}{\hbar} - k_z z \\ &+ \frac{qB}{\hbar c}\left(x - \frac{c\mathcal{E}t}{B}\right)\left(y - \frac{mc^2\mathcal{E}}{qB^2}\right).\end{aligned} \tag{17}$$

asking for the periodicity with respect the variable "z", $\Psi_{n,k_z}(\boldsymbol{x},t) = \Psi_{n,k_z}(z, y, z + L_z, t)$, it follows that $k_z L_z = 2\pi n'$ where n' is an integer number, and the above phase is now written as

$$\phi_{nn'}(\boldsymbol{x},t)=\left[\hbar\omega_c\left(n+1/2\right)+\frac{\hbar^2 2\pi^2 n'^2}{mL_z^2}-\frac{mc^2\mathcal{E}^2}{2B^2}\right]\frac{t}{\hbar}-\frac{2\pi n'}{L_z}z + \frac{qB}{\hbar c}\left(x-\frac{c\mathcal{E}t}{B}\right)\left(y-\frac{mc^2\mathcal{E}}{qB^2}\right). \tag{18}$$

Note from this expression that the term $\mathrm{e}^{-i\phi(\boldsymbol{x},t)}$ contains the element $\mathrm{e}^{i\frac{qB}{\hbar c}xy}$ which characterizes the non separability of the solution with respect these coordinates. Using the same arguments as before (11) to calculate the magnetic flux crossing an area ΔA, one gets

$$\frac{qB(\Delta A)}{\hbar c}=2\pi j,\quad j\in\mathcal{Z}, \tag{19}$$

obtaining the same expression as (12). In this way, from these relations and the expression (16) we have a family of solutions $\left\{\Psi_{nn'}(\boldsymbol{x},t)\right\}_{n,n'\in\mathcal{Z}}$ of the Schrödinger equation,

$$\Psi_{nn'}(\boldsymbol{x},t)=\frac{1}{\sqrt{L_yL_z}}\left(\frac{m\omega_c}{\hbar}\right)^{1/4}\mathrm{e}^{-i\phi_{nn'}(\boldsymbol{x},t)}\psi_n\left(\sqrt{\frac{m\omega_c}{\hbar}}\left(x-\frac{2\pi j\hbar c^2}{q(\Delta A)}\mathcal{E}t\right)\right). \tag{20}$$

Now, by the same arguments we did in the previous case, the general solution would be written of the form

$$\Psi(\boldsymbol{x},t)=\sum_{n,n'}\tilde{C}_{nn'}\Psi_{nn'}(\boldsymbol{x},t), \tag{21}$$

where one must have $\sum_{n,n'}\left|\tilde{C}_{nn'}\right|^2=1$.

2.3. The Analytical Approach for Case $B \| E$

The fields are of form $\boldsymbol{B}=(0,B,0)$ and $\boldsymbol{E}=(0,\mathcal{E},0)$. The scalar and vector potentials are chosen as $\boldsymbol{A}=(Bz,0,0)$ and $\phi=-\mathcal{E}y$. The Shrödinger equation is for this case as

$$i\hbar\frac{\partial\Psi}{\partial t}=\left\{\frac{\left(\hat{p}_x-qBz/c\right)^2}{2m}+\frac{\hat{p}_y^2}{2m}+\frac{\hat{p}_z^2}{2m}-q\mathcal{E}y\right\}\Psi, \tag{22}$$

the eigenvalue problem is now defined by the equation

$$E\Phi=-\frac{\hbar^2}{2m}\frac{\partial^2\Phi}{\partial x^2}+i\frac{qB\hbar z}{mc}\frac{\partial\Phi}{\partial x}+\frac{q^2B^2}{2mc^2}z^2\Phi-\frac{\hbar^2}{2m}\frac{\partial^2\Phi}{\partial y^2}-\frac{\hbar^2}{2m}\frac{\partial^2\Phi}{\partial z^2}-q\mathcal{E}y\Phi. \tag{23}$$

Using again the Fourier transform on the x-variable, it is known [18] (Equation (55)) that one gets the following solution

$$\Phi_{n,n'}(\boldsymbol{x})=a_{n'}\frac{1}{\sqrt{L_yL_z}}\left(\frac{m\omega_c}{\hbar}\right)^{1/4}\mathrm{e}^{-i\frac{m\omega_c}{\hbar}zx}\psi_n\left(\sqrt{\frac{m\omega_c}{\hbar}}x\right)Ai\left(l^{-1}\left(y-y_{n'}\right)\right). \tag{24}$$

where ϕ_n is the solution of the quantum harmonic oscillator, Ai is the Airy function [27], and $a_{n'}$ is its normalization constant $a_{n'}=1\Big/\left|Ai'\left(-l^{-1}y_{n'}\right)\right|$.

Now, using the same arguments as before (11), but with $n_1'=n_2'$ (due to Airy functions) to calculate the magnetic flux crossing an area ΔA, one gets

$$\frac{qB(\Delta A)}{\hbar c} = 2\pi j, \quad j \in \mathcal{Z}, \tag{25}$$

obtaining the same expression as (12). Then, we have obtained a family of solution of the Schrödinger Equation (22),

$$\Psi_{n,n'}(\boldsymbol{x},t) = \mathrm{e}^{-iE_{n,n'}t/\hbar}\Phi_{nn'}(\boldsymbol{x}), \tag{26}$$

where the energies $E_{n,n'}$ are given by $E_{n,n'} = \hbar\omega_c(n+1/2) - q\mathcal{E}y_{n'}$ with $y_{n'} = l\tilde{\xi}_{n'}$ and $Ai(-\xi_{n'}) = 0$. The general solution of (22) can be written as

$$\Psi(\boldsymbol{x},t) = \mathrm{e}^{-i\frac{m\omega_c}{\hbar}xz}\sum_{n,n'}\tilde{C}_{n,n'}\mathrm{e}^{-iE_{n,n'}t/\hbar}\tilde{u}_{n,n'}(x,y), \tag{27}$$

with the condition $\sum_{n,n'}\left|\tilde{C}_{n,n'}\right|^2 = 1$, and where it has been defined the functions $\tilde{u}_{n,n'}$ as

$$\tilde{u}_{n,n'}(x,y) = \frac{a_{n'}}{\sqrt{L_yL_z}}\left(\frac{m\omega_c}{\hbar}\right)^{1/4}\psi_n\left(\sqrt{\frac{m\omega_c}{\hbar}}x\right)Ai\left(l^{-1}(y-y_{n'})\right). \tag{28}$$

3. Analytical Approach with Symmetric Gauge

It is known that the selection of the gauge is not unique, there is always a transform of the form $\boldsymbol{A}_L = \boldsymbol{A}_S + \nabla\chi$, where $\boldsymbol{A}_L = (By,0)$ is the Landau's gauge and $\boldsymbol{A}_S = \frac{B}{2}(y,-x)$ is the symmetric gauge, and the eigenvalue equation limited on the plane *x*-*y* is written as follows

$$E\Psi = \frac{1}{2m}\left(\hat{p}_x^2 + \hat{p}_y^2\right)\Psi + \frac{qB}{2mc}\hat{L}_z\Psi + \frac{q^2B^2}{8mc^2}\left(x^2+y^2\right)\Psi, \tag{29}$$

where $\hat{L}_z$ is the z-component of the angular momentum operator, $\hat{L}_z = x\hat{p}_y - y\hat{p}_x$. This equation cannot be separated in cartesians or polar coordinates. Let us now define a complex variables $z = x+iy$ and $z^* = x-iy$, and the constants

$$\varepsilon = \frac{mE}{2\hbar^2} \quad \text{and} \quad \alpha = \frac{qB}{4\hbar c}, \tag{30}$$

Equation (29) now takes the form of

$$\varepsilon\Psi = -\frac{\partial^2\Psi}{\partial_z\partial_{z^*}} + \alpha\left(z\frac{\partial}{\partial_z} - z^*\frac{\partial}{\partial_{z^*}}\right)\Psi + \alpha^2 zz^*\Psi. \tag{31}$$

Proposing a solution of the form

$$\Psi(z,z^*) = \mathrm{e}^{-\alpha zz^*}\Phi(z,z^*) \tag{32}$$

in the Equation (31), the resulting equation for the function Φ is

$$\frac{\partial^2\Phi}{\partial z\partial z^*} - 2\alpha z\frac{\partial\Phi}{\partial z} = (\alpha-\varepsilon)\Phi. \tag{33}$$

this last expression can be separated. So, let us chose $\Phi(z,z^*) = f(z)g(z^*)$, and by substituting, dividing by $f'(z)g(z^*)$, and making some arrangements,

it follows that

$$\frac{g'\left(z^*\right)}{g\left(z^*\right)} = 2\alpha z + \left(\alpha - \varepsilon\right)\frac{f\left(z\right)}{f'\left(z\right)}, \tag{34}$$

since the expression on the left hand side of the above equality has a different mapping in the complex plane than the one on the right hand side, the latter expression will be generally satisfied if both of them are equal to a complex constant $\lambda \in \mathbb{C}$, and we obtain the next couple of equation

$$\left(2\alpha z + \lambda\right) f'\left(z\right) + \left(\alpha - \varepsilon\right) f\left(z\right) = 0. \tag{35}$$

$$g'\left(z^*\right) = -\lambda g\left(z^*\right), \tag{36}$$

The solution of Equation (36) is straight forward and is given by

$$g(z^*) = Be^{-\lambda z^*}, \tag{37}$$

where B is an arbitrary complex constant. Now, we search for integer complex solution of the expression Equation (35), writing the function as a power series of the variable z

$$f\left(z\right) = \sum_{k=0}^{\infty} a_k z^k, \tag{38}$$

substituting in Equation (35) and making some rearrangements, it follows that

$$\sum_{k=0}^{\infty}\left[a_k\left(2\alpha k + \alpha - \varepsilon\right) + a_{k+1}\left(k+1\right)\lambda\right]z^k = 0, \tag{39}$$

which brings about the following recurrent relation

$$a_{k+1} = -\frac{2\alpha k + \alpha - \varepsilon}{\lambda\left(k+1\right)}a_k. \tag{40}$$

Let us notice that we have the following asymptotic behavior

$$\frac{a_{k+1}}{a_k} \xrightarrow[k\gg 1]{} \frac{2\alpha}{\lambda}. \tag{41}$$

This means that there exist a natural number N such that for $k \geq N$ we have that $a_{k+1} = a_N\left(\frac{2\alpha}{\lambda}\right)^k$. Therefore, one would have the series

$$\sum_{k=0}^{N} a_k z^k + a_N \sum_{k=N+1}^{\infty}\left(\frac{2\alpha z}{\lambda}\right)^k, \tag{42}$$

which diverges for any value such that $\left|2\alpha z\right|/\left|\lambda\right| > 1$. In this way, one must cut the series and obtain a polynomial. To obtain a polynomial solution, we must demand that at some integer number $k = n$, one must have that $a_{n+1} = 0$, and this implies that $2\alpha n + \alpha - \varepsilon = 0$, or

$$\frac{\varepsilon_n - \alpha}{2\alpha} = n \in \mathbb{Z}. \tag{43}$$

Thus, one can obtain that the energies of the system as

$$E_n = \hbar\omega_c\left(n+\frac{1}{2}\right), \tag{44}$$

Note that the direct integration of Equation (35) gives us the solution

$$f(z) = A(2\alpha z+\lambda)^{(\varepsilon-\alpha)/2\alpha}, \tag{45}$$

where A and λ are in general complex constants. Using the expression (43), this function is written as

$$f(z) = A(2\alpha z+\lambda)^n = A\sum_{k=0}^{n}\binom{n}{k}\lambda^{n-k}(2\alpha)^k z^k, \tag{46}$$

where $\binom{n}{k} = \frac{n!}{k!(n-k)!}$ is the binomial number. Therefore, using the expressions (46), (37), and (32), the solution of Equation (31) is

$$\Psi_n(z,z^*) = A_n e^{-\alpha zz^*-\lambda z^*}(2\alpha z+\lambda)^n, \tag{47}$$

where A_n is the normalized constant given by

$$A_n = e^{-|\lambda|^2/4\alpha}\Big/(2\alpha)^{\frac{n-1}{2}}\sqrt{\sum_{k=0}^{n}\binom{n}{k}\Gamma\left(n-k+\frac{1}{2}\right)\Gamma\left(k+\frac{1}{2}\right)} \tag{48}$$

In terms of the variables (x, y), the solution looks as

$$\Psi_n(x,y) = A_n e^{-\alpha\left(x^2+y^2\right)}e^{-\lambda(x-iy)}\left(2\alpha(x+iy)+\lambda\right)^n. \tag{49}$$

One must note that $\left[\hat{L}_z,\hat{H}\right]=0$, where $\hat{L}_z$ is the infinitesimal generator of the element of the group of rotations around z-axis, which is the group of symmetries of our Hamiltonian. Therefore, $\hat{L}_z\Psi_n$ must be other eigenfunction of the Hamiltonian for the same eigenvalue E_n. It is not difficult to see that

$$\hat{L}_z\Psi_n = \hbar\left(\lambda z^*+\frac{2\alpha nz}{2\alpha z+\lambda}\right)\Psi_n, \tag{50}$$

and that

$$\hat{H}\left(\hat{L}_z\Psi_n\right) = E_n\left(\hat{L}_z\Psi_n\right). \tag{51}$$

Note that one gets the following expectetion value

$$\langle n|r^2|n\rangle = 2A_n^2 e^{\frac{|\lambda|^2}{2\alpha}}(2\alpha)^{n-2}\sum_{k=0}^{n}\binom{n}{k}\Gamma\left(n-k+1+\frac{1}{2}\right)\Gamma\left(k+\frac{1}{2}\right)+\frac{|\lambda|^2}{4\alpha^2} \tag{52}$$

which can be used to calculate the area of the surface of a ring of inner radius r_1 and external radius r_2 on the plane x-y, given by $\Delta A = \pi\left(r_2^2-r_1^2\right)$ classically, but in our quantum case, one has

$$\Delta A = \pi\left[\langle n|r^2|n\rangle-\langle n|r^2|n\rangle\right] = \frac{\pi}{\alpha}\times\left\{B(n_2)-B(n_1)\right\}, \tag{53}$$

where $B(n)$ has been defined as

$$B(n) = \frac{\sum_{k=0}^{n}\binom{n}{k}\Gamma\left(n-k+1+\frac{1}{2}\right)\Gamma\left(k+\frac{1}{2}\right)}{\sum_{k=0}^{n}\binom{n}{k}\Gamma\left(n-k+\frac{1}{2}\right)\Gamma\left(k+\frac{1}{2}\right)} \tag{54}$$

Numerically, one finds that $B(2n)=(2n+1)/2$ and $B(2n+1)=n+1$ for $n\in\mathcal{Z}$. Therefore, one gets that

$$B(n_2)-B(n_1)=\begin{cases} n_2-n_1 & \text{even}-\text{even} \\ 2(n_2-n_1) & \text{odd}-\text{odd} \\ n_2-n_1-1/2 & \text{eve}-\text{odd} \\ n_2-n_1+1/2 & \text{odd}-\text{even} \end{cases} \tag{55}$$

Thus, this means that $2\alpha(\Delta A)/\pi$ is an integer number independently on the integers n_1 and n_2, that is (see 12)

$$\frac{qB(\Delta A)}{2\pi\hbar c}\in\mathcal{Z}, \tag{56}$$

or

$$\frac{\Phi}{\Phi_0}=j,\quad j\in\mathcal{Z}, \tag{57}$$

where Φ is the magnetic flux, $\Phi=B(\Delta A)$, and Φ_0 is the quantum magnetic flux, $\Phi_0=2\pi\hbar c/q$.

One needs to mention that Laughlin [28] gave a solution to this problem which is equivalent Landau' solution, and this equivalence was demonstrated by Orion [29]. Their solutions are of separable variable type in the polar coordinates φ and ρ in the space x-y ($x=\rho\cos\varphi$, $y=\rho\sin\kappa$). However, as one can see from (47) or (49), this solution is not of separable variable type in these coordinates, and this is consistent with the fact that the eigenvalue problem (29) written in polar coordinates

$$-\frac{\hbar^2}{2m}\left\{\frac{1}{\rho}\frac{\partial}{\partial\rho}\left(\rho\frac{\partial\Psi}{\partial\rho}\right)+\frac{1}{\rho^2}\frac{\partial^2\Psi}{\partial\varphi}\right\}+\frac{q^2B^2}{8mc^2}\rho^2\Psi-i\hbar\frac{qB}{2mc}\frac{\partial\Psi}{\partial\varphi}=E\Psi, \tag{58}$$

is not of separable variable type in these coordinates. Therefore, the solution (47) cannot be equivalent to Landau-Laughlin solutions.

4. Conclusions and Comments

We have summarized our previous results about the quantization of a charged particle in a flat box and under constants magnetic and electric fields for several electromagnetic static cases using Landau's gauge for the static magnetic field, and using Fourier transformation to solve the linear differential equations resulting from the Shrödinger's equation. We have pointed out again that the full solution obtained is different from Landau's solution for the wave function, but as expected, Landau's levels appear as the solution of the eigenvalues. In all cases, a characteristic phase appears which indicates the non separability on the related variables, which is consistent with the non separability of these variables on the eigenvalue differential equation defined by the Hamiltonian. The quantization of the magnetic flux now appears by considering the number of states between two Landau's levels, and this result is related with the density of states between these levels. Finally, we considered the case for symmetric gauge for the

static magnetic field on the two dimensional plane, and we have shown that a non separable solution exists which is different to Landau-Laughin solution, and the same Landau's levels are obtained. We keep on considering that the approach given here could be very useful to understand quantum Hall effect and related phenomena mainly, because with our solutions a Hall's voltage appears.

Conflicts of Interest

The authors declare no conflicts of interest regarding the publication of this paper.

References

[1] Klitzing, K., Dorda, G. and Pepper, M. (1980) *Physical Review Letters*, **45**, 494-497. https://doi.org/10.1103/PhysRevLett.45.494

[2] Landau, L.D. and Lifshitz, E.M. (2013) Quantum Mechanics: Non-Relativistic Theory, Volume 3. Elsevier, Amsterdam.

[3] Ando, T., Matsumoto, Y. and Uemura, Y. (1975) *Journal of the Physical Society of Japan*, **39**, 279-288. https://doi.org/10.1143/JPSJ.39.279

[4] Laughlin, R.B. (1981) *Physical Review B*, **23**, 5632(R). https://doi.org/10.1103/PhysRevB.23.5632

[5] Halperin, B.I. (1982) *Physical Review B*, **25**, 2185. https://doi.org/10.1103/PhysRevB.25.2185

[6] Laughlin, R.B. (2000) *Uspekhi Fizicheskikh Nauk*, **170**, 292-303. https://doi.org/10.3367/UFNr.0170.200003f.0292

[7] Tsui, D.C., Stormer, H.L. and Gossard, A.C. (1982) *Physical Review Letters*, **48**, 1559-1562. https://doi.org/10.1103/PhysRevLett.48.1559

[8] Laughlin, R.B. (1983) *Physical Review Letters*, **50**, 1395. https://doi.org/10.1103/PhysRevLett.50.1395

[9] Jain, J.K. (1989) *Physical Review Letters*, **63**, 199-202. https://doi.org/10.1103/PhysRevLett.63.199

[10] Konig, M., Wiedmann, S., Brune, C., Roth, A., Buhmann, H., Molenkamp, L.W., Qi, X.-L. and Zhang, S.-C. (2007) *Science*, **318**, 766-770. https://doi.org/10.1126/science.1148047

[11] Zhang, S.-B., Lu, H.-Z. and Shen, S.-Q. (2015) *Scientific Reports*, **5**, 13277, 13279.

[12] MacDonald, A.H. and Streda, P. (1984) *Physical Review B*, **29**, 1616-1619. https://doi.org/10.1103/PhysRevB.29.1616

[13] Yang, Z.H. and Han, J.H. (2011) *Physical Review B*, **83**, Article ID: 045415. https://doi.org/10.1103/PhysRevB.83.045415

[14] MacDonald, A.H., Rice, T.M. and Brinkman, W.F. (1983) *Physical Review B*, **28**, 3648-3650. https://doi.org/10.1103/PhysRevB.28.3648

[15] Fu, L. and Kane, C.L. (2008) *Physical Review Letters*, **100**, Article ID: 096407. https://doi.org/10.1103/PhysRevLett.100.096407

[16] Freedman, M.H., Larsen, M. and Wang, Z.H. (2002) *Communications in Mathematical Physics*, **227**, 605-622. https://doi.org/10.1007/s002200200645

[17] Kitaev, A. (2006) *Annals of Physics*, **321**, 2-111. https://doi.org/10.1016/j.aop.2005.10.005

[18] Gustavo, J.A.L. and Lopez, V. (2020) *Journal of Modern Physics*, **11**, 1731. https://doi.org/10.4236/jmp.2020.1110106

[19] Prange, R.E. (1981) *Physical Review B*, **23**, 4802-4805. https://doi.org/10.1103/PhysRevB.23.4802

[20] Laughlin, R.B. (1999) *Reviews of Modern Physics*, **71**, 863-874. https://doi.org/10.1103/RevModPhys.71.863

[21] Yoshioka, D. (2013) The Quantum Hall Effect. Volume 133, Springer Science & Business Media, Berlin.

[22] Datta, S. (1997) Electronic Transport in Mesoscopic Systems. Cambridge University Press, Cambridge.

[23] Messiah, A. (1999) Quantum Mechanics. Dover Publications, Mineola.

[24] Rudin, W. (1974) Functional Analysis. TATA McGraw-Hill Publishing Co., New Delhi.

[25] Deaver, B.S. and Fairbank, W.M. (1961) *Physical Review Letters*, **7**, 43-46. https://doi.org/10.1103/PhysRevLett.7.43

[26] London, F. (1950) Superuids. John Wiley and Sons, New York.

[27] Lebedev, N.N. (1972) Special Function and Their Applications. Dover Publications, Inc., Mineola.

[28] Laughlin, R.B. (1983) *Physical Review B*, **27**, 3383-3389. https://doi.org/10.1103/PhysRevB.27.3383

[29] Ciftja, O. (2020) *European Journal of Physics*, **41**, Article ID: 035404. https://doi.org/10.1088/1361-6404/ab78a7

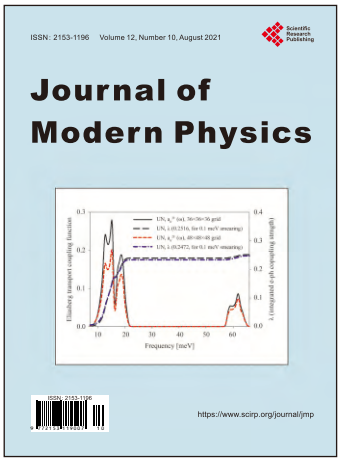

Call for Papers

Journal of Modern Physics

ISSN: 2153-1196 (Print) ISSN: 2153-120X (Online)
https://www.scirp.org/journal/jmp

Journal of Modern Physics **(JMP)** is an international journal dedicated to the latest advancement of modern physics. The goal of this journal is to provide a platform for scientists and academicians all over the world to promote, share, and discuss various new issues and developments in different areas of modern physics.

Editor-in-Chief

Prof. Yang-Hui He City University, UK

Subject Coverage

Journal of Modern Physics publishes original papers including but not limited to the following fields:

Biophysics and Medical Physics
Complex Systems Physics
Computational Physics
Condensed Matter Physics
Cosmology and Early Universe
Earth and Planetary Sciences
General Relativity
High Energy Astrophysics
High Energy/Accelerator Physics
Instrumentation and Measurement
Interdisciplinary Physics
Materials Sciences and Technology
Mathematical Physics
Mechanical Response of Solids and Structures
New Materials: Micro and Nano-Mechanics and Homogeneization
Non-Equilibrium Thermodynamics and Statistical Mechanics
Nuclear Science and Engineering
Optics
Physics of Nanostructures
Plasma Physics
Quantum Mechanical Developments
Quantum Theory
Relativistic Astrophysics
String Theory
Superconducting Physics
Theoretical High Energy Physics
Thermology

We are also interested in: 1) Short Reports—2-5 page papers where an author can either present an idea with theoretical background but has not yet completed the research needed for a complete paper or preliminary data; 2) Book Reviews—Comments and critiques.

Notes for Intending Authors

Submitted papers should not have been previously published nor be currently under consideration for publication elsewhere. Paper submission will be handled electronically through the website. All papers are refereed through a peer review process. For more details about the submissions, please access the website.

Website and E-Mail

https://www.scirp.org/journal/jmp **E-mail: jmp@scirp.org**

What is SCIRP?

Scientific Research Publishing (SCIRP) is one of the largest Open Access journal publishers. It is currently publishing more than 200 open access, online, peer-reviewed journals covering a wide range of academic disciplines. SCIRP serves the worldwide academic communities and contributes to the progress and application of science with its publication.

What is Open Access?

All original research papers published by SCIRP are made freely and permanently accessible online immediately upon publication. To be able to provide open access journals, SCIRP defrays operation costs from authors and subscription charges only for its printed version. Open access publishing allows an immediate, worldwide, barrier-free, open access to the full text of research papers, which is in the best interests of the scientific community.

- High visibility for maximum global exposure with open access publishing model
- Rigorous peer review of research papers
- Prompt faster publication with less cost
- Guaranteed targeted, multidisciplinary audience

Scientific Research Publishing

Website: https://www.scirp.org

Subscription: sub@scirp.org

Advertisement: service@scirp.org